ATOMIC ABSORPTION SPECTRA IN THE RANGE 100 TO 700 Å

by

Michael William Desmond Mansfield, B.Sc., A.R.C.S.

A Thesis submitted for the
degree of Doctor of Philosophy
in the University of London.

Department of Physics,
Imperial College of Science and Technology,
London S.W.7.

April 1969

ABSTRACT

The development of a BRV (Ballofet-Romand-Vodar) source for use as a background continuum source in the study of atomic absorption spectra in the range 100 to 700Å is described. This source has been used in the first place to photograph the atomic absorption spectra of the inert gases, spectra that were originally observed by Madden and Codling using an electron synchotron as a background. A comparison between the BRV source and the electron synchotron as background continuum sources is made on the basis of these results. A hot metal vapour absorption cell has also been developed for use in the wavelength range 100 to 700Å. This cell, which uses arrays of narrow aperture baffles and steep temperature gradients to contain the vapour, does not require the use of solid windows or of buffer gases which would otherwise absorb to a serious extent in this wavelength range. This containment system has been used with the BRV source to photograph the atomic absorption spectra of mercury, rubidium, potassium and sodium at wavelengths below 600Å for the first time. At least 400 new features in the spectra of these elements have been found and tentative assignments, using the (J_cK) coupling scheme, have been made for most of these features. On the basis of the results for Na, K, and Rb, and J.P.Connerade's results for Rb and Cs at wavelengths above 600Å, a comparison has been made between the spectra resulting from the excitation of an electron from the p shell just below the valence shell in the alkali metals.

CONTENTS

Page

ABSTRACT 2

LIST OF ILLUSTRATIONS 7

ACKNOWLEDGEMENTS 8

CHAPTER I INTRODUCTION

1.1 Survey of Previous Work 9

1.2 Beutler's Experiments 13

1.3 Connerade's Experiments 14

1.4 Madden and Codling's Experiments. Fano Profiles . . 15

1.5 The Present Experiments 18

CHAPTER II EXPERIMENTAL

2.1 Spectrographs 20

2.1.1 The 2m Grazing Incidence Spectrograph . . 20

2.1.2 The 3m Normal Incidence Spectrograph . . 25

2.2 The BRV Continuum Source 26

2.3 Source Features. Standards 31

2.3.1 Absorption Lines 31

2.3.2 Emission Lines 44

2.3.3 Accuracy of Measurement 48

2.4 The Furnace and Containment System 49

CHAPTER III THE INERT GASES

3.1 Results 58

3.1.1 Excitation of a Subshell s Electron . . . 58

3.1.2 Excitation of a Subshell d Electron . . . 63

3.1.3 Helium Two-Electron Transitions . . . 66

3.2 Comparison of the Electron Synchotron and the BRV Source 68

CHAPTER IV MERCURY

Page

4.1 Introduction and Experimental Details 71

4.2 Appearance of the Spectrum 73

4.3 Results for Mercury 73

4.3.1 Inner d Shell Excitation 76

4.3.2 Two-Electron Series 79

4.3.3 Other Two-Electron Features 81

4.4 Analysis 85

4.4.1 Inner d Shell Excitation 85

4.4.2 Two-Electron Excitation 86

4.4.2.1 Simultaneous Excitation of Two Valence 6s Electrons . 87

4.4.2.2. Simultaneous Excitation of a Subshell 5d Electron and a Valence 6s Electron . 89

4.5 Excitation from the 5p Shell. Continuous Absorption . 93

4.6 Conclusions 95

CHAPTER V RUBIDIUM

5.1 Introduction and Experimental Details 97

5.2 Appearance of the Rb I Spectrum 98

5.3 Results for Rubidium 100

5.3.1 Series to the (4_1) Limit 102

5.3.2 Series to the (7_1) Limit 103

5.3.3 Series to the (10_1) Limit 103

5.3.4 Other $4p^5(4d+5s)ns,nd$ Lines with Tentative Assignments 106

5.3.5 Simultaneous Excitation of Two Electrons . . 114

Page

5.4 Analysis 116

5.4.1 The $4p^5(4d+5s)$ Limits 116

5.4.2 The $4p^5(4d+5s)ns$ Configuration 118

5.4.3 The $4p^5(4d+5s)nd$ Configuration 120

5.4.4 Two-Electron Excitation 123

5.4.5 The Region 525-350Å 124

5.5 Conclusions 125

CHAPTER VI POTASSIUM

6.1 Introduction and Experimental Details 127

6.2 Appearance of the K I Spectrum 128

6.3 Results for Potassium 131

6.3.1 Series to the (7_1) Limit 132

6.3.2 Other $3p^5(3d+4s)ns,nd$ Features with Tentative Assignments . . 134

6.3.3 Simultaneous Excitation of Two-Electrons . . 141

6.4 Analysis 143

6.4.1 The $3p^5(3d+4s)$ Limits 143

6.4.2 The $3p^5(3d+4s)ns$ Configuration 147

6.4.3 The $3p^5(3d+4s)nd$ Configuration 149

6.4.4 Two-Electron Excitation 151

6.4.5 The 3s Shell. Continuous Absorption 153

6.5 Conclusions 154

CHAPTER VII SODIUM

7.1 Introduction and Experimental Details 155

7.2 Appearance of the Na I Spectrum 157

Page

7.3 Results for Sodium 159

7.3.1 The Leading Doublet $2p^5 3s^2 (^2P_{3/2,1/2})$ . . 160

7.3.2 Series to the $^1P_1$ Limit 160

7.3.3 Other $2p^5 3s$ ns,nd Lines with Tentative Assignments 162

7.3.4 Two-Electron Excitation 166

7.3.5 Excitation from the 2s Shell 166

7.4 Analysis 167

7.4.1 The $2p^5 3s$ ns Configuration 168

7.4.2 The $2p^5 3s$ nd Configuration 171

7.4.3 Two-Electron Excitation 172

7.4.4 Excitation from the 2s Shell 173

7.4.5 The Continuous Absorption Cross Section . . 174

7.5 Conclusions 174

CHAPTER VIII EXCITATION FROM THE SUBVALENCE p SHELL IN THE ALKALI METALS

8.1 Introduction 176

8.2 Parent Ion Levels. Coupling Scheme 176

8.3 The $(n-1)p^5 [(n-1)^d_K + ns]$ ms Configuration 177

8.4 The $(n-1)p^5 [(n-1)^d_K + ns]$ md Configuration 178

8.5 Configuration Interactions of the Orbiting Electron . 179

REFERENCES 181

LIST OF ILLUSTRATIONS

		Page
FIGURE 1	The Performances of Aluminium and Aluminium-backed Iron Filters in the Range 80-320Å . . .	23
FIGURE 2	A Microdensitometer Trace Indicating the Continuous Absorption Cross Section of Hg I, 300-900Å . .	94
PLATE I	A Line Diagram of the BRV Continuum Source . .	27
PLATE II	BRV Source Features, 80-1040Å	32
PLATE III	A Line Diagram of the Containment System . . .	51
PLATE IV	A Photograph of the Apparatus	53
PLATE V	Inner s Shell Excitation in Ar, Kr and Xe	59
PLATE VI	Inner d Shell Excitation in Kr and Xe . . .	64
PLATE VII	The Hg I Absorption Spectrum, 515-765Å . . .	74
PLATE VIII	The Rb I Absorption Spectrum, 525-695Å . . .	99
PLATE IX	The K I Absorption Spectrum, 420-663Å . . .	129
PLATE X	The Na I Absorption Spectrum, 180-195, 295-405Å. .	158

Only the major features of the Hg, Rb, K and Na spectra are indicated on Plates VII-X and many of the assignments given are tentative.

ACKNOWLEDGEMENTS

The author acknowledges with thanks the constant help and encouragement of his Supervisor, Professor W.R.S. Garton, who originally suggested the problem. Thanks are also due to Dr. J.P. Connerade for important help and advice on many topics, and to Mr. J.E.G. Wheaton for help on matters concerned with the BRV source. Work on the glassware by Mr. O.R. Millbank, photographic work by Mr. M. Jackson and typing at very short notice by Mrs. G.L. Locke is also acknowledged with thanks. Finally financial support in the form of a Research Studentship from the Science Research Council is gratefully acknowledged.

CHAPTER I INTRODUCTION

1.1 Survey of Previous Work

Experimental methods of studying the atomic absorption spectra of neutral atoms in the vacuum ultraviolet have, until the past few years, been very limited. In fact, ten years ago, difficulties in obtaining a background continuum source for wavelengths below 600Å meant that few studies of atomic absorption spectra had been possible in this region.

Above 600Å the He_2 discharge of Hopfield (1), developed later by Tanaka (2) and Huffman and co-workers (3), provided a strong continuum in the range 600-900Å. It was this source, supplemented by the Ar_2 continuum (1000-1200Å) and the continuum between the higher members of the H Lyman series (910-980Å), ~~that~~ which was used by Beutler in his pioneering series of experiments in the 1930's (4-12). In these he photographed the absorption spectra of the inert gases Ar, Kr and Xe and of metals easily obtained as atomic vapours. His work is described more fully in section 1.2.

Beutler was prompted to perform these experiments by the discovery of characteristic X-ray spectra. X-ray spectra had been explained by Kossel (13) as due to transitions of electrons from the inner shells of the atom and Beutler considered that the excitation of electrons from shells just beneath the valence shell could be studied by using spectroscopic atomic absorption techniques in the vacuum ultraviolet. This proved to be the case and Beutler's methods brought considerably better resolution to the measurement of inner shell

spectra; furthermore they did not suffer from the difficulty of level broadening encountered in studying the X-ray spectra of solids.

Beutler's experiments with atomic metal vapours have recently been repeated by Connerade (14,15) at Imperial College (1967) who used modern developments in experimental techniques to extend considerably the number of levels observed. He also re-analysed these spectra, completely in most cases. His work is summarised in 1.3.

At wavelengths below 600Å, before the advent of the electron synchotron as a light source, atomic absorption experiments were performed using line sources as backgrounds. With this method, supplemented by the Hopfield continuum above 600Å, continuous photoionization cross sections at many wavelengths in the vacuum ultraviolet were measured for He (16-18), Ne (19-21), Ar (18,22-27,31), Kr (24,28-31) and Xe (22,24,29,31-33). Also Samson (34), using a Garton Flash Tube (35,36) as a background source has detected some of the resonances in the continuous photoionization cross sections of Ar, Kr and Xe due to the excitation of a subshell s electron. This source provides an excellent continuum through much of the ultraviolet but, below 500Å, ~~this~~ the continuum gives way to a dense line spectrum with little usable continuous emission. In experiments such as Samson's the observation of discrete resonance features is difficult as these features often possess asymmetric profiles which are difficult to assess on an irregular background. Samson's accuracy is quoted to be ± 0.1 Å.

Besides the lack of a satisfactory continuum source below 600Å, a second experimental difficulty, that of containment of metal vapours in a windowless system, became prohibitive at wavelengths below 500Å. The usual

experimental method of containing a metal vapour in a system without solid windows has been to contain the vapour between two buffers of helium. However helium absorbs continuously beyond its first ionization potential at 504Å and thus only the inert gases could be studied below this wavelength. The photoionization cross sections of Li (37), Na (37) and K (38) have been studied at wavelengths above 580Å by Hudson and Carter using the Hopfield continuum, helium buffers and photoelectric recording techniques.

The first comprehensive series of atomic absorption experiments at wavelengths below 600Å was that of Madden and Codling (39-45) using an electron synchotron as background, a technique pioneered by Tomboulian and co-workers (46-48). This background extended to very short wavelengths, at least 75Å, and with it Madden and Codling were able to photograph in great detail the discrete spectra of He, Ne, Ar, Kr and Xe below 600Å. Recently electron synchotrons of greater energies have been used to provide continua at wavelengths as low as 20Å (49,50). Madden and Codling's work is surveyed in 1.4.

Two of the resonances photographed by Madden and Codling, the two most prominent lines in helium, had been observed previously in the electron loss experiments of Whiddington and Priestley (51). Recent developments of bombardment techniques with the inert gases have produced important complementary results to those of Madden and Codling as they have enabled optically forbidden transitions from the ground state, in the same energy range as the vacuum ultraviolet spectroscopic measurements, to be observed. Two main experimental techniques have been employed. Firstly, that of Simpson and co-workers (52-54) who measured electron energy losses when the inert gases were bombarded with electrons and, secondly, that of Rudd and

co-workers (55-58) who measured the energies of electrons emitted after the bombardment of the atoms by protons or H_2^+ ions, the energies of the excited states being the energies of the emitted electrons plus the ionization potential of the atom. Numerous forbidden transitions have now been revealed with these techniques although the resolution achieved, 0.1 eV at 60 eV, i.e. 0.2Å, is still an order of magnitude down on the spectroscopic measurements of Madden and Codling. Again these techniques have been limited to easily obtainable non-reactive gases, the inert gases.

A final important experimental development in vacuum ultraviolet absorption techniques, a development that is utilised in the present work (sections 2.2,2.3), is the BRV (Ballofet-Romand-Vodar) flash continuum source, first developed at Bellevue,France (59,60). This source uses the continuous radiation produced, in the region 100-1000Å and above, at the uranium anode in a low pressure impulsive discharge.

The experimental advances in the vacuum ultraviolet that are summarised above have happily coincided to a large extent with advances in the theoretical interpretation of autoionizing lines by Fano (61) and Fano and Cooper (62), described in 1.4. These autoionizing lines are discrete resonances in the continuous photoionization cross sections of atoms; they result from interactions between energy levels beyond the first ionization potential of an atom and the adjacent continuum. Only He (198 305cm^{-1}) and Ne (173 932cm^{-1}) have their first ionization potentials above 167 000cm^{-1} (600Å) and therefore the absorption spectra of atoms at wavelengths less than 600Å provide a large number of Fano profiles.

1.2 Beutler's Experiments

The elements studied by Beutler were Ar, Kr, Xe (5), Hg (6), Cd (7), Zn (8), Tl (12), Cs (9), Rb (11).

He was greatly limited in his work by the experimental facilities available to him. His spectrograph, a 1m normal incidence instrument, had an inverse dispersion of 17.5Å/mm. He had a limited supply of helium for the discharge and gas windows, and only small samples of the elements he was studying. Furthermore his furnace, for vapourising the metals, was made of Supprall glass and could only be heated to 450°C, an inadequate temperature for Zn and Tl.

In Ar, Kr and Xe Beutler was able to see the $np^6\ {}^1S_0 \rightarrow np^5ms,md\ {}^1P_1$ series to the ${}^2P_{3/2,1/2}$ limits and, between these limits, he observed the high series members to the ${}^2P_{1/2}$ limit interacting with the continuum from the ${}^2P_{3/2}$ limit.

In Hg, Cd and Zn he observed the excitation of subshell d electrons, the $nd^{10}(n+1)s^2\ ({}^1S_0) \rightarrow nd^9(n+1)s^2mp,mf$ series of transitions converging on the $nd^9(n+1)s^2\ {}^2D_{5/2,3/2}$ levels of Hg II. He analysed these spectra with a LS scheme comparing them with the normal spectra of Hg, Cd and Zn and with the first spectra of the next elements in the periodic table.

For Rb, Cs and K, Beutler saw the excitation of subshell p electrons, the $np^6(n+1)s\ {}^2S_{1/2} \rightarrow np^5(n+1)s\ ms,md$ series converging on the p^5s levels of the ion. In analysis he used an LS notation but recognised that a j-j scheme was more applicable, neglecting the $\Delta S=0$ selection rule. He did not take the strong mixing of the $np^5(n+1)s$, np^5nd levels of the ion into account though he did appear to have some feeling for this kind of inter-

action, remarking that the $4p^5 5s6s$ level of Rb was difficult to locate because of the nearby $4p^5 5s4d$ level. With Rb he was unable to observe the limits, Rb II levels that lay below 600Å, and, in K, he was only able to see the leading doublet, $3p^5 4s^2$ $(^2P_{3/2,1/2})$.

His work on Tl, observation of the excitation of subshell d electrons, $5d^{10}6s^2 6p \rightarrow 5d^9 6s^2 6p$ np,nf was done before the Tl II levels, $5d^9 6s^2 6p$, were known and can only be regarded as a rough summary. He found 9 features, some of these being doubtful.

1.3 Connerade's Experiments

Connerade repeated Beutler's experiments for Zn, Cd, Hg (14), Cs, Rb and Tl (15).

Experimentally his work represented considerable improvements. His spectrograph was a 3m normal incidence instrument with a 2.75Å/mm. inverse dispersion (this spectrograph was used for much of the work described in the following chapters). He used pyrex and quartz furnaces of greater path lengths than Beutler's, and larger purer samples of the elements studied, and was thus able to extend the spectra of all these elements. Furthermore, since Beutler's experiments, the number and quality of wavelength standards in this part of the spectrum has increased and Connerade was thus able to measure his spectra to a much better accuracy, using the H, He, O, Ne, and C emission lines of the He_2 discharge as wavelength standards.

In his analysis Connerade completely revised Beutler's results. For Cs he was able to use revised Cs II ion levels as limits and for Tl he used the Tl II levels of Ellis and Sawyer (63) not available to Beutler, and, most importantly, he used the $(J_c K)$ coupling scheme of Racah (64) as a model

for his analysis of these spectra. In this model the electrostatic coupling is weak compared with the spin orbit coupling of the parent ion but strong compared with the spin coupling of the external electron. He found this scheme to be good for Zn, Cd, Hg and Tl in which the d^9 shell is screened by a complete s^2 shell, reducing the electrostatic interaction between the outer electron and the core. He also found the $(J_c K)$ scheme a good first approximation for Rb and Cs.

For Rb and Cs Connerade took account of the considerable mixing of the $(n-1)p^5$ ns and $(n-1)p^5(n-1)d$ levels of the ion. For this $a(J_c K)$ notation was ideal for he was then able to consider the excited levels as ns or nd electrons added to ion levels of mixed configuration, these mixed ion levels being specified only by their J values. The excited levels were then described by the parent ion level and the ns or nd of the excited electron through a $(J_c K)$ scheme. For Rb, Connerade, like Beutler, was prevented from seeing the higher series members converging to the Rb II limits by the 600Å short wavelength limit of the He_2 continuum.

1.4 Madden and Codling's Experiments. Fano Profiles

The breakthrough into the region below 600Å came in 1963 when Madden and Codling used the 180 MeV electron synchotron at the National Bureau of Standards as a source of background continuum to wavelengths as low as 75Å. They used a 3m grazing incidence spectrograph at 84.5° incidence with an inverse dispersion of 1.45Å/mm at 500Å to photograph the atomic absorption spectra of He, Ne, Ar, Kr and Xe against the background of synchotron "light". Their accuracy was better than ±0.03Å.

In helium (42) they observed the $1s^2 \rightarrow sp\ 2n+,\ 2n-$ two-electron series.

This notation for the two-electron states represents the highly mixed $2snp\ ^1P_1$, $2pns\ ^1P_1$ and $2pnd\ ^1P_1$ states. Cooper et al. (65) showed that the 2snp, 2pns levels mixed strongly and in approximately equal amounts. The mixed states are represented by

$$(sp,\ 2n\pm) = \frac{1}{\sqrt{2}}\left[U(2snp) \pm U(2pns)\right]$$

where U(2snp), U(2pns) are the symmetrised independent electron wave-functions. Cooper then analysed the overlap of sp $2n\pm$ with the $1s^2$ ground state and predicted that the $2n+$ series would be much stronger than the 2n- series. This was borne out completely by experiment. The $1s^2\ ^1S_o \rightarrow (sp\ 3n\pm)^1P_1$, $(sp\ 4n+)\ ^1P_1$ series to the n=3, n=4 levels of He II were also seen.

In neon (44) Madden and Codling observed the higher series members of the $np^6\ ^1S \rightarrow np^5ms$, md $^1P_1$ series to the $^2P_{3/2,1/2}$ first ionization potentials. These were the transitions seen by Beutler in Ar, Kr and Xe.

For Ne, Ar, Kr and Xe (40,44,45) the excitation of the subshell s electrons, $ns^2np^6\ ^1S_o \rightarrow nsnp^6mp\ ^1P_1$, was seen as a well-developed series in each case and for Kr and Xe the excitation of a subshell d electron, $(n-1)d^{10}ns^2np^6\ ^1S_o \rightarrow (n-1)d^9ns^2np^6mp\ ^1P_1$ was also photographed (41). The other single electron transition seen by Madden and Codling was the excitation of a subshell p electron in Xe (43), $4p^64d^{10}5s^25p^6\ ^1S_o \rightarrow 4p^54d^{10}5s^25p^6ms\ ^1P_1$. These features occurred weakly at 86Å and had previously been recorded by Lukirski et al. (66) using an X-ray continuum source and photoelectric techniques. Recently Nakamura et al. (49) using a 1.3 BeV electron synchotron as a background and Watson and Morgan (50) using a 330 MeV electron synchotron have photographed excitation from the 2p shell in Ar at 50Å, $2p^63s^23p^6\ ^1S_o \rightarrow 2p^53s^23p^6ns$, nd (J=1), a spectrum that is quite similar in appearance to the inner d shell spectra of Kr and Xe.

Watson and Morgan have also detected structure at 58Å in the Kr spectrum due to excitation from the 3p shell and a very weak edge in the Xe spectrum at 58Å due to excitation from the 4s shell.

A considerable number of two-electron transitions have also been observed by Madden and Codling for these gases. These are, for Ne, Ar, Kr and Xe (40,44,45) the excitation of two outer p electrons and the simultaneous excitation of an outer p and an inner s electron and, for Kr and Xe (43) the simultaneous excitation of an inner d electron and an outer p electron. Only the He, Ne and Ar two-electron transitions have so far been analysed and published. Interesting points in these analyses are as follows. With neon it was found that LS coupling did not hold for the excitation of a valence electron but appeared to hold for the excitation of a subshell s electron and was adequate to explain the spectrum of the excitation of two valence electrons (with one slight exception). For argon (45) LS coupling could be used to describe the 3s excitation, although this may have been because, for a second weak series, the spin orbit splitting would have been of the order of the resonance width and this weak series would hence have merged with the strong series. Excitation of a single 3p electron did not obey LS rules, though, and LS coupling was readily violated for the excitation of two 3p electrons. However it also seemed, for the case of two 3p excitation in Ar, that final states almost all involved parents which could form LS allowed states. For Kr and Xe d shell excitation LS was no longer valid and j-j coupling was used.

In these spectra Madden and Codling observed a great number of different autoionization profiles as predicted by Fano (61) and Fano and Cooper (62). For the broader resonances in He, Ne and Ar they studied the

profiles in detail with a photoelectric scanning monochromator, and, from these profiles, they evaluated the important parameters, q, the shape parameter, ρ, the correlation index and $\Gamma/2$ the halfwidth, from which the autoionizing probability of a state can be determined.

These parameters derive from the Fano formula for the absorption cross section of a resonance,

$$\sigma = \sigma_1 \frac{(q+\epsilon)^2}{(1+\epsilon^2)} + \sigma_2$$

Here σ_1 is the background cross section associated with the fraction of the available continua with which the discrete state interacts and σ_2 is the remaining cross section associated with the fraction of the continua which does not enter the interaction. Far from the resonance $\sigma = \sigma_1 + \sigma_2$.

ρ, the correlation index, is defined from $\rho^2 = \dfrac{\sigma_1}{\sigma_1 + \sigma_2}$

ϵ is an energy parameter measuring energy displacement, in units of the halfwidth, $\Gamma/2$, from a point within the resonance

and q is the line shape parameter containing the interaction matrix.

Typical shapes deriving from this formula are broadened absorption resonances, asymmetric resonances (absorption followed sharply by local drops in the continuous absorption cross section to either shorter wavelengths, q negative, or longer wavelengths, q positive) and "window" resonances (purely discrete drops in the continuous cross section with the appearance of emission lines). All these shapes appear frequently in the spectra of Madden and Codling.

1.5 The Present Experiments

The experiments of Madden and Codling, however, were restricted to the

inert gases with which the body of their spectrograph could be filled. The experimental difficulties of containing a metal vapour between regions of high vacuum without He buffers and also the weakness of the synchotron light at that time prevented them from studying other atomic spectra.

In this thesis the methods by which the experimental problems of the background light source, the containment of metal vapours and order sorting are overcome are described. These methods are then used to repeat Madden and Codling's experiments on the inert gases and to photograph, for the first time, the atomic absorption spectra of Hg, Rb, K and Na vapour below 600Å. 400 new features of these spectra are listed and assignments are proposed, although these are only tentative in most cases.

CHAPTER II EXPERIMENTAL

2.1 Spectrographs

2.1.1 The 2 metre Grazing Incidence Spectrograph

The first experiments with the BRV continuum source were performed with a 2m grazing incidence spectrograph designed by A.H. Gabriel (67). This spectrograph, with a platinised 3.5 X 2.5 cm., 600 lines/mm. Bausch and Lomb grating blazed at $1^{\circ}51'$, could be used at 86°, 88° or 89° incidence. For all the experiments described in this thesis it was used at 86° incidence. At this angle spectra could be photographed from 800Å to at least 40Å, although, above 500Å, the intensity was low. The spectrograph had been primarily designed for the observation of emission spectra at wavelengths below 100Å and a smaller angle of incidence would probably have been more suitable for the range studied here. The inverse dispersion of the instrument was about 1.42Å/mm. at 200Å and the resolution was about 0.1Å for emission lines and 0.15Å for absorption lines. The slit width was 10 microns for most experiments but had to be broadened to 15 microns to obtain adequate illumination when a furnace and containment system was inserted between the source and the slit. Unfortunately this did have some adverse effect on resolution.

When the spectrograph was used in the conditions described above, strong emission lines could be observed to their fourth orders. In the observation of continuous emission this threatened to be a serious problem; above 400Å, for example, 4 different orders of continua could overlap. Order sorting devices were therefore sought by which radiation below a certain wavelength λ could be absorbed, ensuring that radiation recorded in the range λ to 2λ was seen in first order. Such a filter would also catch stray light, which, in spite of a zero order catcher on the plate holder,

was evident up to at least 60Å.

The first device to be tested was a plane reflecting mirror of the type described by Astoin et al. (68). This used the fact that, in the vacuum ultraviolet, the low wavelength limit of reflection from an aluminium mirror grows shorter with increasing angle of incidence. The cut-off, though not sharp, is steep e.g. the intensity can decrease by 80% over 10Å (68). Astoin had used a mirror at 30° to 45° incidence and found that the low wavelength cut-off varied from 400 to 290Å for this range. A cut-off of about 200Å was needed in the work described in this thesis and thus an angle of incidence of 60° was employed. It was further intended to make this reflecting mirror toroidal so that, for a given wavelength, it would focus its astigmatic images in such a way that, after reflection by the grating, both the horizontal and vertical astigmatic images would fall at the same point on the photographic plate, as described by Rense and Violett (69). The speed of a grazing incidence spectrograph can be increased considerably by such a method.

It was found, however, that particles emitted from the source very soon damaged the surface of the mirror severely. Moreover the intensity in the region of reflection was extremely low. Astoin et al. partially solved the problem of mirror damage by inserting a gauze in front of the source and a charged plate to deflect charged particles. However the BRV source never produced much illumination to spare and it was felt that to decrease this still further by inserting a gauze and mirror, and by moving the source further from the slit, would be unreasonable, particularly for the slow grazing incidence spectrograph.

The next method of order sorting to be attempted was the insertion of

a self-supporting metal film behind the slit of the grazing incidence spectrograph. It was necessary to insert the film in this position to preserve it from attack by source particles.

The first film to be used was a $\frac{1}{2}$ in. diameter aluminium film of about 800Å thickness. The film thicknesses were determined by comparing their transmission of visible light with that of neutral density filters, a method described by Burton (70). The characteristics of Al films have been studied extensively by Hunter (71,72) and by Madden and Codling (73). The Al film proved effective and robust. It absorbed heavily at wavelengths below the $L_{2,3}$ (2p) edges at 170Å down to about 80Å; below 80Å the intensity of continuum was too low for it to cause trouble in its higher orders. The film transmitted well up to 340Å, above which wavelength second order continuum again appeared.

The transmittance of the film over this wavelength range is indicated in Figure 1, a comparison with the unfiltered source intensity. Figure 1 is a microdensitometer trace of the density of a photographic plate and it should be noted that these traces are of plates taken with different exposure times and that the sensitivity of the microdensitometer was not the same for both traces. This trace is, therefore, in no sense an absolute measurement of the transmittance of the film but it does indicate its performance as a filter. In its region of transmission the aluminium film still absorbs a fair amount (about 40%) and short wavelength emission lines do tend to penetrate in second order, however these effects are minor. The films were kept under vacuum as far as possible because, in air, an Al_2O_3 surface layer soon formed and reduced the transmittance of the film as described by Burton (70). In practice the procedure was to photograph a spectrum with and without a filter, the first photograph was used to

Figure 1

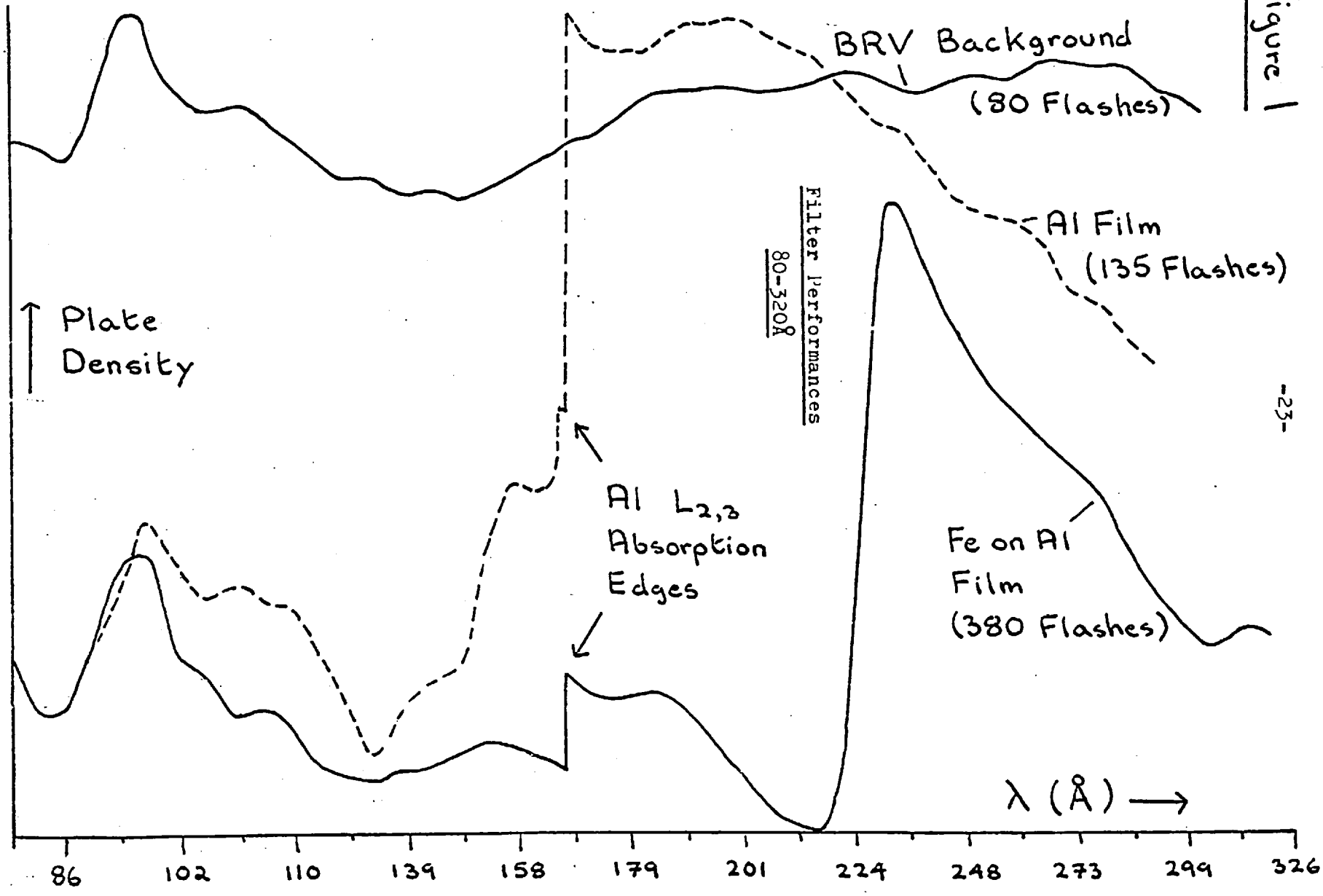
Filter Performances
80-320Å
BRV Background
(80 Flashes)
Al Film
(135 Flashes)
Plate
Density
Al $L_{2,3}$
Absorption
Edges
Fe on Al
Film
(380 Flashes)
λ (Å) →
86
102
110
139
158
179
201
224
248
273
299
326

determine which features were in first order and the second furnished a more intense spectrum with better contrast for measurement. With the metal vapour furnace inserted the continuous emission below 160Å was sufficiently weak to be of little trouble.

The next problem was to find a filter for the 340-600Å range. Consultation of Hunter's papers (71,72), in which he summarises the predicted and observed absorption edges for thin films of 17 elements between 10 and 1000Å, led to attempts to produce an iron filter with an absorption edge at 250Å. The technical problems were great. The crystalline nature of iron meant that self-supporting and gauze-supported Fe films fragmented soon after manufacture. The problem was eventually solved by evaporating the iron onto a self-supporting Al film. The absorption of Al below 170Å was, of course, no problem in this case. Again the films were stored under vacuum to prevent oxidisation. The transmittance of the Fe on Al film is indicated by a microdensitometer trace on Figure 1, again not an absolute measurement of transmittance.

The absorption is due to the excitation of 3p ($M_{2,3}$) electrons to the overlapping 3d ($M_{4,5}$) and 4s (N_1) levels. The diffuseness of the edge is common in transition elements and is accounted for by Skinner (74) as due to Auger transitions of 3d and 4s electrons into the $M_{2,3}$ levels. The absorption spectrum of an iron film, supported on celluloid has been recorded by Carter and Givens (75) using a copper spark line spectrum as a background, but has not been measured continuously by spectroscopic means before.

The nature of the absorption an ill-defined edge around 235Å and a small region of weak transmittance, however, means that Fe is not a satisfactory order sorter.

2.1.2 3 metre Normal Incidence Spectrograph

The problem of photographing the continuum above 340Å without overlapping orders was finally solved by a fortunate discovery regarding the 3m normal incidence spectrograph that had been used by J.P. Connerade to repeat Beutler's experiments (1.3). Connerade had found that the spectrograph grating, though nominally blazed for 800Å, appeared to be blazed nearer to 600Å. The BRV source was then attached directly to the 3m spectrograph and continuum could be seen clearly down to ~~above~~ about 290Å. With this spectrograph a NeI absorption line has been observed at 263Å and an emission line has been seen at 246Å. With an absorption furnace and containment system between the source and the slit the effective low wavelength cut-off moves up to about 330Å. The normal incidence spectrograph can be said to become superior in speed to the grazing incidence instrument at about 350Å, thus these 2 spectrographs cover satisfactorily the entire range of interest in these experiments, 100-700Å.

The 3m normal incidence spectrograph was used with a 2 x 1¼in. 1200 lines/mm. platinised Bausch and Lomb grating of blaze 2°35', givingan inverse dispersion of about 2.75Å/mm. and a resolution of about 0.07Å for sharp absorption lines in this region. A slit width of 10 microns was used throughout, except for mercury (4.1). The experimental advantages of this instrument over the grazing incidence spectrograph were considerable. As well as dispensing with the need for an order sorter, the normal incidence spectrograph was at least twice as fast as the grazing incidence instrument up to 500Å and faster by even greater factors above this wavelength. Furthermore it did not suffer from the usual grazing incidence problems of astigmatism, stray light and troublesome adjustments and it gave an almost

linear dispersion throughout the range 300-1050Å; This was very helpful in identifying source lines (2.3).

2.2 The BRV Continuum Source

The construction of the source, built by J.E.G. Wheaton is shown in Plate I. It closely resembles the source used at Bellevue and described by Romand (59) and by Damany (60). In general the dimensions are about 20% smaller than those of the Bellevue source in the discharge volume and smaller still in the dimensions of the surrounding vacuum housing.

The continuum is created at the end of the $\frac{1}{8}$in. diameter uranium anode by an impulsive discharge between the anode and the earthed brass cathode. The discharge is observed along the axis of the uranium anode through a hole in the cathode. The continuous emission is confined to a very small region probably only a couple of mm across; thus a small aperture of $\frac{1}{8}$in. for the hole through the cathode hardly restricts the continuum light intensity, in fact a narrow aperture tends to suppress the observation of line emission at the edge of the emitting region. Accurate alignment of this source has proved to be essential. The continuous emission deteriorated rapidly with slight changes of alignment, giving way to more emission lines at the edge of the anode, and no emission at all a little beyond that.

An interesting feature of the operation of the source was the shape into which the anode wore. When a new cylindrical uranium anode was inserted a conical pit was worn along its axis by the discharge, indicating a focus of the discharge. The uranium also flaired at its tip, eventually bringing about a weakening of the continuum, but the continuum intensity could be restored by removal of the flairs. The anode as a whole wore slowly and

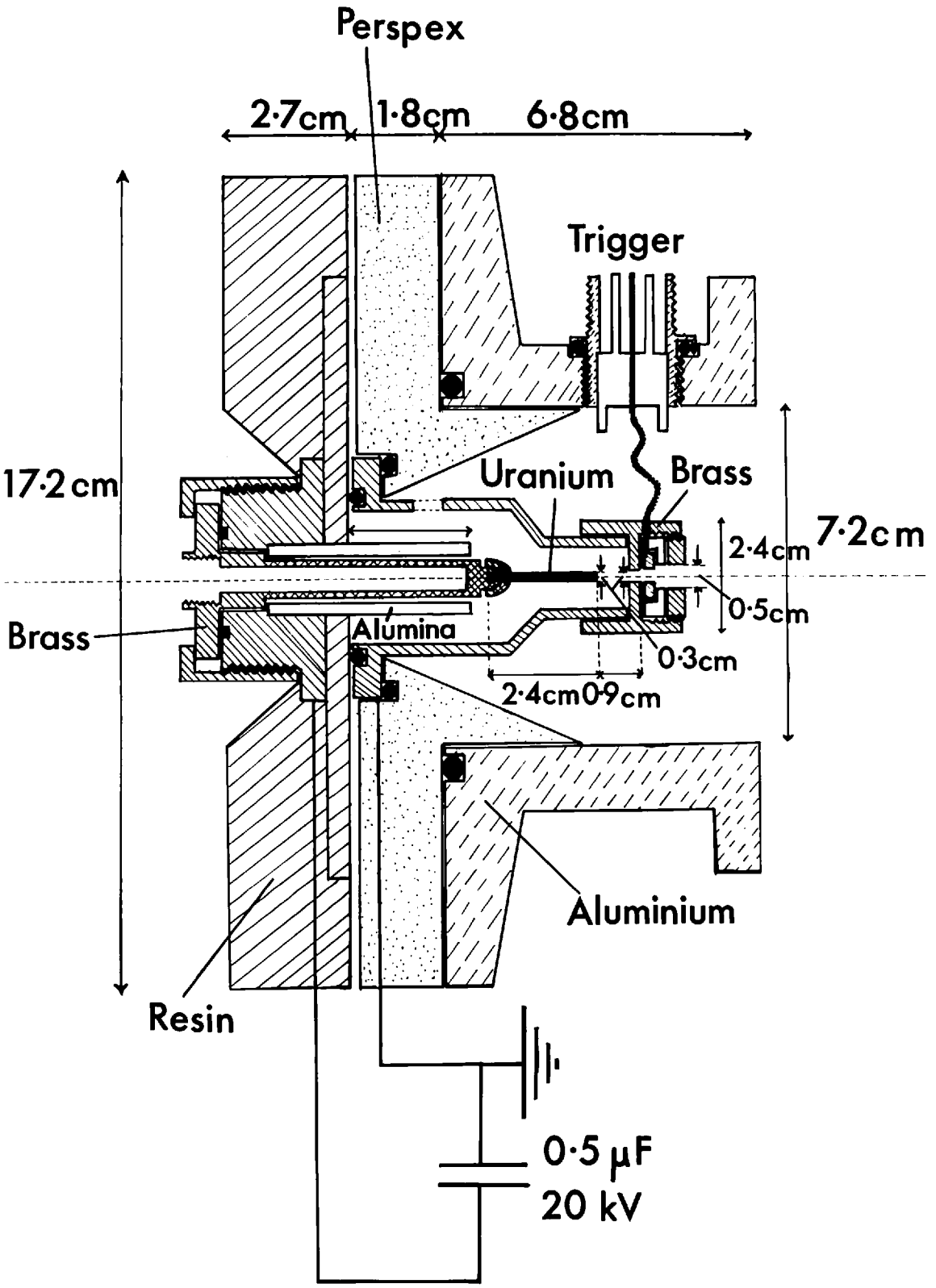
Perspex
2·7cm
1·8cm
6·8cm
Trigger
17·2 cm
Uranium
Brass
7·2cm
2·4cm
0·5cm
Brass
Alumina
0·3cm
2·4cm
0·9cm
Aluminium
Resin
0·5 μF
20 kV

could, in general, be used reliably for about 5,000 flashes.

The discharge was usually operated at 18-20 kV from a 0.5 μFd low inductance condenser. Romand (59) used 22kV and condensers from 0.029 to 0.5 μFd. The inductance of the circuit was not measured but was probably lower than that of the Bellevue source (0.08 μH) due to the smaller volume of the present source. A major difference in operating conditions, however, was that the source could be operated satisfactorily at 10^{-4}mm Hg in the present experiment whereas the Bellevue source required 10^{-6} to 10^{-5}mm Hg. On occasions the source was even operated at 1 micron Hg. This ability to work at higher pressures was, of course, extremely fortunate for the experiments of this thesis in which pressures of mm. Hg of the vapour studied had to be maintained without a window to separate this vapour from the source. It should be mentioned here that the source pressure was monitored about 18 ins. from the discharge region, along the pumping line to the 2 in. diffusion pump. Pressure in the discharge volume was certainly higher.

At higher pressures the source produced many more emission lines and less continuum. It also tended to break down and, once this had happened, it was usually necessary to return the source to high vacuum before it would hold 20 kV again. On some occasions it was necessary to clean the source completely before the high voltage could be used again. For these reasons, whilst operation at 10^{-3}mm. Hg was possible, it was not desirable. 7×10^{-5}mm Hg was a typical operating pressure.

The source was triggered by a vacuum sliding spark (76,77), the propagation of a spark along the surface of a poor conductor. This spark was passed to the cathode across a very thin piece of polythene or PTFE from a third electrode, a small brass ring, coaxial with the anode and the light path. The trigger pulse was 10-25kV.

Triggering was usually the most troublesome feature of source operation. Often the trigger would work for only 500 flashes before it was necessary to renew the polythene. The repitition rate employed was slow, once every ten seconds. This limitation was set by the current capacity of the charging unit. For longer exposures on the grazing incidence spectrograph a faster (though less reliable) charging unit was employed with a firing rate of one flash each 3 seconds. At this rate the anode would get quite hot. Uranium has a fairly low melting point and a low thermal conductivity and thus it was always necessary to check that it was not getting too hot. The overheating of the trigger was often more serious, however, and exposures could suddenly be brought to an end by the polythene in the sliding spark melting. A recent modification has been to use a broader ($\frac{1}{4}$in.) water-cooled anode for more efficient heat dissipation. The anode was earthed in this latter case.

Typical exposures for the BRV source were (in flashes):-

		Ilford Q2	Kodak SWR
With the source directly attached to the spectrograph	Normal Incidence	60	40
	Grazing "	100	60
With a furnace and containment system inserted	Normal Incidence	350	200
	Grazing "	500	250

The number of flashes required of course depended on the level of continuous absorption of the element studied e.g. for mercury on the grazing incidence spectrograph an exposure of 1200 flashes was required. The time for these exposures could thus vary from 6 minutes to 2 hours.

SWR plates were found to be faster and to provide a better contrast

and resolution than the Q2 plates, but they also tended to be variable in quality. For weak exposures patches of emulsion of greater sensitivity on the plate could be troublesome. Q2 plates were more suitable when a large range of wavelengths, with big variations of intensity, was photographed.

The mechanism by which the continuous emission is produced is suggested to be bremsstrahlung from a small plasma sheath at the anode (59). This bremsstrahlung could result from the interaction of cathode electrons with the material of the anode and the high density vapour surrounding it and also from the interaction of ions and electrons in the plasma. Until the degrees of ionization of atoms giving rise to the characteristic source emission lines are known and also the temperatures involved it is difficult to extend this argument.

One further point of interest was the result obtained when an uranium rod was inserted along the axis of a Garton Flash Tube (35,36). The uranium was in contact with the back electrode of the flash tube and protruded as far as the front electrode. This source was then operated at 16kV with a 1 μF capacitor. The familiar O IV, O V, O VI, Al V and Al VI flash tube lines were produced with an enhanced continuum background. The Xe and Kr d shell resonances were observed quite clearly with this arrangement (see Plate VI) although it is difficult to say how distinguishable these would have been without the photograph of these lines taken with the BRV source for comparison. The O and Al lines serve as useful standards in this region but the abundance of lines in the flash tube spectrum makes measurement of absorption lines liable to error when they are overlapped by emission lines.

2.3 Source Features. Standards

The spectrum of the BRV source between 80 and 1040Å is shown in Plate II. This plate is the combination of 7 different exposures on the normal and grazing incidence spectrographs with both Q2 and SWR plates. Allowing for the different wavelength responses of the gratings over this region, the source can be said to produce a moderate and usable continuum at long wavelengths with the intensity of continuum steadily rising towards shorter wavelengths, until it reaches a maximum around 270Å; it then slowly weakens until it is no longer usable at 80Å. The variation in the strength of continuous emission is smooth throughout, the only anomaly being a "hump" of continuum accompanying the strong emission lines between 90 and 100Å.

2.3.1 Absorption lines

Superimposed on this background from the upper wavelength limit of the spectrograph, around 1040Å, to about 200Å are a considerable number of source absorption lines. These lines are fairly sharp but are densely grouped in some regions. They appear to originate in the discharge, for those identified correspond to the second, third and fourth degrees of ionization. They are also very consistent in their appearance. All these absorption lines appear with the same relative intensities, regardless of the pressure at which the source is being operated and the condition of the uranium anode. For example a new anode with an oxide layer and other impurities on its surface produces the same absorption lines as a recently used anode with a shiny surface.

This consistency in the appearance of absorption lines did break down occasionally at short wavelengths (< 250Å) and one slight exception to the

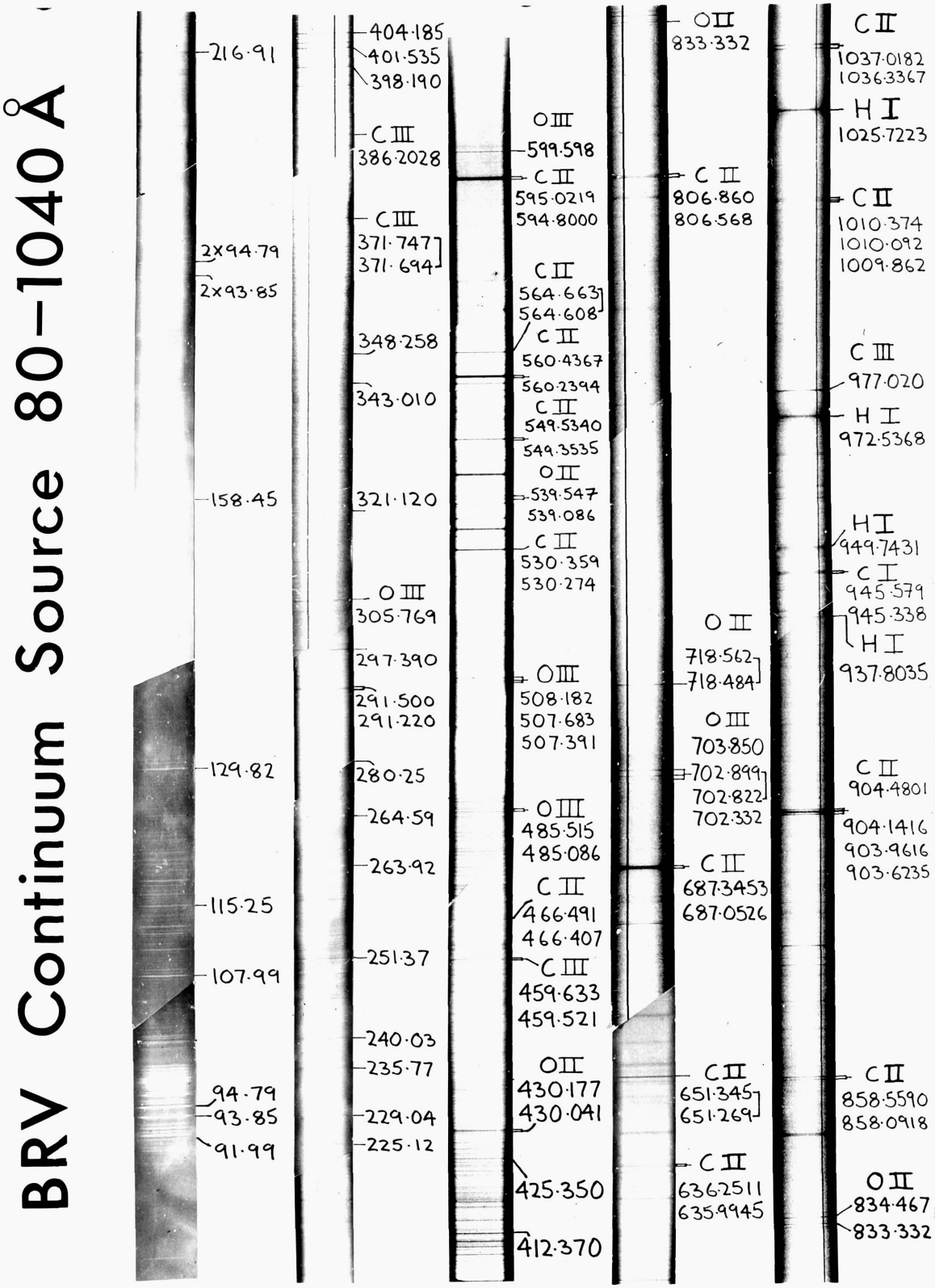
BRV Continuum Source 80–1040 Å
216·91
2x94·79
2x93·85
158·45
129·82
115·25
107·99
94·79
93·85
91·99
404·185
401·535
398·190
C III
386·2028
C III
371·747
371·694
348·258
343·010
321·120
O III
305·769
297·390
291·500
291·220
280·25
264·59
263·92
251·37
240·03
235·77
229·04
225·12
O III
599·598
C II
595·0219
594·8000
C II
564·663
564·608
C II
560·4367
560·2394
C II
549·5340
549·3535
O II
539·547
539·086
C II
530·359
530·274
O III
508·182
507·683
507·391
O III
485·515
485·086
C II
466·491
466·407
C III
459·633
459·521
O II
430·177
430·041
425·350
412·370
O II
833·332
C II
806·860
806·568
O II
718·562
718·484
O III
703·850
702·899
702·822
702·332
C II
687·3453
687·0526
C II
651·345
651·269
C II
636·2511
635·9945
C II
1037·0182
1036·3367
H I
1025·7223
C II
1010·374
1010·092
1009·862
C III
977·020
H I
972·5368
H I
949·7431
C I
945·579
945·338
H I
937·8035
C II
904·4801
904·1416
903·9616
903·6235
C II
858·5590
858·0918
O II
834·467
833·332

regular appearance of the spectrum occurred once when a photograph was taken through a hot empty quartz furnace. Many additional absorption lines were seen converging to a limit at about 685.92Å and, at lower wavelengths, a number of additional sharp absorption lines were also seen for the first time. These sharp features were all identified as Cl II, Cl III and Cl IV from emission spectra. The chlorine almost certainly came from a residue of the $C\,Cl_4$ that had been used to clean the source and furnace. The 685.92Å limit did not correspond to any level of a monatomic chlorine ion and the series were probably due to molecular Cl_2 or CCl_4

These elements that produce absorption features seem to be regular impurities in the anode as their presence is not a function of the amount of surface dirt on the anode. The most easily identified element in absorption, carbon, is a common impurity in uranium. With the Bellevue source only the Hydrogen Lyman series is reported (78), though there seems to have been some evidence of zinc, produced at the brass cathode. This difference may well be due to different processes of manufacture of uranium involving different amounts of impurities, and to the lower resolution of the instruments used at Bellevue.

Absorption features originating in the furnace are molecular, usually N_2, and can be almost eliminated by good pumping. In Plate II, for example, molecular features are hardly noticeable. Discrete molecular features are restricted to the region above 500Å. The absorption spectra of both N_2 and O_2 were photographed so that features from these molecules could be identified when they occurred.

The most immediately recognisable source feature is the group of four CII absorption lines at 904Å. These lines are well-known as emission lines (79).

Using the near linear dispersion of the normal incidence spectrograph as a first approximation, it is soon evident that the great majority of the strong source absorption lines correspond to CII emission lines. This is very fortunate for 17 of these lines were proposed as wavelength standards by Commission 1A of the International Astronomical Union in 1962 (80). The CII spectrum in this region is observed in the expected intensities taken from Kelly's 1968 list of Atomic Emission lines below 2000Å (81) which incorporates Edlen's excellent calculations (79).

Using these CII lines as standards, a considerable number of source absorption features are satisfactorily identified as HI, CII, CIII, CIV, OI, OII, OIII and OIV.

These lines are listed in table I, the standards table. The International Astronomical Union lines are denoted by ST. Measurements with the BRV source relied strongly on CII and, to a lesser extent, on OII as standards, although at times it was necessary to use other lines in table I e.g. when the absorption of the element under study obscured CII or OII lines.

The emission lines from which these standards are taken were narrower than the absorption lines photographed here and some of these observed lines are obviously the combination of up to 4 or 5 lines. In some cases the mean wavelength of a group of lines was calculated, the lines being weighted according to their intensities. This possibility of overlapping lines must always be kept in mind when assessing these standards. For example the CII line, 635.9945 ST always appeared diffuse and was consistently measured to be at 635.95Å. This was attributed to the superposition of another absorption feature.

A further important point is that identifications became much less

certain below 370Å. Intensities in particular were irregular compared with those of published emission species. It is considered that a linear extrapolation with the normal incidence spectrograph is not reliable over more than 50Å and lines measured below 370Å rely rather heavily on 3 Madden and Codling Ne I lines (44) at 275.64, 272.21 and 263.11Å that were superimposed, and on an O III line at 305.769Å. Prominent source lines, in this region, which had not been identified were measured by extrapolation and were occasionally used as standards, particularly for the grazing incidence instrument. They are listed in Table I and are identified as "measured". There is no evidence to throw doubt on the values for these lines, in fact, measurements made with these lines as standards are encouraging; however, they are certainly much less satisfactory than the standards used above 370Å. Accuracy in the range 250-370Å is discussed in 2.3.3.

It was necessary to measure the wavelength of every source feature so that these wavelengths could be compared in detail with those obtained for the absorption spectra of the element under study and a critical distinction between the two sets of features could be made. 565 absorption lines were thus measured in the source; the stronger lines and the lines for which possible identifications have been made are listed in Table II. It will be noted that Cu and Zn lines are listed, presumably originating from the brass cathode. There are many possibilities for identification of unknown lines in Table II. The spectrum of U in this region is little known and there is the possibility of inner electron transitions in C I - IV, O I - IV that have not been seen in the spark spectra.

Finally, those lines listed in Table II with wavelengths below 280Å were measured on the grazing incidence instrument from emission standards (2.3.2).

TABLE I. List of BRV Absorption Standards

The appearance of a line is sharp unless otherwise stated.

Code	Published λ (Å) (81)	Identity	Appearance
2	1036.3367ST	CII	Moderate strength
3	1025.7223	HI	Strong, diffuse
4	1010.374	CII	Weak
7	977.020	CIII	Strong
8	972.5368	HI	Moderate, diffuse
12	949.7431	HI	Weak, diffuse
21	904.4801ST	CII	Strong
22	904.1416ST	CII	Strong
23	903.9616ST	CII	Strong
24	903.6235ST	CII	Strong
35	858.5590ST	CII	Strong
36	858.0918ST	CII	Moderate
39	835.292	OIII	Weak
40	834.467	OII	Moderate
41	833.742	OIII	Very Weak
42	833.332	OII	Moderate
43	832.762	OII	Weak
47	806.860	CII	Quite Weak
50	799.944	CII	Very Weak
52	792.968	OI	Very Weak
58	718.562 > .523 718.484	OII	Moderate
59	703.850	OIII	Moderate

Code	Published λ (Å)	(81)	Identity	Appearance
60	702.899 702.822	.862	OIII	Moderate
61	702.332		OIII	Weak
62	687.3453ST		CII	Very Strong
63	687.0526ST		CII	Very Strong
71	651.345 651.269	.309	CII	Very Strong, broad.
72	641.888		CII	Moderate
73AA	641.800 641.771	.785	CII	Moderate
73AB	641.627 641.593	.610	CII	Moderate
74	636.2511ST		CII	Moderate
75	635.9945ST		CII	Moderate
79	616.291		OII	Moderate
80	599.598		OIII	Moderate
81	595.0219ST		CII	Very Strong
82	594.8000ST		CII	Very Strong
83	577.0859		CII	Weak
84	574.2809		CIII	Weak
85	564.663 564.608	.644	CII	Strong
85A	562.562		CII	Weak
87	560.4367ST		CII	Very Strong
88	560.2394ST		CII	Very Strong
93	554.514		OIV	Weak
94	554.074		OIV	Weak
95	549.5700ST 549.5110ST	.5340	CII	Strong

Code	Published λ (Å)		Identity	Appearance
96	549.3785ST 549.3195ST	.3535	CII	Strong
97	543.444		"	"
97F	543.257		"	"
97A	539.853		OII	Weak
99	539.547		OII	Moderate
100	539.086		OII	Moderate
101	538.318 538.312 538.256	.281	OII CIII OII	Moderate
101A	537.830		OII	Weak
104	532.705 532.659	.690	CII	Moderate
105	530.359 530.274	.323	CII	Very Strong
106	525.795		OIII	Moderate
107	508.182		OIII	Moderate
108	507.683		OIII	Weak
110	485.515		OII	Weak
111	485.086		OII	Moderate
113	466.491 466.407	.480	CII	Strong
116	459.633		CIII	Strong
117	459.521		CIII	Strong
121	438.897		CII	Weak
122	437.102		CII	Moderate
125	430.177		OII	Strong
126	430.041		OII	Strong
127	425.350		Measured	Moderate

Code	Published λ (Å)	Identity	Appearance
128	412.370	Measured	Strong
132A	404.185	Measured	Strong
132D	401.535	Measured	Moderate
135	398.190	Measured	Strong
138	386.2028	CIII	Strong
139G	384.178	CIV	Moderate, diffuse
141	371.747 } 371.694 } .720	CIII	Strong
157	305.769	OIII	Strong
163	297.390	Measured	Strong
166	291.500	Measured	Moderate
167	291.220	Measured	Strong

TABLE II. List of Stronger BRV Absorption Features and Source Features for which possible identifications have been made.

These lines are sharp unless otherwise indicated.

For Zn and Cu the published λ are as listed in Kelly (1959) (82)

Code	Measured λ (Å)	Possible Identity	Published λ (Å)	Appearance
1	1037.048	CII	1037.0182ST	Quite strong
5	1010.127	CII	1010.092	Weak
6	1009.885	CII	1009.862	Weak
13	945.597	CI	945.579	Moderate strength
14	945.293	CI	945.338	Moderate
16	937.815	HI	937.8035	Veryweak, diffuse
26	888.614	ZnII	888.62	Weak

Code	Measured λ (Å)	Possible Identity	Published λ (Å)	Appearance
28	881.054	ZnII	881.05	Quite strong
29	877.847	OI	877.882	Moderately strong
37	848.886			Strong
38	848.625			Strong
39A	835.004	OIII	835.096	Very weak
48	806.529	CII	806.568	Quite strong
49	802.891	CuIII	802.841	Moderate, diffuse
51	799.616	CII	799.660	Weak
55	790.149	OIV	790.203 } .160 790.103 }	Weak
56	767.027	ZnII	767.02	Moderate
66	677.940	ZnIII	677.93	Moderate
67	677.609	ZnIII	677.56	Quite strong
67E	676.576	CuIII	676.564	Very weak
68	661.894			Moderate, diffuse
69	653.505			Moderate
70	653.137			Moderate
71A	644.140	OII	644.148	Weak
76	634.903			Moderate
77	630.366			Strong
78	617.052	OII	617.051	Moderate
79C	610.740	OIII	610.746	Very weak
79B	609.791	OIV	609.829	Very weak
79A	600.554			Very weak, diffuse
82C	580.913	OII	580.967	Weak
82B	580.486	OII	580.400	Weak

Code	Measured λ (Å)	Possible Identity	Published λ (Å)	Appearance
86	562.360	CII	562.497 562.473 562.367 562.338 } .417	Weak
89	559.205			Quite strong
90	558.006			Quite strong
92	555.052	OII	555.026	Weak
96C	545.699			Moderate
103	533.983	CII?	533.935	Very strong
103A	533.753	NII	533.729	Very strong
104A	531.938	CII	531.917	Moderate
109	507.387	OIII	507.391	Weak
109C	487.434			Moderate
109B	486.846			Moderate
112V	482.705			Weak
112U	480.074			Weak
112R	478.205			Moderate
112M	474.038			Quite strong
112L	472.512			Moderate
112K	472.209			Moderate
112J	471.787			Moderate
113C	464.575			Quite strong
113B	463.410			Quite strong
114	461.997			Quite strong, diffuse
115	461.219	CII	461.120	Quite strong, diffuse
117H	458.795			Weak
118	452.557			Moderate
119	449.997			Moderate, diffuse

Code	Measured λ (Å)	Possible Identity	Published λ(Å)	Appearance
119A	440.979			Quite weak
120	440.172			Moderate, diffuse
121B	437.718	OII	437.683	Weak
121A	437.425	OII	437.332	Weak
122A	435.835			Weak
123	435.334			Weak
126E	429.691			Moderate
126C	428.127			Moderate
127P	424.680			Moderate
127O	423.122			Moderate, diffuse
127M	419.543	CIV	419.525	Weak
127K	417.917			Moderate
127J	417.018			Moderate
127F	414.627			Moderate
129	411.069			Strong
130	410.112			Strong
131	408.819			Quite strong
132	407.667			Moderate
132C	402.494			Moderate
135A	395.444	OIII	395.558	Weak, diffuse
136A	392.312	OII	392.322	Quite weak
137	391.934	OII	392.002 } .978 391.943 }	Moderate
139H	384.349			Moderate
139F	383.981	CIV	384.032	Moderate
140G	377.766			Moderate, diffuse
140F	377.454			Moderate, diffuse

Code	Measured λ(Å)	Possible Identity	Published λ(Å)	Appearance
140B	374.077	OIII	374.075	Quite weak
140A	373.234			Quite weak
143A	366.173	CIII	366.169	Weak
144	365.713	CIII	365.778	Quite strong
145	347.997			Moderate, asymmetric?
145A	334.343			Quite strong
148	322.600	CIII	322.5741	Moderate
149	321.090	OIII	320.979	Quite strong, asymmetric?
151	312.472	CIV	312.453 } .438 312.422 }	Moderate
152	308.432			Moderate
153	308.072			Moderate
155	306.760	OIV	306.882 } .760 306.621 }	Weak
156A	306.002			Moderate
158	304.160			Moderate
159	303.950			Moderate
162	298.672			Weak
187	263.920			Moderate
189	260.296			Moderate
190	259.864			Moderate
191	259.689			Moderate
198	251.37			Quite strong
200	249.17			Weak
202	247.69			Weak
204	245.66			Moderate
205	240.03			Strong

Code	Measured λ(Å)	Possible Identity	Published λ(Å)	Appearance
207	235.77			Strong
208	229.10			Moderate
210	225.12			Moderate
212	216.91			Weak

2.3.2 Emission lines

The source emission lines lie in the range 40 to 450Å for the operating conditions of the source chosen in the experiments of this thesis.

In many senses the occurrence of emission lines is in complete contrast to that of absorption lines as described in the previous section. The abundance and relative intensities of emission lines are very much dependent on the operating pressure of the source, its alignment and the cleanliness of the uranium anode. It was usual to clean a new anode with about 100 preliminary discharges to reduce the amount of line emission.

Even when these precautions of a clean anode, low pressure and good alignment were adhered to there was still irregularity in the amount of line emission. For some experiments there was only one noticeable emission line, that at 158.45Å, though it was more usual to see the stronger lines between 90 and 100Å in 2 or 3 orders as well as a few other strong lines between 100 and 200Å.

None of these stronger lines have been related to published emission line wavelengths though occasionally some oxygen lines could be identified. These O lines, listed in Table III, were rare however and never strong. The main line emission seems to have been from uranium ions, whose spectra in this region are not adequately documented. There is also a possibility of Zn and

Cu emission though this is not indicated by the wavelengths of lines published for these elements (82).

The source emission lines have been measured by the following method. It had been noticed that line emission from the source was more intense at higher pressures and, with this in mind, the source was operated with about 0.2mm Hg of neon present in the discharge volume in the hope that some of the many Ne IV, V and VI lines in this region would be seen and could be used as standards. Many of these lines were in fact seen, though O IV, V and VI lines were more prominent. It seems likely that the neon, though not filling the discharge volume as much as had been expected, had inhibited the pumping of oxygen produced in the discharge. These oxygen lines were as useful as the neon lines as standards however for they are very strong features of the Garton Flash Tube (35,36) spectrum in this region and could easily be identified by comparison with Flash Tube photographs.

In this way 27 O IV, V, VI and Ne IV standards were produced in the region 150-240Å. Most of the BRV emission lines are at shorter wavelengths, but the stronger lines appear clearly in second order, particularly in the range 180-200Å. Thus, by measuring the stronger lines in second order and using these measurements as standards for shorter wavelengths, the characteristic BRV lines were measured. The strong lines are also seen clearly in third order, between 270 and 300Å.

Altogether, with neon in the source, about 400 lines were seen between 40 and 350Å. 110 of these were correlated with lines seen in the source at low pressure (5×10^{-5}mm. Hg), the remainder being Flash Tube oxygen lines, neon lines and higher orders of source lines. Above 250Å the lines became too densely grouped to allow satisfactory sorting; however source lines above this wavelength have been measured with the normal incidence spectrograph.

The more prominent source emission lines are listed in Table IV. Those below 250Å were measured by the method described above, those above 250Å were measured with the normal incidence spectrograph. Some of the stronger lines listed in Table IV have been used as standards in the short wavelength region where there are no identified lines; these are marked by an asterisk. The absorption lines below 250Å in Table II were measured using these standards, the lines at 93.85, 94.79 and 158.45Å being relied on heavily for this. Accuracy in this region is discussed in the next section.

TABLE III. Oxygen Emission Lines in the BRV Source

Code	Published λ (Å)		Identity
120	150.089 150.124	150.100	O VI
123	151.449 151.481 151.548	151.500	O V
163	172.935		O VI
164	173.082		"
181	183.937 184.117	184.050	"

TABLE IV. Stronger BRV Emission Lines

Code	Measured λ (Å)	Appearance	Code	Measured λ (Å)	Appearance
136BL	392.944	Moderate strength	145L	324.258	Quite strong
139BL	382.101	Moderate, sharp	145UL	343.010*	Moderate, sharp
141BL	370.850*	Quite strong	145NL	337.779	Moderate
144BL	362.321	Strong, diffuse	149L	321.120*	Strong
			168L	290.398	Moderate

Code	Measured λ (Å)	Appearance	Code	Measured λ (Å)	Appearance
169L	289.729	Moderate	63	117.34*	Moderate
174L	280.251*	Strong	62	116.77	Moderate
182L	271.830*	Quite strong	61	116.46	Moderate
186L	264.585*	Moderate	57	115.25*	Quite strong
166	174.08	Moderate	51	113.10*	Quite strong
145	165.58	Moderate	49	112.32*	Moderate
144	165.16	Moderate	48	112.10	Moderate
143	164.68	Moderate, diffuse	45	110.69*	Quite strong
			40	108.64*	Moderate
141	163.34	Moderate	38	107.99*	Strong
139	162.71	Moderate	34	101.83	Moderate
133	158.45*	Very strong, persistent	33	101.59	Moderate
130	156.08	Strong	32	101.23	Moderate, diffuse
91	129.82	Diffuse	26	97.60	Moderate, diffuse
82	124.68*	Weak			
81	124.38*	Weak, diffuse	25	97.29	Moderate, diffuse
77	122.63	Moderate, diffuse	24	96.22	Moderate
76	122.18	Moderate	23	95.97	Moderate, diffuse
75	121.94	Moderate	22	95.34	Moderate
72	121.09	Moderate, diffuse	21	95.11*	Moderate
71	120.68	Moderate	20	94.79*	Very strong
68	120.06*	Moderate	19	93.85*	Very strong
67	119.65	Moderate, diffuse	17	92.76*	Quite strong

Code	Measured λ (Å)	Appearance	Code	Measured λ (Å)	Appearance
16	92.46	Moderate	4	68.8 ± 0.1	Weak
15	91.99	Moderate	0	40.8 ± 0.2	Persistent
9	87.45	Very weak			

2.3.3 Accuracy of Measurement

All plates were measured with a Zeiss Abbé microcomparator. From repeated measurements, this instrument was considered to have an accuracy of ±0.002 mm. which is ±0.005Å for the normal incidence spectrograph and ±0.003Å for the grazing incidence instrument.

The error of measurement however is to a much greater extent a function of the accuracy of the standards used and therefore a function of wavelength region.

Typically, for the normal incidence spectrograph, 15 to 45 standards were used for each plate covering a wavelength range of 600Å. A second degree polynomial was necessary to fit these points for ranges over 100Å. The scale seemed to depart from linear particularly at the ends of the plate holder; below 400Å and above 900Å it could be as much as 0.07Å away from a linear fit. A third degree polynomial made little difference to the standard deviation which was usually between 0.02 and 0.01Å.

For the grazing incidence spectrograph 15 to 25 standards were used for a range of 300Å. A fourth degree polynomial was necessary for the non-linear dispersion of this instrument. The scale changed very rapidly at the ends of the plate where presumably the edges did not bend completely to the 2m radius of the Rowland circle and this part of the plate was not used. The standard deviation was between 0.03 and 0.01Å.

The predicted errors of measurement for sharp features in the different wavelength regions are listed below.

a) 700-1050Å. The standards in this region are reliable but are separated by gaps of as much as 70Å. The measurements for Rb agree well with those of J-P. Connerade but there are discrepancies for Hg. The error should not be more than ±0.025Å.

b) 400-700Å. There are many reliable standards in this region which is the region in which the vast majority of new spectra lie. The measurements for the inert gases and Rb in this region are in satisfactory agreement with published wavelengths. The error is about ±0.015Å.

c) 270-400Å. The standards become less reliable as the wavelength decreases but the measurements made of 3 Madden and Codling Ne lines around 270Å are satisfactory. The error is about ±0.025Å.

d) 80-270Å. This range was covered by the grazing incidence spectrograph and measurements here rely heavily on standards measured by the method described in 2.3.2. In particular there is a large gap between 158 and 260Å on some plates and thus the error may be as high as ±0.25Å. No new spectra except a very diffuse Na feature at 186Å are measured in this region though.

2.4 The Furnace and Containment System

The metals whose absorption spectra were studied in these experiments were those that were easily obtained as monatomic vapours at relatively low temperatures. Pressures of up to 10 mm. Hg were required and thus the highest temperature needed, for Na, was 610°C. These temperatures were achieved in pyrex (up to 430°C) and fused quartz tubes of 1½ in. diameter

heated by coils of nichrome wire wound round them. Two layers of asbestos tape separated the wire from the glass or quartz and 2 or 3 layers of asbestos cord lagged the furnace. The heated length was 12 in. for the pyrex furnace and 12 in. and 26 in. for the quartz furnaces.

Whenever temperatures below 430°C were required (for Hg and Rb) the pyrex furnace was preferred as it was much cleaner and could be pumped to a lower pressure than the quartz. Furthermore the quartz was more liable to vicious attack from the hot metal vapours and required a complete lining of thin stainless steel in the heated region. This problem was worst for sodium, causing the quartz to flake greatly on cooling.

The furnaces were roughly calibrated from a Hg thermometer placed in contact with the inner wall of the furnace, at the centre, and from a Pt/Pt-Rh thermocouple in contact with the outer wall, also at the centre. The readings of these 2 thermometers were noted as the current in the nichrome wire increased. The Hg thermometer of course could only be used up to 300°C but, as the thermocouple tended to consistently read the same fraction of the mercury thermometer reading (typically 0.7), the thermocouple readings were adjusted by this factor above 300°C. This method was of course very crude but it served well in predicting the current reading needed for a particular level of absorption. It was noted that the temperature could vary considerably along the length of a furnace for a given temperature e.g. at "270°C" for the pyrex furnace the temperature could vary by 80°C along the furnace. For quartz this effect was much worse; thus quotations of temperature have only a comparative meaning.

A further precaution taken was to calibrate the furnaces on their second heating cycles because the resistive properties of nichrome wire were

PLATE III LINE DIAGRAM OF THE CONTAINMENT SYSTEM

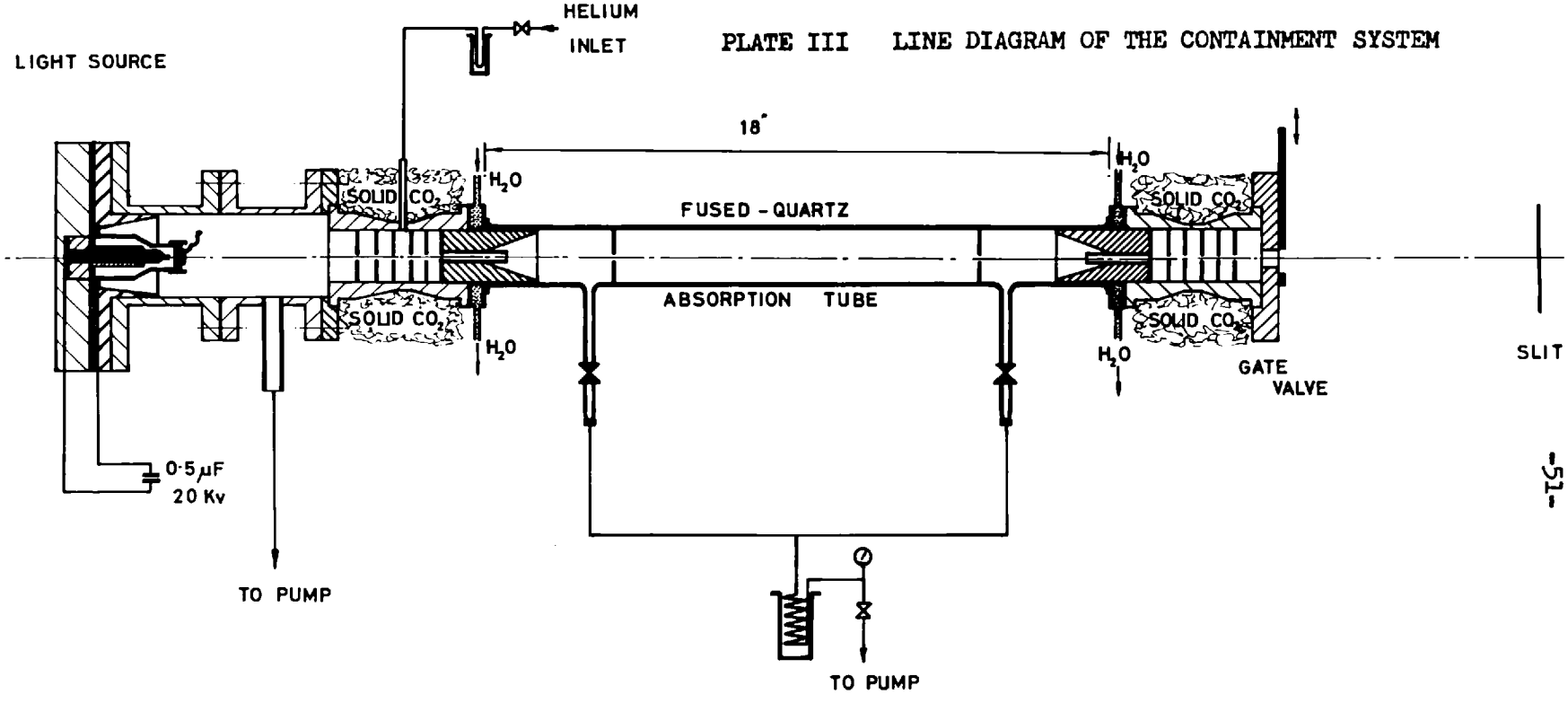

very irregular the first time it was heated. In both calibration and experiment the furnaces were allowed 20-30 minutes to reach a stable temperature.

The final experimental problem concerned the containment system. The problem was to maintain up to 10mm. Hg of a highly reactive metal vapour between 2 regions of high vacuum, 10^{-5}mm. Hg for the spectrograph and 5×10^{-5} mm. Hg for the source. There are no solids from which transmitting windows can be made in this region and no buffer gases that would transmit at pressures comparable to that of the metal vapour.

The principles by which this difficulty was overcome are illustrated in Plate III, a line diagram of the containment system and Plate IV, a photograph of the source and 12 in pyrex furnace in use on the grazing incidence spectrograph. In this system an array of many small diameter baffles was placed on either side of the furnace to inhibit the diffusion of metal vapour atoms from the furnace. Also a steep temperature gradient was applied between the furnace and the baffles so that vapour that was scattered by the baffles condensed before leaving the baffle system.

In the discussion on the operation of the BRV source (2.2) it was concluded that the continuum was emitted by a very small volume of plasma, only a couple of mm. across. It seemed likely, therefore, that apertures as small as $\frac{1}{8}$in. along the light path would have little adverse effect on the light intensity at the spectrograph slit. This proved to be so for the baffles used in the containment system. The baffling system employed consisted firstly of a $\frac{1}{4}$in. diameter, $1\frac{3}{4}$in. long aperture in the water-cooled furnace end-pieces and then of a series of six $\frac{1}{8}$in. baffles, $\frac{1}{2}$in. apart, at either end of the vapour column.

PLATE IV PHOTOGRAPH OF THE APPARATUS

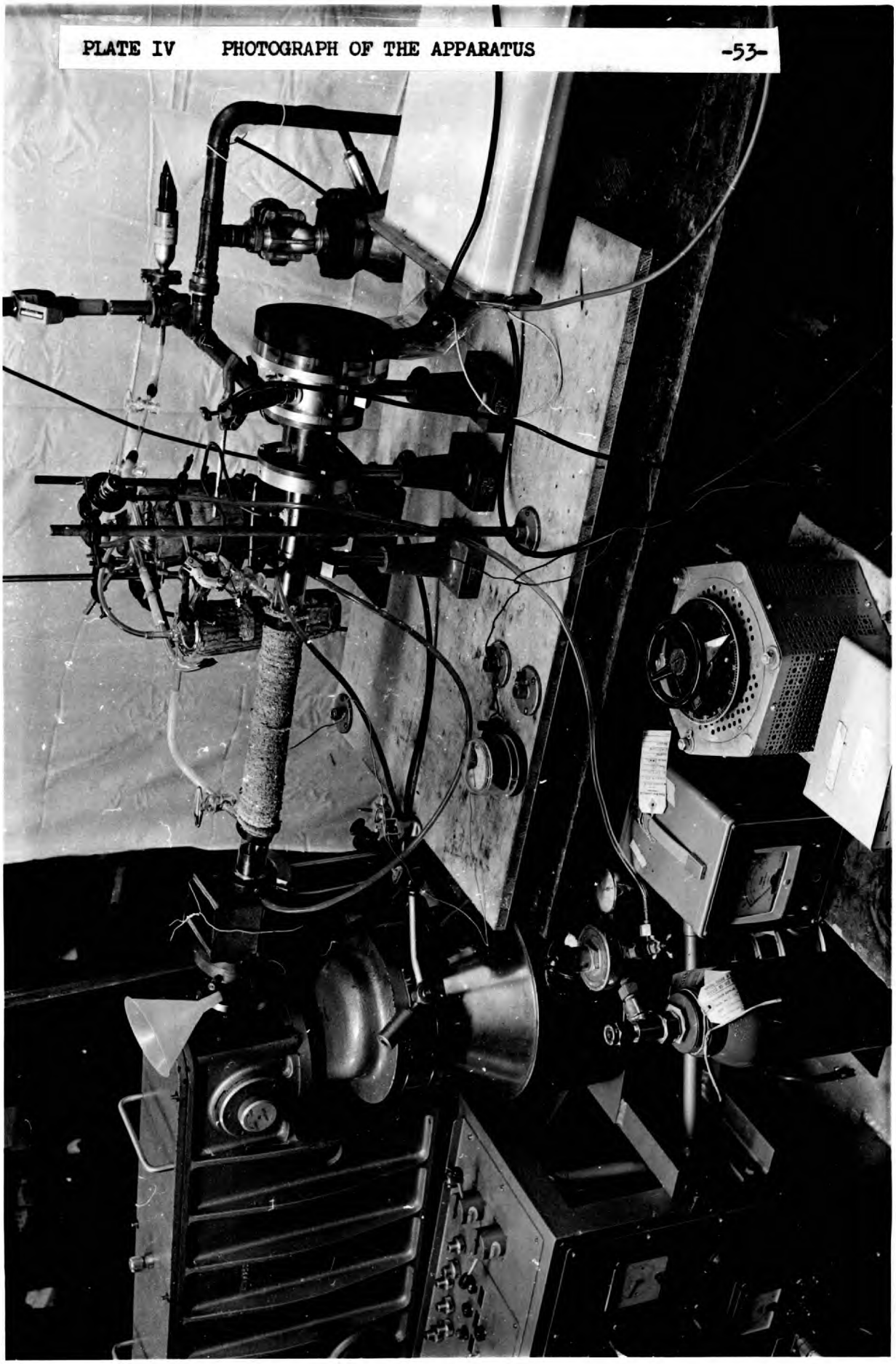

The temperature gradient was maintained firstly by water-cooling the stainless steel furnace end-pieces and then by surrounding the sets of baffles by closely packed solid CO_2. The baffles were made of copper to ensure rapid radial conduction of heat from the vapour and they were held in a stainless steel housing to prevent excessive conduction of heat from the end-piece 'O' ring seals which might otherwise have frozen.

It was expected, however, that, even with these precautions of baffling and a temperature gradient, there was a danger that a monatomic beam of metal atoms travelling along the light path would reach the source and the spectrograph. This was because, at the residual gas pressures of 10^{-4}mm. Hg employed, the mean free path of metal atoms was typically 50cm, greater than the path to the source or spectrograph. It was considered, therefore, that the minimum tolerable pressure of He, about 30microns Hg, should be maintained to reduce the mean free path to a few mm. This He was injected in the middle of the set of baffles by the source (see Plate III). It transpired, however, that the containment system was considerably more effective than had been expected and the helium was not used for metal vapour pressures up to 5 mm. Hg, without ill effect.

The water-cooled end-pieces had been given a conical shape for the mercury experiments so that the condensed mercury would run back towards the furnace and not block the light path. In fact clogging was not a problem but it seemed that the conical shape might have produced a pumping action, thus explaining the surprising efficiency of the system.

The furthest obvious penetration of metal vapour was to the third copper baffles, though, on one occasion at a very high mercury pressure, some vapour did condense in the source when the baffles were not adequately

cooled. No damage was done that could not be remedied by cleaning.

One final experimental development proved necessary in the containment system. In the first experiments with mercury, at temperatures corresponding to tens of mm. Hg, no absorption could be detected although the sample was obviously evaporating fast and condensing rapidly at the end-pieces. It was thought that, although the mercury was being evaporated at high pressures, it was clinging to the walls of the furnace on its journey to the end-pieces and was not reaching the light path, the furnace axis, at all. To remedy this a $\frac{1}{4}$in. aperture stainless steel baffle was placed inside the furnace, at either end of the wire-heated pyrex, to inhibit the movement of vapour along the walls. The effect was dramatic; strong mercury absorption, that of the inner 5 d shell, was immediately seen. A further sophistication of this technique was to add up to 3 further thin copper baffles of varying aperture at either end, inside the wire-heated portion of the furnace. A dramatic example of the effectiveness of such a system was an experiment in which a one gram sample of Rb was used to maintain rubidium vapour at 5mm. Hg pressure for 2 hours while 2 exposures were made.

The furnace was initially pumped through the two arms illustrated in Plate III, as pumping through the baffles and spectrograph slit was a long and inefficient process. The connection from the source pump to the arms was then closed and the arms were used as points at which the residual gas pressure could be monitored during an exposure, by a Pirani gauge through a liquid nitrogen cold trap.

The experimental procedure was as follows:-

1) Once aligned the whole apparatus was thoroughly evacuated. The furnace was then brought to a high temperature for outgassing, and then all allowed to cool.

2) The furnace and source were brought to atmospheric pressure by the injection of He. The element under study was then quickly introduced at the centre of the furnace. For Rb, K and Na, which reacted with air, this was done with He streaming through the furnace arms. The samples of Rb and K were in argon filled capsules whose seals were broken in the He stream from the furnace.

3) The furnace and source were immediately pumped down again to a high vacuum, with a glass window at the end of the source where the anode was usually inserted.

4) To check alignment a light was shone through this window and through all the baffles to the slit of the spectrograph. When the grating was rotated slightly, the zero order could be seen through the window of the spectrograph plate chamber when the alignment was good.

5) The source and spectrograph were again brought to atmospheric pressure by He injection and the window was replaced by the anode; the system was then brought back to high vacuum by at least an hour's pumping.

6) The connection from the pump to the furnace arms was then closed and the cold trap by the furnace pirani gauge was filled with liquid nitrogen. The boxes around the baffle housings were packed with CO_2.

7) The furnace was heated on a temperature curve leading to a slightly higher temperature than that selected. After about 20 or 30 mins the metal would begin to condense at the ends. The furnace current would then be put to the required setting and the exposure begun.

8) The exposure could last as long as there was evidence that the sample was still being evaporated. This could be verified by observation of the pyrex or quartz at the ends of the furnace. At first a silver film of the

condensed metal could be seen there and, as long as evaporation was still in progress, coalescing drops of the molten metal could be seen.

CHAPTER III THE INERT GASES

3.1 Results

3.1.1 Excitation of a subshell s electron

The absorption spectra of Ne, Ar, Kr and Xe in the region 270-1040Å were photographed by attaching the BRV source directly to the normal incidence spectrograph slit and passing these respective gases slowly through the housing of the spectrograph. In each case the $^2P_{3/2}$ edge, the first ionization potential of the element, was seen with the Beutler-Fano lines converging onto the higher $^2P_{1/2}$ limit. Plates were taken at different pressures around one micron Hg, with a path length of 6 m, longer than Madden and Codling's path length which varied with wavelength but was nominally 70-100 cm.

Above the first ionization potential, in the region of high continuous absorption, the discrete features due to the excitation of a sub-shell s electron and the simultaneous excitation of two outer p electrons were seen, though, for neon with the normal incidence instrument, only the first 3 resonances were seen as they lay at the short wavelength limit of the spectrograph. The most dramatic features, the window resonances for Ar, Kr and Xe are illustrated in Plate V.

These resonance features were measured, using the standards described in 2.3.1. Altogether, with the normal incidence instrument, 3 features were measured for Ne, 45 for Ar, about 65 for Kr and about 68 for Xe. With the fainter 20% or so of these features there was some confusion as to whether or not they were definitely distinguishable from source features,

Autoionization Resonances in Ar, Kr and Xe

Excitation of sub shell s electron

3 metre Normal-Incidence

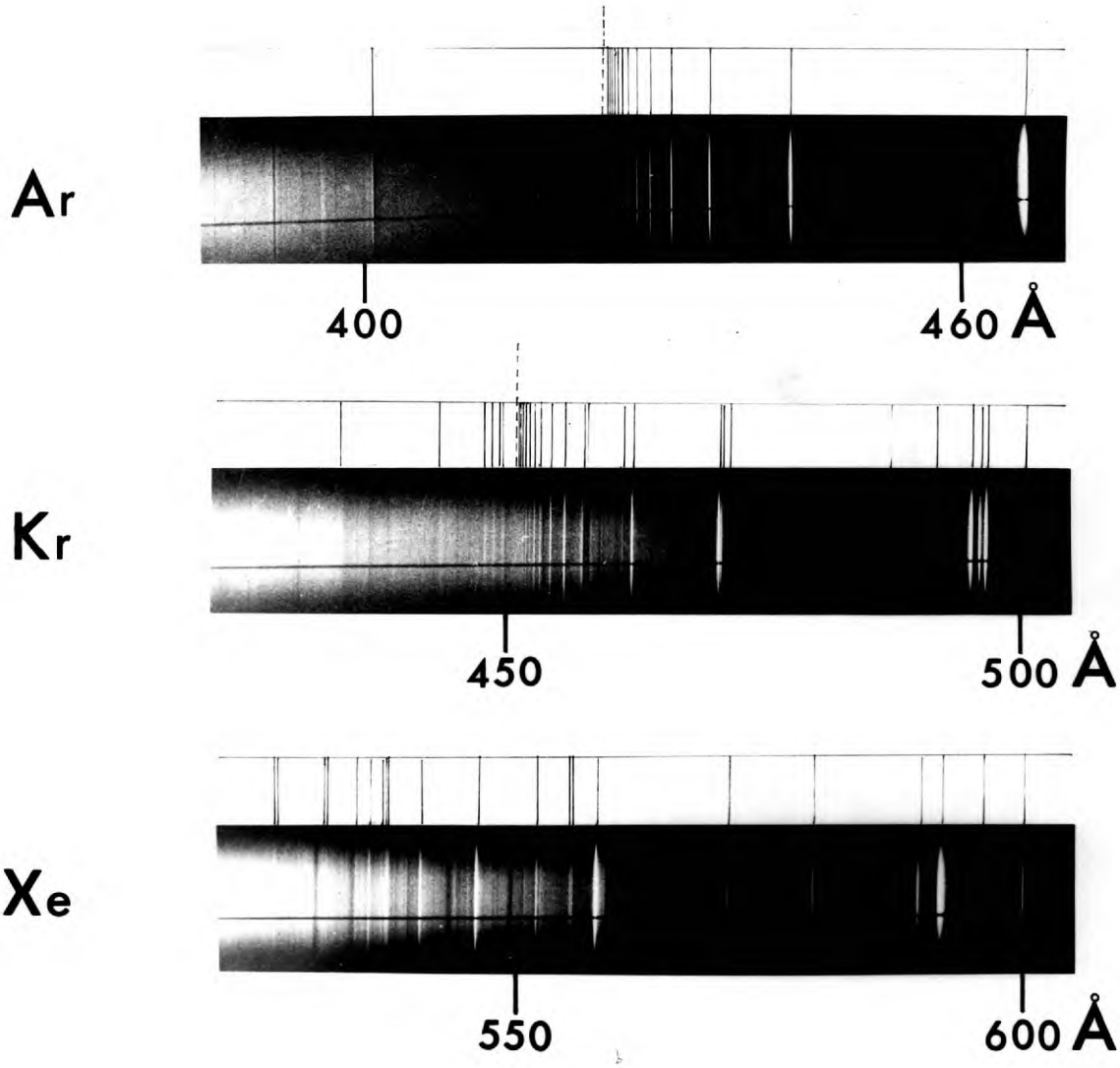

even after a detailed comparison with background features had been made.

These measured values were then compared with those of Madden and Codling (44) (45) and Samson (31) (34). The line lists for Madden and Codling's Kr and Xe resonances have not yet been published but the major features have been confirmed by private communication.

For argon the first 14 members of the $3s^2 3p^6\ {}^1S_o \rightarrow 3s3p^6np\ {}^1P_1$ series were measured. This compares with the 16 seen by MC (Madden and Codling) (45) and 8 seen by Samson (31). The measured wavelengths were in excellent agreement with MC's values, the maximum difference being 0.02Å. The Samson values showed differences of up to 0.15Å, but, as the quoted accuracy of Samson's Ar work was ±0.5Å, this is not surprising. The observation of 2 extra series members by MC may well have only been the difference between the SWR plates used by them and the Q2 plates used in the present experiments. However, for the weaker two-electron transitions at shorter wavelengths, MC's work was clearly superior. These resonances, due to the simultaneous excitation of two 3 p electrons, possessed a considerable variety of Fano profiles and it was very difficult to separate them from the background features which are particularly densely grouped below 450Å. The high level of continuous absorption also meant that these background features could not be "filled in" by a long exposure. MC, with a featureless background, measured 133 two-electron resonances; the present experiment revealed only 30 with any certainty. Agreement with MC was good for stronger features but there were differences of up to 0.1Å for the weaker features. In many cases it was clear that resonances measured by MC as asymmetric (measured where the rate of change of absorption cross section was greatest) were measured as absorption or transmission peaks in the present experiment.

For krypton the measurements for the $4s^2 4p^6\ {}^1S_0 \rightarrow 4s4p^6 np\ {}^1P_1$ transitions were all in agreement with those of Samson (34) and the values of the stronger transitions privately communicated by Codling. In fact the maximum difference between Samson's results and the present results was 0.06Å, considerably better than Samson's quoted accuracy of ±0.1Å. 14 members of the series were seen compared with 5 seen by Samson. From a study of MC's best photograph, it is expected that they will observe 16 or 17 members. The quantum defect for the series is steady except for the obviously perturbed 8 p electron (also seen by Samson) and for a slightly perturbed 11 p electron. The same remarks concerning two-electron transitions apply as those made for argon; MC's observations are again superior.

For xenon the measurements of the $5s^2 5p^6\ {}^1S_0 \rightarrow 5s5p^6 np\ {}^1P_1$ transitions did not agree with those of Samson (34) and MC as well as those for equivalent Ar and Kr transitions had done. The present results were in general below those of Samson in wavelength, the maximum difference being 0.14Å and agreement becoming better at short wavelengths. As Samson's accuracy is again ±0.1Å this difference is not too serious. The measurements for major features communicated by Codling were in satisfactory agreement (within 0.02Å) below 560Å, but became progressively less in agreement for longer wavelengths.

It is interesting that for both MC's experiments and the present experiments some difficulty with standards was expected above 560Å. MC had superimposed the absorption spectrum of helium to provide standards for measurement of the Kr and Xe lines. These measurements from 540 to 600Å leaned heavily on the He I line at 584.3340Å, and the fitting of a polynomial for a grazing incidence instrument in this way must mean that wavelengths

measured away from this standard must be subject to uncertainty, though it should be mentioned that the dispersion of their instrument was reliably described by a grating equation. For the present experiment the CII lines at 595.0219, 594.8000Å were the only standards used above 560Å. Due to the high level of continuous absorption around 600Å, these absorption standards were not seen with much contrast and greater error than is usual may have resulted. However, these two lines fitted well onto a linear fit through the other standards and, with the near linear dispersion of the normal incidence spectrograph, should be more satisfactory than MC's standards.

Due to a very strong perturbation near the limit of the xenon inner s shell transitions only the first 7 members (to 12 p) were recorded plus transitions that could be attributed to the 14 p and 17 p states. Samson (34) had measured the first 6 members though the quantum defect was much more regular for the present measurements. It is expected that the MC results will reveal little more of this series. Again the Madden and Codling Xe photographs indicate that their measurements of the two-electron resonanoes will be greatly superior to the present measurements.

The 3 neon resonances observed with the normal incidence spectrograph are in excellent agreement with MC's results (44). 6 Ne resonances were observed with the grazing incidence spectrograph as described in 3.1.3.

In general, the results for the inner s shell and nearby two-electron transitions are impressive and support the standards used from 350 to 550Å very satisfactorily. However it is obvious that they are surpassed on most accounts by MC's work and it is not considered worthwhile to analyse and tabulate them here. As there seems to be some doubt about the Xe measurements from 550 to 600Å, though, these measurements are tabulated as they may prove a useful supplement to MC's measurements.

TABLE XE I RESONANCES 550-600Å

Code	λ (Å)	ν (cm^{-1})	Appearance
XE1	599.81	166 720	Sharp window
XE2	595.83	167 833	Moderate window
XE3	591.67	169 013	Broad strong window
XE4	589.50	169 636	Strong window
XE5	586.24	170 579	Very weak window
XE6	582.72	171 607	Weak AS* (q negative)
XE7	581.07	172 098	Very weak window
XE8	579.94	172 431	Very weak window
XE9	579.15	172 665	Sharp window
XE10	570.80	175 192	Moderate window (AS q -ve?)
XE11	558.78	178 961	Moderate AS (q negative)
XE12	557.86	179 258	Strong window
XE13	555.53	180 009	Moderate window
XE14	555.32	180 075	Moderate window
XE15	552.32	181 055	Weak window
XE16	552.02	181 152	Sharp window
XE17	550.77	181 564	Moderate AS (q positive)

* AS = Asymmetric, measured where the rate of change of absorption cross section is greatest.

3.1.2 Excitation of subshell d electron

The inner d shell absorption spectra of Kr (115-150Å) and Xe (170-205Å) are illustrated in Plate VI. These are transitions of the type

d SUBSHELL EXCITATION IN KR AND XE

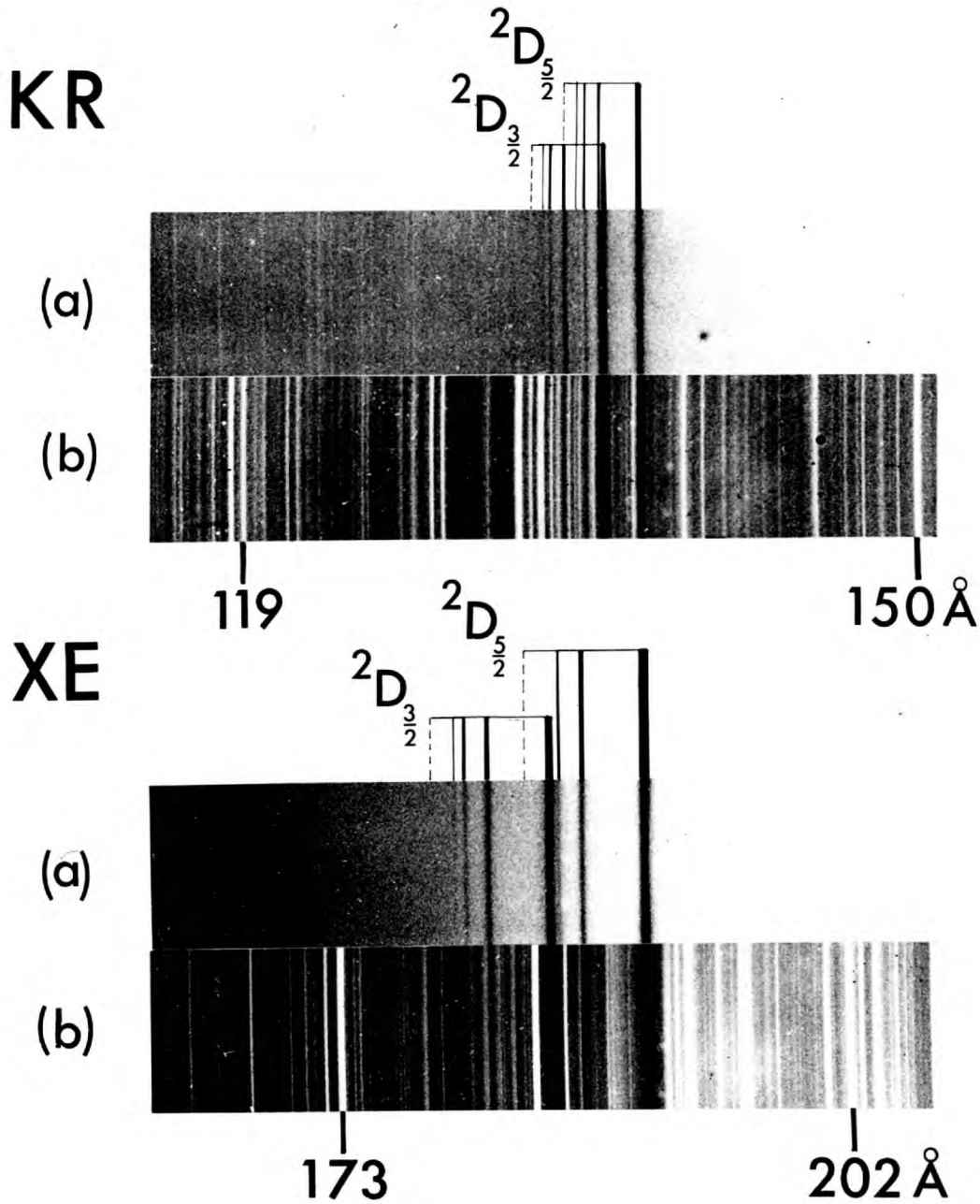

$(n-1)d^{10}ns^2np^6\ {}^1S_o \rightarrow (n-1)d^9ns^2np^6({}^2D_{3/2,5/2})\ mp\ {}^1P_1$. They were photographed with a pure BRV source (a) and also with the Flash Tube modified with an uranium anode along its axis (b), as described at the end of 2.2. The gases were passed slowly through the body of the grazing incidence spectrograph.

Although the spectra were seen clearly with the BRV source, they were difficult to measure due to the lack of standard emission lines on the plate. The measurements of these spectra were therefore made with the modified flash tube source, using the well known O and Al lines as standards.

In the spectra obtained with the BRV source, for Xe 7 absorption lines were seen, one less than MC had seen and, for Kr, 8 absorption lines were observed, the same number as in MC's experiments. With the flash tube the 7 Xe lines were measurable, but only 5 of the Kr lines were sufficiently distinguishable for measurement with this source. The measurements made were broadly in agreement with MC's (41), the maximum difference being 0.08Å, a not unreasonable value in these conditions where the true centres of absorption lines can be obscured by overlying emission lines.

The two-electron transitions, involving a subshell d and a valence p electron, observed by Madden and Codling (43) were not seen. They were probably too weak and easily confused with the ill-defined emission lines in this region. The weak subshell p transitions in Xe, $4p^64d^{10}5s^25p^6\ {}^1S_o \rightarrow 4p^54d^{10}5s^25p^6({}^2P_{3/2})\ ns\ {}^1P_1$, reported by MC (43), lay in a region of declining continuum (87Å) and were not seen either and, of course, the 2p shell excitation in Ar observed by Nakamura et al. (49) and the Ar, Kr and Xe discrete features in the 40-60Å region seen by Watson and Morgan (50) lay in a region of little or no continuum in the present experiment.

One further point of interest involving excitation from the d shell is worth mentioning here as it may be of relevance to the mercury spectrum reported in the next chapter. This phenomenom is the very broad absorption feature centering around 120Å in Xe. It manifests itself dramatically by removing completely all emission lines between 110 and 140Å in the flash tube spectrum. Ederer (33) has measured the magnitude of this cross section and found that the maximum of continuous absorption was shifted 2Ry from the $^2D_{5/2,3/2}$ limits for d shell excitation and was 10 times as large as the cross section at the $^2D_{3/2}$ edge. Furthermore the strength was distributed over a range of 4Ry, 10 times that expected for the hydrogen model.

Ederer's results were explained by Cooper (83) who attributed this delayed onset of continuous absorption to excitations to f states which were not seen as discrete levels below the limit. Cooper showed that the f-wave was excluded by the centrifugal barrier at these lower energies and thus the $d \rightarrow p$ transitions were dominant. However at higher energies the f-wave began to overlap the 4d wave function and thus the $d \rightarrow f$ possibility rises rapidly causing this broad maximum at 120Å.

3.1.3 Helium 2-electron transitions

Further experiments with the inert gases and the grazing incidence instrument were not as successful as the results of the previous section however. The helium 2-electron series (42) revealed only its first 5 members, even with helium pressures in the spectrograph high enough to turn these asymmetric resonances into apparent window features. Similarly the Ne subshell s series was only seen to the fifth member and the Ar s subshell

series to the eighth member (compared with the 14 members measured on the normal incidence spectrograph). Damany (60) in a similar experiment with helium and the Bellevue BRV source also only reports the first 5 members of the He series.

While the source features of the BRV source account for some of this lack of resolution, e.g. the He two-electron series gets lost in second order emission lines, it also seems evident that the grazing incidence spectrograph does not possess as good a resolution as MC's instrument in this region. MC used a longer path length, 70 to 100 cm., compared with 35-50 cm. in the present experiment, but it should have been possible to compensate for this by using higher pressures in the spectrograph.

Though it is true that as many members of subshell d series (3.1.2) were observed as had been observed by MC, this seems to have been more a matter of the breadth of absorption lines not decreasing so rapidly for high series members of series excited from low-lying shells. This is accounted for (84) as due to the increasing dominance of Auger transitions in determining the life times of high energy excited states. For less energetic transitions from shells just below the valence shell, the life time of a state is primarily determined by the autoionization of the excited electron. This life time will increase roughly with the cube of the effective quantum number and the length of a series will be determined eventually by instrumental resolution. The life time for an internal Auger transition, however, varies slowly with energy and can be regarded as constant for the span of a Rydberg series. Thus, for high energy transitions, while the lower members of the series may have life times determined by autoionization, the higher members, with the Auger effect dominant, will not decrease in breadth with increasing effective quantum number. The series will loose contrast

and will no longer be observable experimentally; thus instrumental resolution is not so important in determining the number of series members seen.

3.2 Comparison of the Electron synchotron and the BRV Source

Using the results of 3.1 it should now be possible to evaluate to some extent the relative usefulnesses of the BRV source and the electron synchotron as background continuum sources.

The obvious advantages of the BRV source are its small size and the ease with which it can be attached to an apparatus. It also has the advantages that it can be operated at higher pressures than the electron synchotron and is not too adversely affected when, for a short period, some of the element under study enters the source . While similar principles of metal vapour containment to those described in 2.4 could be developed for use with an electron synchotron, the precautions ensuring containment would need to be more rigorous.

The time exposures required for the BRV source were a little longer than those needed for the electron synchotron. However both types of source have been undergoing considerable modifications in the past year and exposure times should be cut by at least a factor of ten in both cases.

With regard to the quality of continuum produced, though, it seems that the electron synchotron has a clear advantage. Allowing for the different responses of the instruments used to record spectra, and, in some cases, for different photographic emulsions, it is clear that the source features of the BRV source can often cause confusion when weak asymmetric features are photographed. With the featureless steadily varying continuum of the electron synchotron there is no doubt whether or not features are

attributable to the element under study.

It is also true, though, that this difficulty, of confusion with BRV features, is at its worst for elements with high continuous absorption e.g. the inert gases and mercury. This continuous absorption also reduces the accuracy of the source standards which are no longer seen in good contrast to the continuum background. Furthermore the removal of continuous emission means that emission lines become more obvious above the background and thus "window" features of the element under study can become difficult to distinguish from the more noticeable emission lines in this case.

For elements with low continuous absorption cross sections, whose first ionization potentials lie at wavelengths a long way above the region of interest, 100-700Å, however, these difficulties are greatly reduced. In the case of these elements it is possible to fill in awkward source absorption features, leaving only the strong sharp standards. Furthermore the autoionization profiles for elements a long way above their first ionization potentials tend to be broadened, but still well-defined, absorption peaks. The alkali metals, studied in chapters V to VII are, of course, excellent examples of elements with low first ionization potentials and, below the limits of the inner p shell spectra studied in this thesis, there is little confusion with source features. Above the p shell limits, though, the onset of further continuous absorption does bring out the source features again with ensuing difficulties.

As far as accuracy of measurement with the respective sources is concerned, the source standards of the BRV source should be more reliable, at least in the region 400-700Å, as the use of superimposed He and Ne absorption standards in the case of the electron synchotron does leave some fairly

large gaps ill-served by standards. With improved intensity of illumination, however, it should be possible to insert, in front of either source, devices which would superimpose well-known emission standards without troublesome loss of illumination.

The electron synchotron has also been used for the absolute determination of continuous photoionization cross sections (42,45) by photometric recording techniques. Although a flash by flash record of the consistency of the intensity and energy distribution of the light from the BRV source has not been made, it does seem to have been very consistent for exposures of 25-30 flashes made under regular conditions. The BRV source should also be useful as a background for photometric work, therefore, when the technical difficulties of shielding the photoelectric recorder from interference by the discharge has been overcome. A further point that should be mentioned in favour of the electron synchotron though is that it produces polarised light and thus has an unique advantage when polarised light is required, e.g. in investigating the optical properties of solids. Also the angular confinement of the electron-synchotron radiation and the fact that the intensity and distribution of its radiation can be reliably calculated are important points in its favour.

In conclusion, therefore, while the electron synchotron will always have the advantage of being able to produce a purer continuum, it is expected that the BRV source should be competitive in many applications; in particular it is well-suited to the measurement of the absorption spectra of the alkali metals in this region.

CHAPTER IV MERCURY

4.1 Introduction and Experimental Details

The initial development of the containment system, as described in 2.4 was performed with mercury as this element is readily obtainable in relatively large quantities and is easily produced as a monatomic vapour.

Garton and Connerade (14), in repeating Beutler's experiments (6), had extensively studied the spectrum due to excitation from the 5d shell in Hg I, $5d^{10}6s^2\ {}^1S_0 \rightarrow 5d^9 6s^2 np$, nf (J=1). 50 transitions of this type, grouped in well-developed series, were found and these were all accounted for satisfactorily by the use of a $(J_c K)$ scheme (4.4.1). The higher of the two Hg II levels, $5d^9 6s^2\ {}^2D_{3/2,5/2}$, that serve as limits for this spectrum, the $5d^9 6s^2\ {}^2D_{3/2}$ level, lay at 742Å and no further features had been observed between this wavelength and the 600Å short wavelength limit of the He_2 continuum. It was hoped therefore that extension of the Hg I spectrum below 600Å would reveal excitation from the 5p shell and possibly two-electron transitions.

The temperatures required to study the Hg I spectrum over a large range of pressures were low and the pyrex furnace with a 12 in. heated path length was adequate for all Hg experiments. The containment system and experimental procedure described in 2.4 were used although, as mercury did not react strongly with air, it was not necessary to stream He through the furnace while the sample was inserted.

The sample was held in a trough, 5.3cm x 1.2cm x 1cm (deep), made of copper sheet and placed at the centre of the furnace. The surface of the copper in contact with the hot mercury formed an amalgam, but this effect

was minor and the more rapid heating of the sample that could be achieved in a copper container was felt to be a more important consideration. A typical sample was 50 gms. of triply distilled Hg; this large quantity could easily sustain a 10mm Hg pressure for 2 hours and it was not necessary to attempt to recirculate the mercury condensed from the conical end pieces. The sample was usually preheated to drive off impurities.

A considerable experimental problem encountered in experiments with mercury at wavelengths below 742Å was that the heavy continuous absorption beyond the limit of the valence spectrum at 1188Å and beyond the d shell limits at 835Å and 742Å necessitated very long exposures in order that a reasonable light intensity should be obtained at the photographic plate. The problems of differentiating between source features and mercury features, discussed in 3.2, also became acute. Very long exposures were therefore employed - 650 flashes for the normal incidence spectrograph and 1000 flashes for the grazing incidence instrument, with the BRV source being used at its maximum repitition rate viz. one flash each 3 seconds. Even so it was necessary to resort to a broadening of the slit to 20μ for both instruments to ensure that resonances could be photographed in good contrast. This led to a detectable loss of resolution for both spectrographs.

The level of continuous absorption is indicated in Figure 2 for a temperature of about 230°C. Temperatures used varied from 180 to 250°C which should have entailed pressures of 8 to 100 mm. Hg. However, as well as the heating irregularities of the furnace, mentioned in 2.4, the pressure must also have depended very much on surface impurities, oxides etc. The optical thickness was also a function of the amount of internal furnace baffling used and, therefore, quotations of temperature, and of pressure from the standard

pressure versus temperature charts, are hardly meaningful in an absolute sense.

4.2 Appearance of the Spectrum (Plate VII)

At wavelengths above the $5d^9 6s^2\ ^2D_{3/2}$ limit the mercury spectrum is as described by Connerade (14). The absorption lines converging on the $5d^9 6s\ ^2D_{3/2, 5/2}$ limits are broadened but well defined at low pressures. With increasing pressure a region of reduced absorption (a "window") appears on the long wavelength side of each line until, at very high pressures, only the windows can be seen.

Between the $^2D_{3/2}$ limit, at 742Å, and about 525Å there is a large number of resonances with a great variety of intensities and Fano profiles (61,62); 2 series are just apparent. The continuous absorption is very heavy in this region.

From 525 to about 370Å, the lower limit of the normal incidence spectrograph in this case, there are no further resonances but the level of continuous absorption remains very high.

The region 370-90Å was studied with the grazing incidence spectrograph. The continuous absorption remained high but dropped to some extent below 200Å. No resonances were observed in this region but the experimental difficulties resulting from the high level of absorption meant that a rigorous examination of the region could not be made.

4.3 Results For Mercury

TABLE I Hg II level notation used in analysis.

Hg I ABSORPTION SPECTRUM

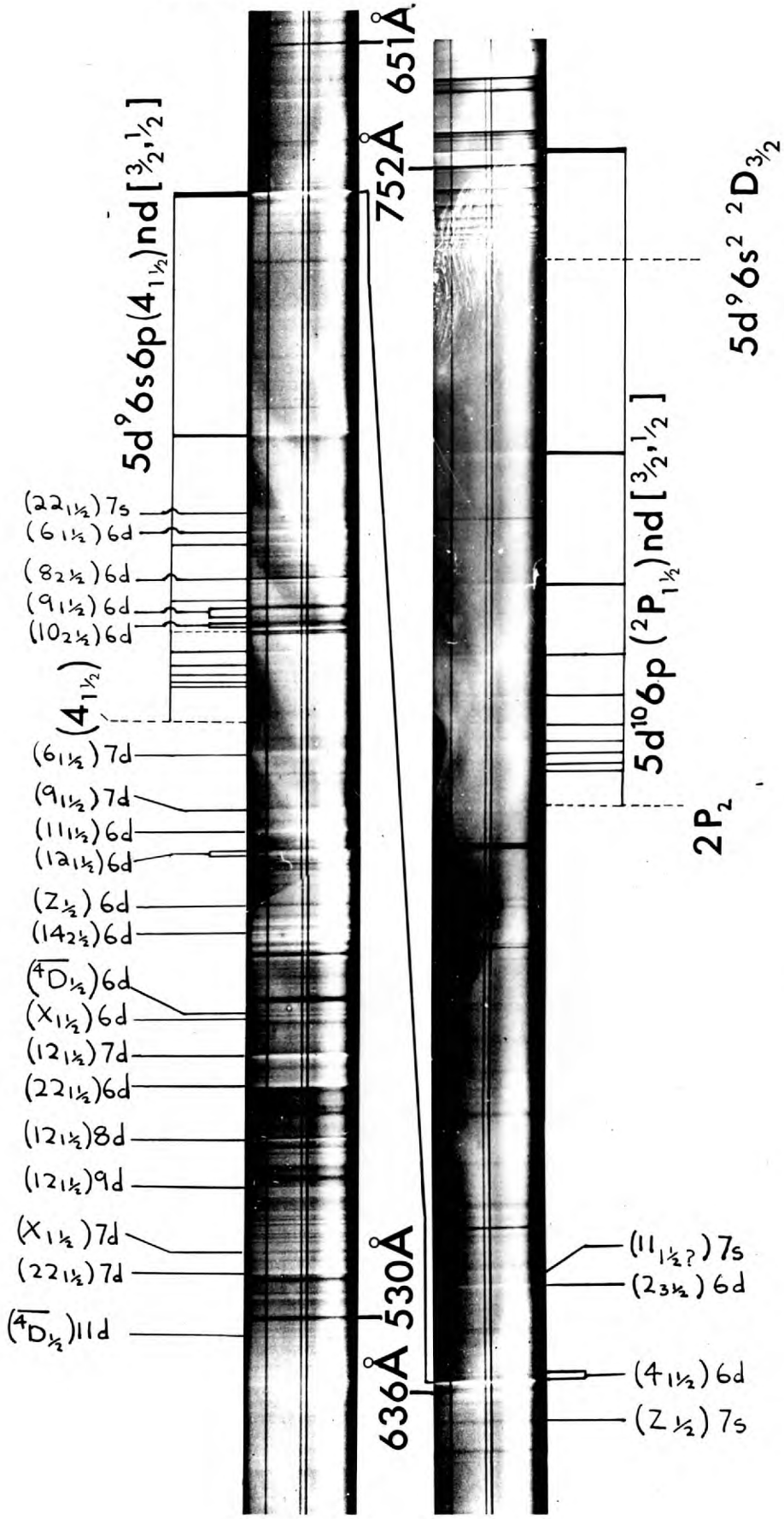

Notation (Atomic Energy Levels Vol.III)	Configuration	Energy (cm^{-1}) from Hg I ground state	J
$2P_1$	$5d^{10}6p\ (^2P_{1/2})$	135 669	$\frac{1}{2}$
$2P_2$	$5d^{10}6p\ (^2P_{3/2})$	144 792	$1\frac{1}{2}$
2S	$5d^{10}7s\ (^2S_{1/2})$	179 898	$\frac{1}{2}$
$3D_2$	$5d^{10}6d\ (^2D_{3/2})$	189 167	$1\frac{1}{2}$
$3D_3$	$5d^{10}6d\ (^2D_{5/2})$	189 727	$2\frac{1}{2}$
$^2D_{5/2}$	$5d^9 6s^2\ (^2D_{5/2})$	119 698	$2\frac{1}{2}$
$^2D_{3/2}$	$5d^9 6s^2\ (^2D_{3/2})$	134 736	$1\frac{1}{2}$
$1_{2\frac{1}{2}}$	$5d^9{}_{2\frac{1}{2}}\ 6s_{\frac{1}{2}}\ 6p_{\frac{1}{2}}$	163 888	$2\frac{1}{2}$
$2_{3\frac{1}{2}}$	"	168 393	$3\frac{1}{2}$
$3_{2\frac{1}{2}}$	"	169 018	$2\frac{1}{2}$
$4_{1\frac{1}{2}}$	"	170 361	$1\frac{1}{2}$
$5_{4\frac{1}{2}}$	$5d^9{}_{2\frac{1}{2}}\ 6s_{\frac{1}{2}}\ 6p_{1\frac{1}{2}}$	176 750?	$4\frac{1}{2}$
$6_{1\frac{1}{2}}$	"	178 275	$1\frac{1}{2}$
$7_{3\frac{1}{2}}$	"	179 170	$3\frac{1}{2}$
$8_{2\frac{1}{2}}$	"	179 486	$2\frac{1}{2}$
$9_{\frac{1}{2}}$	"	180 369	$1\frac{1}{2}$
$10_{2\frac{1}{2}}$	"	181 178	$2\frac{1}{2}$
11	$5d^9{}_{1\frac{1}{2}}\ 6s_{\frac{1}{2}}\ 6p_{\frac{1}{2}}$?	185 043	$1\frac{1}{2}$?
$12_{1\frac{1}{2}}$	"	187 367	$1\frac{1}{2}$
Z	"	188 054	$\frac{1}{2}$

Notation (Atomic Energy Levels Vol.III)	Configuration	Energy (cm^{-1}) from Hg I ground state	J
14	$5d^9 1\frac{1}{2}\ 6s_{\frac{1}{2}}\ 6p_{\frac{1}{2}}$?	188 220	$2\frac{1}{2}$?
U	$5d^9 1\frac{1}{2}\ 6s_{\frac{1}{2}}\ 6p_{1\frac{1}{2}}$	190 477	$\frac{1}{2}$
$\overline{{}^4D_{\frac{1}{2}}}$	"	190 796	$\frac{1}{2}$
X	$5d^9 1\frac{1}{2}\ 6s_{\frac{1}{2}}\ 6p_{1\frac{1}{2}}$	193 373	$1\frac{1}{2}$
$22_{1\frac{1}{2}}$	"	194 787	$1\frac{1}{2}$
$23_{3\frac{1}{2}}$	"	195 356	$3\frac{1}{2}$
$16_{3\frac{1}{2}}$	Unclassified	190 397	$3\frac{1}{2}$

The levels labelled ${}^2D_{5/2,3/2}$, 2P, 2S, 3D, Z, U, X, $\overline{{}^4D}$ are from Paschen (85).

The levels labelled by numerals are from McLennan et al. (86).

4.3.1 Inner d shell excitation

The transitions listed by Connerade (14), $5d^{10}6s^2 \rightarrow 5d^9 6s^2\ ({}^2D_{5/2,3/2})$ np, nf, are all confirmed by the present experiment but there are discrepancies that do not fall within the respective error estimates. In general the results of the present experiments, taken from 2 photographs at low and medium/low pressure, give wavelengths consistently above those of Connerade. For series converging on both the ${}^2D_{5/2,3/2}$ limits the discrepancy is greatest for lower members, the maximum difference being about 0.07Å. This difference could be due to the different sets of standards used, in which case Connerade's results are certainly more reliable in view of the large gaps between standards at wavelengths above 700Å (2.3.3) in the present experiment.

The reason for these discrepancies, however, could well lie in the asymmetric profiles of these lines. At low pressures the lines appear as reasonably sharp absorption peaks, the window accompanying each resonance to the long wavelength side not showing above the background continuum, which is hardly diminished by continuous absorption beyond the Hg I 1st ionization potential at these very low pressures. At very high pressures only the windows are seen but at moderate pressures the asymmetry is seen more as a broadening of the absorption lines to their short wavelength sides. It is known that Connerade's measurements were the mean of measurements at several pressures and the fact that new splittings were observed in the present experiments indicates that the 2 plates used for the present measurements were taken at lower pressures than Connerade's.

Thus Connerade's measurements at higher pressures would tend to measure an absorption centre at a shorter wavelength. This effect was noticed in the measurements made at 2 different pressures in the present experiments and the fact that the difference in measurements became progressively smaller for high series members also supports this explanation of the discrepancies.

The measurements of the present experiments yield a steadier course of quantum defects along the series, though the variation recorded by Connerade is quite reasonable for a p series.

Listed below are the splittings in the first two members of the $5d^{10}6s^2 \rightarrow 5d^9 6s^2\ (^2D_{5/2})\ nf\ [3/2,\ 1/2]_1$ series and the extensions made to Connerade's series in the present experiment. Connerade measured the splitting of the first member, 5f, of the $(^2D_{5/2})\ nf\ [3/2,\ 1/2]_1$ series but there was some suspicion that this apparent splitting might merely be the result of the superposition of an emission line. The significance of this

splitting and the meaning of the letter notation used for the np series is explained in 4.4.1.

(i) $(^2D_{5/2})$ np $[^3/2]_1$ series extension

λ (Å)	ν (cm^{-1})	n*	n
837.588	119 390	18.88	23
837.361	119 423	19.98	24
837.176	119 449	20.99	25

(ii) $(^2D_{3/2})$ np 1 b series extension

λ (Å)	ν (cm^{-1})	n*	n
744.573	134 305	15.96	20
744.306	134 353	16.97	21
744.066	134 397	17.99	22
743.858	134 434	19.06	23
743.698	134 463	20.05	24
743.570	134 486	20.95	25

(iii) $(^2D_{5/2})$ nf $[^3/2, {}^1/2]_1$ splittings and series extension

λ (Å)	ν (cm^{-1})	n*	n
887.301	112 701	3.960	5
887.127	112 723	3.966	
867.852	115 227	4.962	6
867.723	115 244	4.964	
	. . . . .	. . . . .	
840.827	118 930	11.95	13

(iv) $(^2D_{3/2})$ nf $[^3/2]_1$ series extension

λ (Å)	ν (cm^{-1})	n*	n
746.543	133 951	11.82	13

(v) $(^2D_{3/2})$ np 1c series extension

λ (Å)	ν (cm^{-1})	n*	n
755.368	132 385	6.832	11
752.070	132 966	7.87	12
749.960	133 340	8.87	13

4.3.2 Two-Electron Series (Plate VII)

(i) $5d^{10}6s^2\ ^1S_0 \rightarrow 5d^{10}6p\ (^2P_{3/2})$ nd $[^3/2, ^1/2]_1$

λ (Å)	ν (cm^{-1})	n*	n
753.705 ±0.02	132 678	3.010	6
724.78 ±0.05	137 972	4.012	7
712.23 "	140 405	5.00	8
705.51 "	141 742	6.00	9
701.46 "	142 560	7.01	10
699.20 ±0.08	143 020	7.87	11
697.11 "	143 448	9.04	12
695.94 "	143 691	9.98	13
694.91 "	143 905	11.12	14
694.21 "	144 049	12.15	15

This series is asymmetric with q negative (q, the profile index is as described in 1.4). The first member is quite strong and well-defined but all

the other members are weak and diffuse. The error of measurement on these latter members is thus quite large.

The n=6 line can be seen on Connerade's photograph of the spectrum but he does not record it; presumably he was not sure whether or not it was a mercury feature.

(ii) $5d^{10}6s^2\ {}^1S_0 \rightarrow 5d^9 6s\ 6p\ (4_{1\frac{1}{2}})\ nd\ [{}^3/2,\ {}^1/2]_1$

λ (Å)	ν (cm⁻¹)	n*	n	Appearance
636.916 ±0.02	157 007	2.867	6	Very strong window
613.706 ±0.03	162 945	3.871	7	Diffuse AS (q + ve)
603.469	165 709	4.857	8	AS (q - ve)
597.918	167 247	6.03	9	Weak AS (q - ve)
	. . . . .	. . . . .		
593.053 ±0.02	168 619	7.94	11	AS (q - ve)
591.81 ±0.03	168 974	8.89	12	Weak AS (q -ve)
590.87	169 245	9.92	13	"
590.05 ±0.07	169 478	11.15	14	Very weak AS (q - ve)
589.59	169 608	12.07	15	"

AS denotes asymmetric."-ve"denotes negative.

The first 2 members are strong with different profiles; a reason for this is suggested in the analysis (4.4.2.2). The members n= 8, 9, 10 lie in a region with many other resonances, then the n= 11 to 15 members can be seen beyond this region. The error on higher members is quite large.

The n=6 window is the strongest feature in the two-electron spectrum. It lies above 600Å and therefore it is surprising that Connerade did not see it. Its resemblance to an emission line may have caused Connerade to mistake it for one of the impurity emission lines superimposed on the He_2 continuum.

4.3.3 Other Two-Electron Features

It was concluded previously (3.2) that the BRV source is not well-suited for elements of high continuous absorption cross section because of the likely confusion of the spectrum of the element with the background features. This difficulty arises with mercury and therefore 2 tables are given. The first comprises features that are reasonably distinct from the background and on which there are no source features superimposed to cause confusion. All Hg wavelengths have been checked against the wavelengths measured for source features from photographs of the background alone (2.3.1). The second table comprises features for which there is some confusion, by reason either of their weakness or the proximity of source features. These lines in Table (ii) are believed to be due to Hg I but there is some doubt.

(i) Other mercury two-electron features with tentative assignments

Code	λ (Å)	ν (cm^{-1})	Assignment	n*	Appearance
HG 12	777.670	128 589	$(2P_1)$ 7d	3.937	Sharp A
HG 31	647.217	154 508	$(11_{1\frac{1}{2}?})$ 7s	1.896	Weak W
HG 32	645.926	154 817	$(2_{3\frac{1}{2}})$ 6d	2.843	W
HG 32B	640.007	156 248	$(3_{2\frac{1}{2}})$ 6d	2.931	Weak W
HG 33	637.629	156 831	$(4_{1\frac{1}{2}})$ 6d	2.848	"
HG 35	633.137	157 007	$(Z_{\frac{1}{2}})$ 7s	1.909	Diffuse A
HG 38	610.754	163 732	$(2_{3\frac{1}{2}})$ 8d	4.852	Weak W
HG 39	606.326	164 928	$(22_{1\frac{1}{2}})$ 7s	1.917	Diffuse W
HG 40	605.249	165 221	$(2_{3\frac{1}{2}})$ 9d	5.882	W
HG 41	604.552	165 412	$(6_{1\frac{1}{2}})$ 6d	2.921	"
HG 42A	602.399	166 003	$(2_{3\frac{1}{2}})$ 10d	6.770	Weak W
HG 43	602.174	166 065	(2S) 7p	2.817	A

Code	λ (Å)	ν (cm^{-1})	Assignment		n*	Appearance
HG 44A	601.306	166 305	$(7_{3\frac{1}{2}})$	6d	2.921	Broad weak A
HG 44B	600.087	166 642	$(8_{2\frac{1}{2}})$	6d	2.923	Strong sharp A
HG 46	597.308	167 418	$(9_{1\frac{1}{2}})$	6d	2.911	Strong broad A
HG 47	596.382	167 678	$(9_{1\frac{1}{2}})$	6d	2.941	Quite weak A
HG 48	595.783	167 846	$(10_{2\frac{1}{2}})$	6d	2.869	Strong A
HG 49	595.462	167 937	$(10_{2\frac{1}{2}})$	6d	2.890	"
HG 55	583.573	171 358	$(6_{1\frac{1}{2}})$	7d	3.983	Broad diffuse W
HG 56	581.491	171 972	$(8_{2\frac{1}{2}})$	7d	3.822	A
HG 57	578.344	172 908	$(9_{1\frac{1}{2}})$	7d	3.831	Diffuse A (AS)
HG 59	576.098	173 582	$(11_{1\frac{1}{2}?})$	6d	3.094	Quite strong W
HG 61	574.261	174 137	$(12_{1\frac{1}{2}})$	6d	3.948	Quite strong W (AS)
HG 62	573.902	174 246	$(12_{1\frac{1}{2}})$	6d	3.978	" " "
HG 64	572.950	174 535	$(10_{2\frac{1}{2}})$	7d	4.064	Quite strong A
HG 66	572.141	174 782	(2S)	9p	4.631	Diffuse W
HG 68	569.207	175 683	$(Z_{\frac{1}{2}})$	6d	2.978	Quite strong A
HG 70	567.862	176 099	$(7_{3\frac{1}{2}})$	9d	5.978	W
HG 71	567.397	176 243	$(14_{2\frac{1}{2}})$	6d	3.027	W (AS)
HG 72	566.641	176 479	$(6_{1\frac{1}{2}})$	11d	7.82	AS (q + v e)
HG 73	565.988	176 682	$(16_{3\frac{1}{2}})$	6d	2.829	W
HG 73A	565.384	176 871	$(10_{2\frac{1}{2}})$	8d	5.048	Broad diffuse AS(q-ve)
HG 73C	564.298	177 211	$(8_{2\frac{1}{2}})$	10d	6.95	Broad diffuse W
HG 76	561.621	178 056	$(11_{1\frac{1}{2}?})$	7d	3.963	Weak W
HG 77	559.038	178 879	$(\overline{^4D}_{\frac{1}{2}})$	6d	3.035	W
HG 78	558.636	179 008	$(X_{1\frac{1}{2}})$	6d	2.764	"
HG 79	556.406	179 725	$(10_{2\frac{1}{2}})$	12d	8.69	"
HG 80	555.192	180 129	$(12_{1\frac{1}{2}})$	7d	3.894	Very strong AS (q-ve)

Code	λ (Å)	ν (cm^{-1})	Assignment	n*	Appearance
HG 81	552.037	181 147	$(22_{1\frac{1}{2}})$ 6d	2.836	Very Strong AS (q+ve)
HG 81A	551.577	181 298	$(Z_{\frac{1}{2}})$ 7d	4.030	A
HG 82	550.709	181 584	$(3D_2)$ 8p	3.804	Weak A
HG 83	550.048	181 802	$(23_{3\frac{1}{2}})$ 6d	2.845	Diffuse A
HG 84	547.131	182 772	$(12_{1\frac{1}{2}})$ 8d	4.892	Strong AS (q - ve)
HG 86	545.591	183 287	$(U_{\frac{1}{2}})$ 7d	3.907	A (AS)
HG 87	545.254	183 400	$(U_{\frac{1}{2}})$ 7d	3.852	Weak A
HG 87A	544.543	183 640	$(\overline{^4D_{\frac{1}{2}}})$ 7d	3.916	Broad weak AS (q +ve)
HG 89	542.540	184 318	$(12_{1\frac{1}{2}})$ 9d	3.999	W
HG 90	541.686	184 609	$(3D_2)$ 9p	4.907	Weak Edge
HG 91	540.447	185 032	$(Z_{\frac{1}{2}})$ 9d	6.026	A
HG 93	537.499	186 047	$(U_{\frac{1}{2}})$ 8d	4.977	A
HG 94	536.515	186 388	$(X_{1\frac{1}{2}})$ 7d	3.968	A
HG 95	534.462	187 104	$(22_{1\frac{1}{2}})$ 7d	3.779	AS (q + ve)
HG 96	532.188	187 903	$(23_{3\frac{1}{2}})$ 7d	3.837	Broad weak W
HG 97	529.896	188 716	$(U_{\frac{1}{2}})$ 11d	7.89	Weak W
HG 98	529.554	188 838	$(X_{1\frac{1}{2}})$ 8d	4.919	Weak W
HG 99	528.762	189 121	$(\overline{^4D_{\frac{1}{2}}})$ 11d	8.09	W

A = Absorption. W = Window. AS = Asymmetric (measured where the rate of change of cross section is greatest). "Appearance" describes where a measurement was made on a line. When there is a suspicion that the actual profile is different, this profile is indicated in brackets.

(ii) Possible Mercury two-electron features with tentative assignments

Code	λ (Å)	ν (cm^{-1})	Assignment	n*	Appearance
HG 6	863.203	115 848	$(2P_2)$ 7s	1.947	Weak AS (q - ve)
HG 7	862.009	116 008			Weak A
HG 9	812.741	123 040	$(2P_1)$ 6d	2.948	Weak A
HG 14	771.739	129 577			Weak A
HG 16	762.577	131 134	$(2P_1)$ 8d	4.919	A
HG 19	730.337	136 923	$(2P_2)$	3.73	Very Weak A
HG 21	715.55	139 752	$(2P_2)$	4.67	Very Weak A
HG 23	707.47	141 349	$(2P_2)$	5.65	Extremely Weak A
HG 25	702.87	142 275	$(2P_2)$	6.60	Extremely Weak A
HG 32A	641.280	155 938	$(3_{2\frac{1}{2}})$ 6d	2.897	Very Weak A
HG 36	614.337	162 777	$(4_{1\frac{1}{2}})$ 7d	3.804	Weak A
LIMIT	587.14	170 318	$(4_{1\frac{1}{2}})$ Limit		Weak feature
HG 54	584.845	170 985	$(6_{1\frac{1}{2}})$ 7d	3.880	Weak diffuse A
HG 60	574.871	173 952	$(6_{1\frac{1}{2}})$ 8d	5.038	Weak AS (q - ve)
HG 63	573.312	174 425	$(7_{3\frac{1}{2}})$ 8d	4.861	Weak A
HG 65	572.412	174 699	$(8_{2\frac{1}{2}})$ 8d	4.788	Weak A
HG 67	571.054	175 115	$(3D_2)$ 7p	2.792	A
HG 69	568.399	175 933	$(9_{1\frac{1}{2}})$ 8d	4.974	Weak AS (q +ve)
HG 74A	563.615	177 426	$(7_{3\frac{1}{2}})$ 11d	7.93	Weak A
HG 75	563.238	177 545			Weak A
HG 75A	562.841	177 670			Very Weak A
HG 80A	553.837	180 559	$(X_{1\frac{1}{2}})$ 6d	2.926	Diffuse A
HG 85A	546.185	183 088			AS (q - ve)

Some of these features, in particular HG 19, 21, 23 and 25, are

extremely weak and little significance should be attached to them. Normally HG 19, 21, 23 and 25 would be disregarded completely but they are included in this case because of the regular course of their quantum defects to the $2P_2$ limit and because the line HG 12 would make a plausible first member for such a series ($n^* = 2.602$ to the $2P_2$ limit).

4.4. Analysis

4.4.1 Inner d Shell Excitation

The notation used for the analysis of the extensions to the $5d^{10}6s^2\ {}^1S_0 \rightarrow 5d^9_K(\overset{6s^2}{{}^2D_{5/2,3/2}})$ np, nf series is exactly the same as that used by Connerade (14) for these configurations.

In his scheme Connerade found that (J_cK) coupling held very well for the d^9s^2nf configuration. He considered that this was probably due to screening by the s^2 shell, which reduced electrostatic interactions between the nf electron and the core, thus satisfying a condition of the (J_cK) model in which the electrostatic coupling is weak compared with the spin orbit coupling of the core but strong compared with the spin coupling of the outer electron (64).

As was expected, in view of the greater penetration of the core by np electrons, Connerade found (J_cK) coupling less appropriate to the d^9s^2 np configuration. He therefore used the letter notation of Condon and Shortley (88) for these series.

The (J_cK) scheme for adding nf electrons to the ${}^2D_{5/2}$ limit leads to the expectation of 2 series, with $K = 3/2,\ 1/2$, that should yield a final $J = 1$. Only one series is apparent but Connerade calculated that the 2 series should lie very close together (87). He detected a splitting in the first 5f member

but was not altogether sure that this was not an effect of an overlying emission line. Thus the observation of a clear splitting in both the 5f and 6f levels in the present experiment is an important verification of Connerade's scheme.

4.4.2 Two-Electron Excitation

Above the higher limit for excitation of a single 5d shell electron, the next one electron excitation expected energetically is excitation of a sub shell 5p electron. Such a transition has not been observed in optical spectroscopy but a rough estimate of its position may be made from characteristic X-ray spectra. The lowest energy required to remove a 5p electron is the energy of the O_3 edge. This is given (89) as 57.6eV which corresponds to 215Å. The difference between this value for a solid (amalgam for Hg) and a gas should not be more than 1 Ryd i.e. 50Å in this case. Thus the discrete structure between 742 and 525Å cannot be accounted for by 5p excitation.

The only other possibility energetically for resonances in this region is multiple electron excitation. Excitation of 3 or more electrons simultaneously would be expected to be as weak in relation to two-electron transitions as two-electron transitions are in relation to single electron transitions. They would also for the most part take place at higher energies than the region under consideration and have thus been disregarded in this analysis.

Only the possibility of two-electron excitations remains. These can broadly be divided into 2 types, simultaneous excitation of the 2 valence 6s electrons and simultaneous excitation of 5d and 6s electrons.

4.4.2.1 Simultaneous Excitation of Two Valence Electrons

Possible excitation scheme involving the 6s electrons are

$5d^{10}6s^2 \rightarrow 5d^{10}6p$ ns, nd

$\rightarrow 5d^{10}6d$ np, nf

$\rightarrow 5d^{10}7s$ np

$\rightarrow 5d^{10}5f$ nd

and then $\rightarrow 5d^{10}7p$ ns, nd etc.

Excitation to the states $5d^{10}7s$ nf, $5d^{10}5f$ ns are excluded by the ΔJ selection rule which necessitates a final J = 1 for transitions from the $^1S_0$ ground state of Hg I.

A generalised $(J_c K)$ notation, with J_c referring to the entended core $5d^{10}6p$ etc. has been adopted as most convenient for these transitions. However, as there is no longer a $6s^2$ screening shell and as the ns, np and nd electrons penetrate further into the core than the nf electrons, the $(J_c K)$ model will not be rigorously applicable.

(i) $5d^{10}6p$ ns, nd

These resonances, converging on the $5d^{10}6p$ $(2P_1, 2P_2)$ levels of Hg II would be expected to possess the lowest energies for two-electron transitions. One ns and one nd series can be built on the lower energy $J = \frac{1}{2}$ limit, and one ns and two nd series can be built on the $J = 3/2$ limit.

One series (4.3.2 Table (ii)) does converge on the $2P_2$ limit. In the normal spectrum of Hg I the effective quantum numbers, n* , for the ns and (n-2) d electrons lie quite close together and are also quite close to the n* for the series to the $^2P_2$ limit. The ns series in the normal spectrum, however, starts with a n* of 2.2 (for 7s) whereas the nd series starts with n* $\sim$ 2.9 (6d), so, as the first strong member of the series to the $2P_2$ limit

has $n^* = 3.01$, the series has been classified as a nd series. There is also a weak feature (HG 6) with a n^* of 1.95 referred to the $2P_2$ limit and there is a possibility of ns, nd interactions throughout the series. 2 series of nd features with, $K = \frac{1}{2}, {}^3/2$, are possible to the $2P_2$ limit, and it is difficult to determine which the observed series is attributable to; it is quite likely that the two series are merged.

Notable features of the series are that the first member, 6d, is considerably stronger than the other members and that the series is not very well developed. The series is eventually lost more through its weakness than instrumental resolution. This is not unexpected as two-electron transitions tend to occur where configuration interactions are prominent and the 6s, nd interaction should be small. Furthermore the breadth of the lines in this case indicates, to some extent, penetration of the electron into the core and thus departure from a good $(J_c K)$ model. These lines are quite broad though ns features could well be broader.

A few other lines in the list of tentative assignments are attributed to the $5d^{10}$ 6p $(2P_1, 2P_2)$ ns, nd configuration, though these are not well established. The methods by which these assignments were made are discussed in 4.4.2.2. In particular the group of 5 doubtful lines in table (ii) of 4.3.3 that show a fairly steady course of quantum defects to the ${}^2P_2$ limit are very uncertain as they would normally have been disregarded as Hg features due to their extreme weakness.

Connerade (14) lists a feature at 879Å as possibly $5d^{10}$ 6p 6d with $n^* = 2.25$ referred to the $2P_1$ limit. In view of the experience of quantum defects in the present work a $5d^{10}$ 6p 7s classification built on the $2P_1$ limit would seem more likely. This feature was not observed in the present experiments but this is almost certainly because it is only detectable, as a window, at

a very high pressure such as that attained by Connerade.

(ii) $5d^{10}6d$ np

No convincing evidence of these series to the $^3D_2$, $^3D_3$ limits has been observed except for the $5d^{10}6p6d$ first members that are shared with the $5d^{10}6p$ nd series. A few tentative assignments have been made for levels of this type from a knowledge of the ion levels and typical quantum defects for np electrons.

(iii) $5d^{10}7s$ np

Again, recognisable series to the 2S limit have not been seen and only a few tentative assignments are made. These series share their first members with the first members of the $5d^{10}6p$ ns series.

(iv) $5d^{10}6d$ nf, $5d^{10}5f$ nd

No assignments have been made for these series to the $^3D_2$, $^3D_3$, $^4F_3$ and $^4F_4$ limits. Series to Hg II levels that lie above the $5d^{10}8s$ limits at about 205 600 cm^{-1} (486Å) would lie outside the 740-525Å region in which the resonances occur and therefore they are disregarded in this analysis.

It is evident however that the resonance spectrum observed is much too complex to be described in terms of the series suggested so far and thus levels involving simultaneous excitation of a 6s and a 5d electron are now examined.

4.4.2.2 Simultaneous Excitation of Subshell 5d and Valence 6s Electrons

Possible excitation schemes of this sort are

$$5d^{10}6s^2 \longrightarrow 5d^9 6s6p \text{ ns, nd}$$
$$\longrightarrow 5d^9 6s6d \text{ np, nf}$$
$$\longrightarrow 5d^9 6s7s \text{ np, nf}$$
$$\longrightarrow 5d^9 5f\ 6s \text{ ns, nd}$$
$$\text{and then} \longrightarrow 5d^9 6s\ 7p \text{ ns, nd etc.}$$

Final J values of 1 are possible for all these transitions.

Again, a generalised $(J_c K)$ notation is used in the tables of 4.3.2 and 4.3.3, specifying levels by the ion limit (J_c), the nl of the electron added and the effective quantum number to the ion limit. In this case also the $(J_c K)$ model would not be expected to apply rigorously in view of the lack of a $6s^2$ screening shell and the penetrating orbits of the outer electrons.

(i) $5d^9 6s6p$ ns, nd

These resonances converge on the Hg II $5d^9 6s6p$ levels. 23 Hg II levels are possible with this notation, with J = $^1/2$ ... $4\frac{1}{2}$. 19 of these levels have been identified by McLennan et al. (86) (table I of 4.3) who used a $(j_c j)$ scheme in the same way as they had used it in their analysis of this configuration in Au I and Tl III. Two of the J values attributed to these levels are doubtful and are denoted by question marks in table I (4.3)

A final J=1 value can be obtained by adding an s electron to a $J=\frac{1}{2}$ or $^3/2$ ion level and thus 11 series are possible to these limits. A d electron can produce J=1 when it is added to any of the ion levels except the $J=4\frac{1}{2}$ level, 2 series being possible to the $J=2\frac{1}{2}$, $3\frac{1}{2}$ levels. Thus 36 nd series are possible in all. It can be seen immediately that a very complex spectrum can result from this configuration alone. The known ion levels of this type lie between 605 and 510Å and must therefore be regarded as likely parents for many of the resonances observed.

A series, 4.3.2 table (ii), is seen converging on the $5d^9 6s6p$ $(4_{1\frac{1}{2}})$ limit. The last 5 members emerge from a region in which there are many resonances. Their effective quantum numbers, n* , are close to the n* of the $5d^{10}6p$ $(2P_2)$ nd series discussed in the previous section. Again these n* could be correlated with either ns or nd electrons in the valence spectrum.

When positions of lower members of this series are estimated, on the assumption of a regular quantum defect, the series can be followed to the very strong window resonance, HG 34, which gives an n^* of 2.87 to the $(4_{1\frac{1}{2}})$ limit. No resonance is found in the region that would give a n^* of 1.9, which would be expected of a 7s electron, and thus the series is identified as an nd series. The first 2 members of the series have profiles markedly different from the higher members, but calculations on the assumption of quantum defects for ns, nd electrons similar to the valence spectrum show that a $(Z_{\frac{1}{2}})$7s level could overlie the 6d window resonance and a $(X_{\frac{1}{2}})$ 7s level could lie on top of the 7d level. Thus the irregular profiles of these 2 levels could well be accounted for by interactions with levels of this type. The 10d member is missing and the 9d level is weak but these lie amongst a dense group of resonances; the 10d member is probably lost in the 595.0219Å source line.

From the 2 two-electron series identified so far some useful guidelines can be deduced that should be helpful in analysing the remaining resonances. Firstly, the first member of each series is much stronger than the other members and the series are not well-developed. Thus it may be assumed that the remaining features are likely to be due to low lying series members. Secondly both series were identified as nd series rather than ns series and nd configurations are probably more likely; furthermore the ns levels lie close to (n-2)d levels and interactions should be common. Thirdly the quantum defects of the running electrons were similar to those of the running electrons of the same l-value in the normal spectrum and estimations of the positions of levels using these quantum defects and the ion limits should give a useful first approximation.

Using these guidelines tentative assignments have been made for all the

more certain resonances, 4.3.3 table (i). On the whole it has also been assumed that to a large extent members of the same series would have similar profiles as, for the span of a Rydberg series, the parameters that determine profile, q and ρ^2 (see 1.4), are largely constant. Also it has been assumed that, in general, intensity decreases progressively along a series.

All these assumptions may have exceptions however for a spectrum so rich in screening and configuration interactions. These interactions can mean that only the high or low members of a series can be seen, that unlikely resonances become visible through intensity sharing interactions with nearby strong resonances, that intermediate members may be missing and that the quantum defect can be very irregular for a series. The possibility of exceptions of this sort have been borne in mind throughout analysis and exceptions to all the guidelines discussed above have been made.

(ii) $5d^9 6s6d$ np, nf, $5d^9 6s7s$ np, nf, $5d^9 5f$ 6s ns, nd etc.

The ion limits to which these series converge are not known but they would be expected to lie at energies greater than those in the region we are concerned with. The $5d^9 6s6d$ np series share their first members with the $5d^9 6s6p$ nd series, with the possibility of another 36 series, but, apart from the first members, no assignments have been made for any of these series. However the possibility of configuration interactions with levels of this sort remains. Apart from energy considerations, these series appear to be less likely when they are compared with the configurations that were found to be dominant in the spectrum resulting from the excitation of two valence electrons.

One assignment has been made by adding a 6d electron to an unclassified Hg II level, the $(16_{3\frac{1}{2}})$ level.

4.5 Excitation from the 5p Shell. Continuous Absorption

In 4.4.2 it was estimated, from characteristic X-ray data, that the spectrum of excitation from the 5p shell should lie around 210Å. Although the mercury spectrum was observed to 90Å no evidence of such discrete structure was found.

The experimental difficulties below 300Å, however, were such that only obvious discrete structure was likely to be detected. The continuous absorption in this region necessitated exposures of up to 3 times the normal length and a consequence was that source emission lines, which were not reduced in intensity to the same extent as the continuum was, became much more prominent. In particular the group between 90 and 100Å, where the continuous absorption of Hg was apparently reduced, appeared strongly in 2 or 3 orders. Thus many "new" emission features were observed and it was difficult to ascertain whether or not any of these features could be window-type resonances of Hg I.

A particularly striking group of 3 "new" lines was seen around 280Å. However it is very unlikely that these are attributable to Hg I as their intensities are considered to be too great to be caused by windows in the continuous absorption cross section.

The level of continuous absorption between 900 and 300Å is indicated on Figure 2. This is a plot of plate density against wavelength. It should be noted that the plot of plate density for the case when there is mercury absorption is made at a much greater sensitivity than the plot of the BRV background. The continuous absorption of mercury is in fact over 95% and it is thus necessary to show the mercury absorption plot on a larger scale to compare shapes.

Figure 2

A Microdensitometer Trace Indicating the Continuous Absorption Cross Section of Hg I, 300-900Å

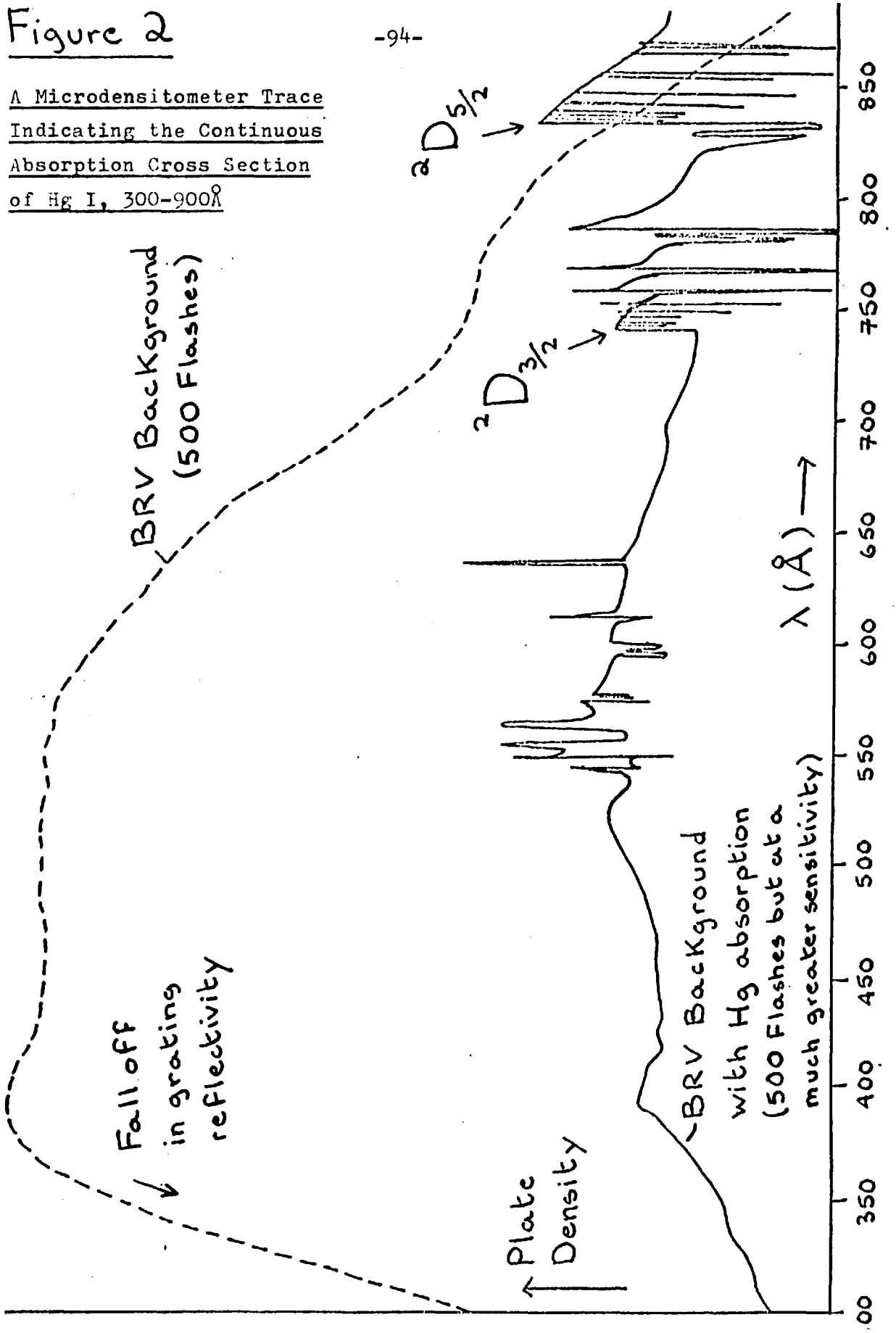

While these curves are in no sense an absolute indication of the absorption cross section of mercury, they do at least indicate that the level of absorption does not decrease steadily beyond the $^2D_{5/2,3/2}$ limits or the two-electron limits discussed in the previous section.

In discussing the continuous absorption of Xe beyond its $4d^9 5s^2 5p^6$ $^2D_{5/2,3/2}$ limits, in 3.1.2, it was noted that there could be a delayed onset of continuous absorption when the f-wave was excluded by the centrifugal barrier at lower energies. When higher energies were reached, though, the f-wave began to overlap the 4d wave function and the $d \rightarrow f$ possibility was greatly increased. The result was that the maximum absorption cross section occurred 2 Ry from the $^2D_{5/2,3/2}$ limits and was spread over a range of 4 Ry.

Cooper and Manson (83) (90) expect effects of this sort to be typical of the behaviour of photoelectric cross sections in this energy region and, for the case of gold, they find that this overlap is more critical for the 5d shell than the 4d shell. In the case of mercury the onset of continuous absorption at the $^2D_{5/2,3/2}$ limits is pronounced and the nf series to these limits are clear. Therefore this case is not completely comparable to Xe, but it does seem possible, though, that a similar phenomenon could cause a second maximum in the continuous absorption cross section and thus account for the persistence of continuous absorption to short wavelengths. Continuous absorption beyond the two-electron limits may also make a contribution although, on the evidence of the two two-electron series observed, this contribution is not obvious.

4.6 Conclusions

In this analysis 91 new features of Hg I spectrum have been observed,

measured and assigned, tentatively in most cases.

Observation of a splitting in the first two members of the nf series to the $^2D_{5/2}$ limit has provided support for Connerade's analysis of the single electron excitation d shell spectrum. 2 series of two-electron excitations have been established and, while detailed assignments of other two-electron resonances are only tentative, the dominant configurations in the two-electron spectrum have largely been established.

Experimentally the development of faster sources and faster photographic emulsions should provide the opportunities needed to extend this spectrum. Assignments of the two-electron spectrum will probably require updating when reliable theoretical calculations of the energies of the two-electron excitation states become available. Finally there is also a need for more absolute experimental and theoretical results concerning the continuous absorption cross section of mercury beyond its $^2D_{5/2,3/2}$ limits.

CHAPTER V RUBIDIUM

5.1 Introduction and Experimental Details

In repeating Beutler's Rb experiments (10) Connerade (15) measured 73 lines of the $4p^6 5s\ (^2S_{\frac{1}{2}}) \rightarrow 4p^5(4d + 5s)$ ns, nd (Rb I^b) spectrum. However, like Beutler, he was handicapped in his analysis by the 600Å short wavelength limit of the He_2 continuum that he used as a background. The Rb II levels on which these series converge, the $4p^5$ (4d + 5s) levels, lie between 625 and 555Å and thus Connerade was unable to observe the higher members of series converging on these limits. It was expected, therefore, that extension of the Rb I spectrum below 600Å with the BRV source would reveal something of the high series members and thus enable the analysis of Connerade's spectra to be extended.

Experimentally Rb, the most reactive element used in the present work, was expected to be troublesome. Hot Rb can heavily attack 'O' rings, brass and even pyrex in the space of a few hours. In practice though, it proved quite well-behaved. The procedure for inserting a one gram capsule of the element described in 2.4 proved to be satisfactory and the attack of the element on the vacuum housing was limited to a slight etching of the pyrex furnace. The 12 in pyrex furnace was adequate for the temperature range used, 290-335°C, corresponding to Rb pressures from 0.8 to 4.5mm. Hg. However, as with Hg (4.1), the level of absorption achieved seemed to be more a function of the amount of baffling used inside the furnace. Strong Rb absorption could easily be achieved.

The level of continuous absorption for Rb in the vacuum ultraviolet, at wavelengths far shorter than the first ionization potential of Rb, at 2968Å,

was very low and in this respect Rb was an excellent element for study with the BRV source (3.2). It almost seemed, in fact, that the intensity of the source radiation increased slightly when passed through the hot Rb and the continuum also appeared to be a little cleaner. Such an effect could be caused by a gettering action of the hot Rb vapour. At energies above the $4p^5$ (4d + 5s) limits, though, the continuous absorption introduced the problems of distinguishing between source features and further Rb features.

The Rb spectrum was measured at both high and medium pressures, the standards described in 2.3 being particularly reliable in this region. The 2 spectra at different pressures were useful in assessing the relative strengths of broad lines and thus in analysing them.

Finally the procedure for cleaning Rb from the furnace should be mentioned. The Rb completely oxidised in about a day when exposed to air (having, of course, been allowed to cool) and it was then washed from the furnace with water without any violent reactions.

5.2 Appearance of the Rb I Spectrum (Plate VIII)

At wavelengths above 600Å the Rb spectrum consists of many broadened but well-defined absorption lines. The lowest lying feature of the spectrum, at long wavelengths, is the strong $4p^5 5s^2$ ($^2P_{3/2,1/2}$) doublet. Towards shorter wavelengths the lines become considerably more closely packed and sharper although there are no obvious series. In general the spectrum above 600Å is of a doublet structure suggesting ($J_c j$) or ($J_c K$) coupling. The features above 600Å retain their symmetric absorption profiles at the highest pressure used in this experiment.

Between 600Å and 574Å the spectrum becomes very complex. Lines of many

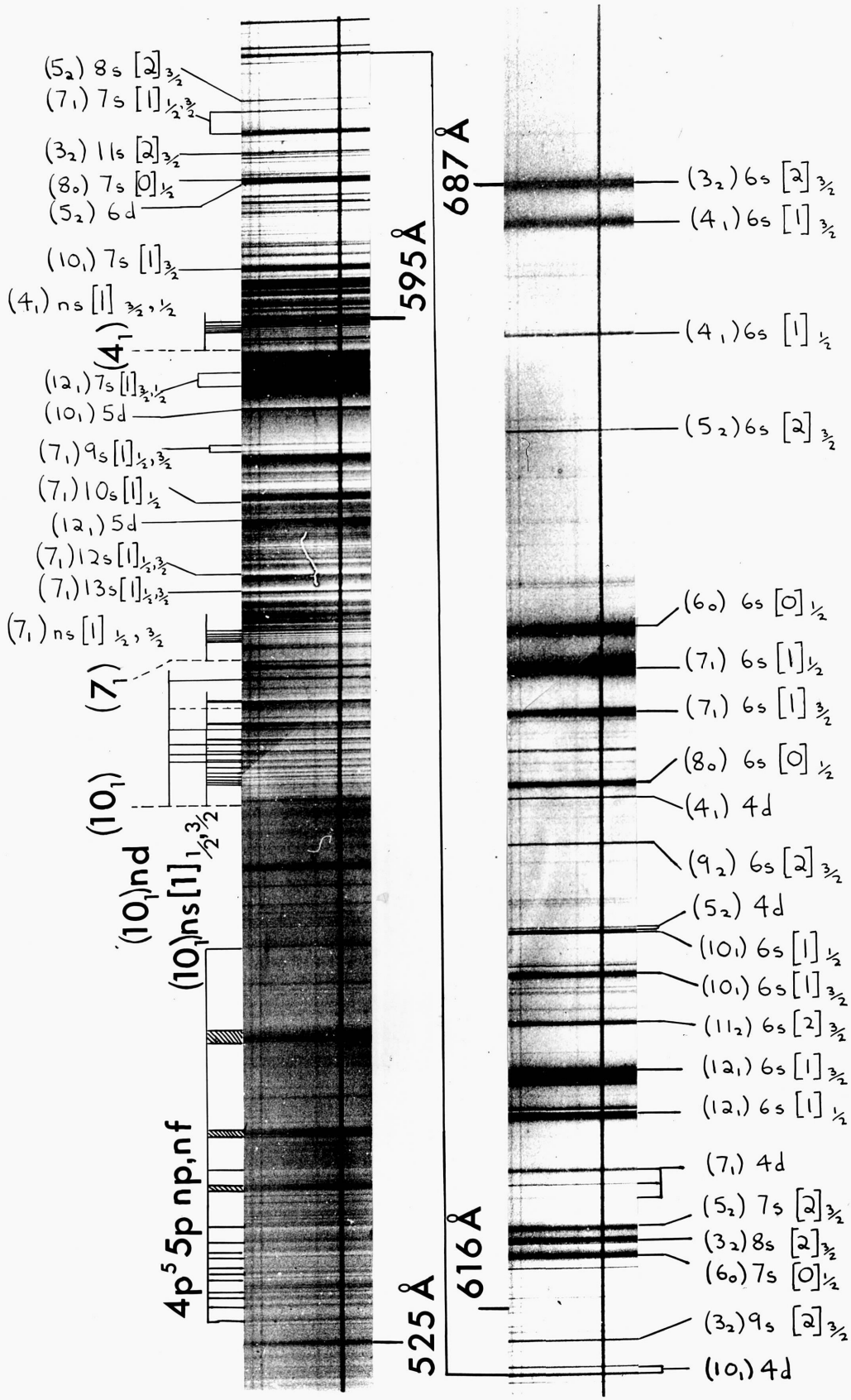

RbI Absorption Spectrum

different autoionizing profiles can be seen and it is difficult to ascertain which parts of a structure should be measured. In this region 2 groups of high series members (about 6 members in each case) can be seen converging on their respective limits without any obvious lower members preceding them.

At wavelengths below 574Å the spectrum simplifies with 2 series emerging that converge on the same limit. The strong spectrum seems to terminate with this limit and a moderately strong continuous absorption sets in at higher pressures.

Beyond this last limit, at about 564Å, more asymmetric features can be seen until the discrete spectrum seems to terminate finally around 525Å. These latter features, between 525 and 550Å, are much less well-defined than those seen at longer wavelengths. One group of particularly broad weak features appears to make up the lower members of a series.

At wavelengths below 525Å only two rather doubtful Rb features were seen. These lay around 475Å; other wise the level of continuous absorption remained quite high though it diminished steadily towards shorter wavelengths. At fairly high pressures the background became too weak for further observation around 350Å and it would have been difficult to observe further discrete features at wavelengths shorter than this.

5.3 Results for Rubidium

TABLE I Rb II level notation used in analysis.

Notation (Atomic Energy Levels Vol.III)	Notation (J. P. Connerade)	Configuration	Energy (cm^{-1}) from Rb I ground state	J
$4d\ 1_1$	1_1	$4p^5\ (4d + 5s)$	160 145	1
$4d\ 2_2$	2_2	"	162 385	2

Notation (Atomic Energy Levels Vol.III)	Notation (J. P. Connerade)	Configuration	Energy (cm^{-1}) from Rb I ground state	J
5s $^3P_2$	3_2	$4p^5$ (4d + 5s)	167 038	2
5s $^3P_1$	4_1	"	168 566	1
4d 3_2	5_2	"	170 356	2
4d 4_o	6_o	"	172 491	0
4d 5_1	7_1	"	174 306	1
5s $3P_o$	8_o	"	175 570	0
4d $6_{1,2}$	9_2	"	176 718	2
5s $^1P_1$	10_1	"	177 158	1
4d 7_2	11_2	"	177 652	2
4d $8_{1,2}$	12_1	"	179 321	1
5p 1_1		$4p^5$ ($^2P_{1\frac{1}{2}}$) 5p	187 970	1
5p 2_2		"	190 433	2
5p 3_3		"	190 592	3
5p 4_1		"	191 848	1
5p 5_2		"	192 408	2
5p 6_o		"	194 896	0
5p 7_1		$4p^5$ ($^2P_{\frac{1}{2}}$) 5p	197 618	1
5p 8_2		"	198 664	2
5p 9_1		"	198 786	1
5p 10_o		"	201 328	0

These levels are all from Laporte, Miller and Sawyer (91).

5.3.1 Series to the (4_1) Limit

Code	λ(Å)	ν (cm^{-1})	n*	Assignment
RB 107A	595.047	168 054	14.640	(4_1) 18s [1] $_{3/2,1/2}$
RB 107B	594.820	168 118	15.651	19s
RB 107C	594.651	168 166	16.563	20s
RB 107D	594.502	168 208	17.508	21s
RB 107E	594.381	168 242	18.695	22s
RB 107F	594.286	168 269	19.622	23s

These 6 high series members emerge from a group of complex asymmetric features. It will be noted that in 5.3.4 assignments are made for all the othe (4_1) ns members of this series except 13s and 17s. The (4_1) ns assignments of 5.3.4 are only tentative, however, as there are irregularities in intensities and profiles and they cannot be listed with the same certainty as the 6 lines above. The missing 13s, 17s lines would coincide with other strong features in the spectrum.

It should also be noted that the 18s and 19s lines listed above very nearly coincide with the source CII lines at 595.0219, 594.8000Å and are thus liable to distortion; they are, for example, much stronger than the other 4 lines.

These 6 lines are fairly sharp absorption lines. Their effective quantum numbers could represent either a ns or nd series. The analysis of the Rb I^b spectrum in general suggests that ns features are more prominent than nd and these 6 lines have been assigned accordingly. The two possible ns series, with J = $3/2, 1/2$, are considered to have merged for these high

series members.

These lines are not listed by Connerade.

5.3.2 Series to the (7_1) Limit

Code	λ (Å)	ν (cm^{-1})	n*	Assignment
RB 144	573.395	173 794	14.640	(7_1) 18s [1] $1/2, 3/2$
RB 145	575.198	173 853	15.564	19s
RB 146	575.039	173 905	16.481	20s
RB 147	574.903	173 942	17.411	21s
RB 148	574.782	173 979	18.319	22s
RB 149	574.685	174 008	19.190	23s

These 6 high series members are very similar to the 6 members to the (4_1) limit described in 5.3.1. They also emerge from a complex region without obvious lower members preceding them. Tentative assignments are made for all the other ns members in 5.3.4, with the (7_1) 15s line in particular fitting in well with the above series (the 14s assignment is in the second list (ii), the possible Rb features).

Again the features are assigned as ns as the more likely configuration with the J = $^1/2$, $^3/2$ series considered to have merged. The steady increase in quantum defect through the series would suggest the (7_1) level to be at 140 585 rather than the published 140 615 (91). However the value from the spark spectrum should be much more accurate than that of the present experiments.

These lines are not listed by Connerade.

5.3.3 Series to the (10_1) Limit

(i) $(10_1)ns[1]_{\frac{1}{2},3/2}$ series

Code	λ (Å)	ν (cm^{-1})	n*	Assignment
RB 158	570.937	175 151	7.394	(10_1) 11s $[1]_{1/2,3/2}$
RB 160	569.584	175 567	8.305	12s
RB 163	568.518	175 896	9.325	13s
RB 165	567.755	176 132	10.342	14s
RB 167	567.147	176 321	11.450	15s
RB 169	566.710	176 457	12.512	16s
RB 170	566.381	176 559	13.535	17s
RB 171	566.124	176 640	14.56	18s
RB 172	565.928	176 701	15.50	19s
RB 173	565.773	176 749	16.38	20s

This strong series, the best developed in the Rb I^b spectrum, finally emerges from the complex region to terminate the main group of Rb I^b features. The series is asymmetric with q positive though, from the 14s member, it is measured as an absorption series. The quantum defect indicates a ns series; it changes a little at the 15s member where the (10_1) ns and (10_1) nd (next table) series merge.

The absorption part of each resonance stretches quite a way to short wavelengths, particularly in the 11s, 12s members, and this could correspond to the merging of the $[1]_{\frac{1}{2}}$, $[1]_{3/2}$ series. It is notable that line RB 152 (5.3.4) has a similar profile to the profiles of this series although it has an anomalous intensity. There is a strong absorption line (RB 153) to the short wavelength side of this line and these 2 are assigned in the tentative list as the (10_1) 10s $[1]_{\frac{1}{2},3/2}$ lines before merging. Assignments are also made for the other members of this series in 5.3.4.

These lines were not observed by Connerade.

(ii) (10_1) nd series

Code	λ (Å)	ν (cm^{-1})	n*	Assignment
RB 155	572.357	174 716	6.703	8d
	. . . . .	. . . . .		
RB 162	569.137	175 705	8.690	10d
RB 164	568.173	176 003	9.747	11d
RB 166	567.536	176 200	10.70	12d
RB 168	567.022	176 360	11.73	13d

This series of moderately strong broadened absorption lines accompanies the ns series described above, merging with it after the 13d member. The 9d member would lie near the strong (10_1) 11s level and this may account for its absence. A tentative assignment is made for this transition in 5.3.4 with a highly anomalous effective quantum number. Tentative assignments are also made for transitions to the other nd levels except the 7d level which lies amongst the high members to the (7_1) limit (5.3.2).

The quantum defect of the series corresponds well with the typical value used for nd electrons in this analysis. 3 series are possible for the addition of a nd electron to the (10_1) ion level; they are (10_1) nd $[1]_{1/2,3/2}$, (10_1) nd $[2]_{3/2}$. It is difficult to ascertain which this series may be; it is considered likely that the 3 series would have merged for the higher series members considered here.

These features, for (10_1) ns, nd, were not observed by Connerade.

5.3.4 Other Rb $4p^6\ 5s\ {}^2S_{\frac{1}{2}} \rightarrow 4p^5\ (4d + 5s)$ ns, nd lines with Tentative Assignments

As it is concluded in the discussion of 5.4.1 that the $4p^5 4d$ ion levels with J = 0, 1, 2 contain an admixture of $4p^5 5s$, transitions of the type $4p^6 5s\ {}^2S_{\frac{1}{2}} \rightarrow 4p^5 4d$ ns, nd are included in this section, in effect as one-electron transitions.

As with mercury, there are 2 tables, the first comprising lines that can almost certainly be attributed to Rb after a comparison with source features and the second comprising those lines that are possible Rb features. With the weak continuous absorption of Rb in this region, source features are, to a large extent, filled in and thus the second list is short.

73 transitions were listed by Connerade (15) and they are all confirmed in the present analysis excepting the weak 723.337Å line listed by Connerade. This line lies in a region of weak BRV continuum and it is not surprising that it is not detected in the present investigation. On the whole the measurements of Connerade and of the present work are in satisfactory agreement. For those lines for which the difference between Connerade's measurements and those of the present experiment lies outside the respective estimated errors, the wavelengths measured are marked by asterisks. In many cases this discrepancy is accounted for by overlying source lines.

Connerade lists, among these 73 lines, about 15 lines below 598Å seen against the He emission lines following the He_2 continuum at shorter wavelengths. A comparison between the photographs of Connerade and of the present experiment shows that these "lines" are indeed associated with Rb features; however, in the present experiments, features in this region have invariably been measured at different points of their profiles and a

comparison with Connerade's results is not made. This same argument applies to 4 weak window features measured by Connerade from a microdensitometer trace (92).

The SWR plates used in the present experiment have enabled a greater resolution to be achieved than Connerade was able to attain with his Q2 plates. Thus quite a few new lines have been observed above 600Å, as well as below, and some splittings have been detected in Connerade's lines. The new lines are denoted by asterisks by their code numbers and newly observed splittings are indicated by a bracket with an asterisk e.g. $\left.\begin{matrix}\text{RB 64}\\ \text{RB 65}\end{matrix}\right\rangle$ *

Finally the assignments of lines observed by Connerade are changed in some cases. In general the assignments follow Connerade's scheme closely and confirm it (5.4); however assignments have been changed in some cases in the light of the observation of additional splittings and higher series members at lower wavelengths. Assignments different from Connerade's are indicated by an asterisk by the assignment. The lower 6s lines are regarded in Connerade's analysis to be well-established, but, for convenience, they are included in the tentative list here. The $4p^5 5s^2\ (^2P_{3/2,1/2})$ doublet is, of course, also well-established. (5.4.2)

(i) Rb Line list for "single electron" transitions with tentative assignments

Code	λ (Å)	ν (cm^{-1})	n*	Assignment	Appearance
RB 1	809.73 ±0.05	123 497		$4p^5 5s^2\ (^2P_{3/2})$	Very Broad
RB 6	767.41 ±0.15	130 309		$4p^5 5s^2\ (^2P_{\frac{1}{2}})$	Very Broad
RB 9	738.82* ±0.015	135 351		$4p^5 4d^2$	Sharp
RB10	720.43 ±0.05	138 806	2.268	$(1_1)\ 6s\ [1]_{3/2}$	Broad weak
RB11	714.83 ±0.05	139 894	2.209	$(2_2)\ 6s\ [2]_{3/2}$	Broad

Code	λ (Å)	ν(cm^{-1})	n*	Assignment	Appearance
RB12A	687.967	145 356	2.724	(1_1) 4d	Sharp weak
RB13	687.143 ±0.05	145 530	2.259	(3_2) 6s [2] $_{3/2}$	Broad
RB14	684.72 ±0.05	146 045	2.207	(4_1) 6s [1] $_{3/2}$	Broad
RB15	677.616*	147 576	2.287	(4_1) 6s [1] $_{\frac{1}{2}}$	Sharp Strong
RB16	671.555	148 908	2.262	(5_2) 6s [2] $_{3/2}$	Sharp Strong
RB17	658.923*	151 763	2.301	(6_o) 6s [0] $_{\frac{1}{2}}$	Broad Strong
RB18	656.544	152 313	2.234	(7_1) 6s [1] $_{\frac{1}{2}}$	Broad Strong
RB19	653.740	152 966	2.268	(7_1) 6s [1] $_{3/2}$	Broad Strong
RB20	649.167	154 043	2.279	(8_o) 6s [0] $_{\frac{1}{2}}$	Quite Broad Strong
RB21	648.279	154 255	2.769	(4_1) 4d	Sharp Strong
RB22	645.374*	154 949	2.245	(9_2) 6s [2] $_{3/2}$	Sharp Strong
RB23*	640.064	156 234	2.788	(5_2) 4d	Sharp
RB24	639.857	156 285	2.793	(5_2) 4d*	Sharp
RB25*	639.699	156 323	2.294	(10_1) 6s [1] $_{\frac{1}{2}}$	Sharp Strong
RB26	637.646	156 827	3.278	(3_2) 7s [2] $_{3/2}$	Sharp
RB27	637.051	156 973	2.332	(10_1) 6s [1] $_{3/2}$	Strong
RB29	634.000	157 729	2.347	(11_2) 6s [2] $_{3/2}$	Strong
RB31	630.796	158 530	2.245	(12_1) 6s [1] $_{3/2}$	Broad Strong
RB32	630.170	158 687	3.333	(4_1) 7s [1] $_{3/2}$	Sharp Strong
RB34	628.588*	159 087	3.385	(4_1) 7s [1] $_{\frac{1}{2}}$	Sharp Strong
RB35	628.327	159 153	2.864	(6_o) 4d	Sharp
RB36	628.094	159 212	2.336	(12_1) 6s [1] $_{\frac{1}{2}}$	Strong
RB38	624.738	160 067	2.776	(7_1) 4d	Quite Strong
RB39	623.838	160 298	2.799	(7_1) 4d	Sharp
RB40	623.008	160 512	2.821	(7_1) 4d	Weak
RB41	622.154	160 732	3.743	(4_1) 5d	Very Weak

Code	λ (Å)	ν (cm^{-1})	n*	Assignment	Appearance
RB42	621.119	161 000	3.425	(5_2) 7s [2] $_{3/2}$	Quite Broad, Quite Strong
RB43	620.399	161 187	4.331	(3_2) 8s [2] $_{3/2}$	Strong
RB44*	620.136	161 255	3.874	(4_1) 5d	Sharp
RB45	619.410	161 444	3.152	(6_o) 7s [0] $_{\frac{1}{2}}$	Quite Broad, Strong
RB46*	618.611	161 653	2.712	(8_o) 4d	Sharp
RB47	617.505*	161 942	2.739	(8_o) 4d	Weak
RB49	616.815*	162 123	4.725	(3_2) 6d *	Sharp
RB51	615.934	162 355	2.764	(9_2) 4d	Weak
RB52	615.063*	162 585	4.284	(4_1) 8s [1] $_{3/2}$	Weak
RB53	614.721*	162 675	4.316	(4_1) 8s [1] $_{\frac{1}{2}}$	Sharp
RB53A	614.150	162 827	5.105	(3_2) 9s [2] $_{3/2}$	Sharp Strong
RB54*	613.500	162 999	2.828	(9_2) 4d	Sharp Weak
RB56	612.526	163 120	2.810	(10_1) 4d	Sharp Strong
RB57	612.037	163 258	2.823	(10_1) 4d*	Strong
RB58	611.556	163 517	4.662	(4_1) 6d *	Sharp
RB59	610.926	163 686	4.742	(4_1) 6d *	Weak
RB60	609.195	164 151	4.205	(5_2) 8s [2] $_{3/2}$ *	Sharp
RB61 *	609.007	164 202	5.349	(3_2) 10s [2] $_{3/2}$	Weak
RB62	608.492	164 341	3.318	(7_1) 7s [1] $_{\frac{1}{2}}$	Sharp
RB64	607.207	164 689	3.380	(7_1) 7s [1] $_{3/2}$	Strong
RB65 *	607.080	164 723	5.344	(4_1) 9s [1] $_{3/2}$	Strong
RB66	606.578	164 859	5.441	(4_1) 9s [1] $_{\frac{1}{2}}$	Sharp
RB67	605.836	165 061	7.450	(3_2) 11s [2] $_{3/2}$	Sharp Strong
RB68*	605.698	165 099	3.854	(6_o) 5d	Sharp
RB69	605.514	165 149	2.783	(12_1) 4d	Sharp Strong

Code	λ(Å)	ν(cm^{-1})	n*	Assignment	Appearance
RB70	605.222	165 229	2.791	(12_1) 4d	Sharp
RB71*	604.628	165 391	5.879	(4_1) 7d	Weak
RB72*	604.463	165 436	5.921	(4_1) 7d	Sharp
RB73*	604.353	165 466	8.355	(3_2) 12s [2] $_{3/2}$	Sharp
RB74	604.144	165 524	3.305	(8_o) 7s [0] $_{\frac{1}{2}}$	Strong
RB75*	603.930	165 582	4.794	(5_2) 6d	Strong
RB77	603.067	165 819	6.320	(4_1) 10s [1] $_{3/2}$	Sharp Strong
RB78*	602.869	165 874	4.948	(5_2) 6d	Weak
RB79	602.629	165 940	6.464	(4_1) 10s [1] $_{\frac{1}{2}}$	Strong
RB80*	602.450	165 989	10.228	(3_2) 14s [2] $_{3/2}$	Sharp
RB81*	602.259	166 042	6.594	(4_1) 8d	Sharp
RB82	602.111	166 082	6.647	(4_1) 8d	Weak
RB83*	602.011	166 110	10.874	(3_2) 12d *	Sharp Strong
RB84*	601.923	166 134	6.717	(4_1) 8d	Sharp
RB85*	601.727	166 188	11.362	(3_2) 15s [2] $_{3/2}$	Sharp
RB86*	601.550	166 237	11.705	(3_2) 13d	Quite Weak
RB87*	601.290	166 309	12.269	(3_2) 16s [2] $_{3/2}$	Quite Weak
RB88*	601.122	166 356	12.685	(3_2) 14d	Sharp
RB89*	600.842	166 433	7.173	(4_1) 11s [1] $_{3/2}$	Sharp
RB90*	600.584	166 505	7.297	(4_1) 11s [1] $_{\frac{1}{2}}$	Quite Strong Sharp
RB92*	600.041	166 655	4.336	(6_o) 8s [0] $_{\frac{1}{2}}$	Weak Diffuse
RB93*	599.949	166 681	3.794	(7_1) 5d	Moderate
RB94	599.798	166 723	3.313	(9_2) 7s [2] $_{3/2}$	Moderate
RB96	599.217	166 884	3.269	(10_1) 7s [1] $_{\frac{1}{2}}$	Strong
RB97A	598.379*	167 118	3.306	(10_1) 7s [1] $_{3/2}$	Strong Broad

Code	λ(Å)	ν (cm^{-1})	n*	Assignment	Appearance
RB98 *	597.899	167 252	5.946	(5_2) 7d	Diffuse
RB99 *	597.445	167 397	3.271	(11_2) 7s [2] $_{3/2}$	Broad
RB100 *	597.105	167 475	10.020	(4_1) 11d	Moderate
RB101A	596.923	167 526	10.272	(4_1) 14s [1] $_{3/2,1/2}$	Quite Strong
RB101B *	596.737	167 578	3.300	(11_2) 7s [2] $_{3/2}$	Quite Strong
RB102 *	596.550	167 630	10.828	(4_1) 12d	Strong W
RB103 *	596.432	167 664	4.768	(6_o) 6d	Moderate
RB104 *	596.258	167 713	11.342	(4_1) 15s [1] $_{3/2,1/2}$	Moderate
RB104A *	596.081	167 763	7.802	(4_1) 13d	Strong
RB105A *	595.724	167 863	12.493	(4_1) 16s [1] $_{3/2,1/2}$	Quite Strong
RB107 *	595.266	167 992	4.939	(6_o) 6d	Strong
RB108 *	593.849	168 393	4.308	(7_1) 8s [1] $_{\frac{1}{2}\text{or}3/2}$	Strong
RB109 *	593.022	168 628	5.400	(6_o) 9s [0] $_{\frac{1}{2}}$	Strong W (AS q+ve)
RB110 *	591.796	168 977	3.257	(12_1) 7s [1] $_{3/2}$	Strong
RB111 *	590.896	169 235	3.299	(12_1) 7s [1] $_{\frac{1}{2}}$	Strong, very diffuse
RB112 *	589.415	169 660	3.826	(10_1) 5d	Strong AS (q+ve)
RB113 *	588.951	169 794	3.622	(10_1) 5d	Very Weak
RB114 *	587.168	170 309	5.240	(7_1) 9s [1] $_{\frac{1}{2}}$	Sharp
RB115 *	586.772	170 424	5.317	(7_1) 9s [1] $_{3/2}$	Sharp
RB116 *	586.555	170 487	7.400	(6_o) 11s [0] $_{\frac{1}{2}}$	Strong AS(q+ve)(Edge)
RB117 *	585.396	170 825	8.116	(6_o) 12s [0] $_{\frac{1}{2}}$	AS (q + ve)
RB117A *	585.001	170 940	4.868	(8_o) 6d	Weak
RB118 *	584.811	170 995	5.046	(7_1) 7d	Quite Strong
RB120 *	584.270	171 151	4.274	(10_1) 8s [1] $_{\frac{1}{2}}$	Quite Strong
RB120A *	583.824	171 284	4.322	(10_1) 8s [1] $_{3/2}$	Strong, broad
RB121 *	583.502	171 379	6.026	(7_1) 10s [1] $_{\frac{1}{2}}$	Sharp W

Code	λ(Å)	ν(cm^{-1})	n*	Assignment	Appearance
RB122*	582.906	171 554	6.315	(7_1) 10s [1] $_{3/2}$	Weak W
RB123*	582.655	171 628	5.333	(8_o) 9s [0] $_{\frac{1}{2}}$	W
RB124*	582.370	171 712	4.299	(11_2) 8s [2] $_{3/2}$	Strong
RB125*	581.900	171 851	3.833	(12_1) 5d	Weak
RB126*	581.470	171 978	6.866	(7_1) 8d	Weak
RB128*	581.260	172 040	6.959	(7_1) 8d	Quite Weak
RB129*	581.111	172 084	16.420	(6_o) 20s [0] $_{\frac{1}{2}}$	Quite Weak
RB130A*	580.662	172 218	7.249	(7_1) 11s [1] $_{\frac{1}{2}, 3/2}$	Moderate
RB132*	580.210	172 351	4.778	(10_1) 6d	Moderate
RB133*	579.817	172 468	4.837	(10_1) 6d	Moderate
RB134*	579.589	172 536	7.874	(7_1) 9d	Strong AS (q +v e)
RB135*	578.936	172 731	8.347	(7_1)12s [1] $_{\frac{1}{2}, 3/2}$	Very Strong AS(q+ve)
RB135A*	578.439	172 879	8.769	(7_1) 10d	Weak W
RB136*	577.897	173 041	9.314	(7_1)13s [1] $_{\frac{1}{2}, 3/2}$	Very Strong AS(q+ve)
RB137*	577.378	173 197	5.264	(10_1) 9s [1] $_{\frac{1}{2}, 3/2}$	Strong W
RB137A*	577.082	173 283	10.357	(7_1) 14s [1] $_{\frac{1}{2}, 3/2}$	Moderate
RB139A*	576.592	173 433	11.212	(7_1) 13d	Weak
RB140*	576.372	173 499	11.661	(7_1) 15s [1] $_{\frac{1}{2}, 3/2}$	Quite Strong
RB141*	576.112	173 577	12.27	(7_1) 16s [1] $_{\frac{1}{2}, 3/2}$	Weak W
RB142*	575.776	173 679	13.23	(7_1) 17s [1] $_{\frac{1}{2}, 3/2}$	Sharp W
RB143*	575.641	173 720	5.283	(11_2) 9s [2] $_{3/2}$	Diffuse
RB150*	574.437	174 083	8.59	(8_o) 12s [0] $_{\frac{1}{2}}$	Diffuse
RB152*	573.430	174 389	6.295	(10_1) 10s [1] $_{\frac{1}{2}}$	Moderate (AS q+ve)
RB153*	573.085	174 494	6.418	(10_1) 10s [1] $_{3/2}$	Strong
RB159*	569.904	175 468	8.058	(10_1) 9d	Moderate

Code	λ(Å)	ν(cm^{-1})	n*	Assignment	Appearance
RB161 *	569.335	175 643	5.462	(12_1) 10s $[1]_{3/2}$, $\frac{1}{2}$	Weak
RB175 *	565.620	176 797	11.215	(11_2) 15s $[2]_{3/2}$	Diffuse
RB177 *	565.131	176 950	12.503	(11_2) 16s $[2]_{3/2}$	Diffuse
RB178 *	564.831	177 044	13.435	(11_2) 17s $[2]_{3/2}$	Diffuse

All these features are measured as absorption lines unless otherwise stated. AS denotes asymmetric features. W denotes window features. Between 598 and 575Å, in particular, interactions tended to be very complex and it is not always clear whether features should be measured as absorption or transmission peaks. Somewhat arbitrary decisions have been taken in many cases. Where there is an indication that profile is different from that measured, this profile is shown in brackets.

(ii) Line list of possible Rb single electron features with tentative assignments

Code	λ(Å)	ν(cm^{-1})	n*	Assignment	Appearance
RB 8*	743.065	134 578		$4p^5 4d^2$	Sharp Weak
RB 30*	632.178	158 183	5.110	(2_2) 9s $[2]_{3/2}$	Weak
RB 53B*	613.832	162 911	3.839	(5_2) 5d	Very Weak
RB 55	613.046	163 120	2.796	(10_1) 4d	Very Weak
RB 63*	607.491	164 611	6.724	(3_2) 8d	Very Weak
RB 91*	600.373	166 563	3.765	(7_1) 5d	Very Weak. Diffuse
RB157*	571.357	175 022	6.459	(11_2) 10s $[2]_{3/2}$	Very Weak. Diffuse
RB176*	565.360	176 879	6.704	(12_1) 8d	Weak. Diffuse

RB55 is close to one of Connerade's lines, 613.140Å.

From 750 to 810Å, there are a number of features that appear on the plates of Connerade and those of the present experiment. They are weak, diffuse absorption features unlike the rest of the spectrum in this region. Connerade thought that they may be attributable to molecular Rb compounds. They seem to be definitely associated with Rb but are too weak to measure on the plates of the present experiment. A further possibility is that such features could be attributable to the diatomic Rb_2 molecule. This possibility is suggested by Hudson and Carter (37) who consider that alkali molecules can account for 1 to 10% of alkali metal vapours at these pressures. These features are also noted in the discussion of the $4p^5(4d + 5s)^2$ configuration, (5.4.3).

5.3.5 Simultaneous Excitation of Two Electrons. $4p^6 5s\ ^2S_{\frac{1}{2}} \rightarrow 4p^5\ 5p\ np,\ nf$

The $4p^5 5p$ ion levels are listed in Table I and the AEL notation quoted there is used in the possible assignment column.

Code	λ(Å)	ν(cm^{-1})	Appearance	n*	Possible Assignment
RB181	555.334	180 072	Quite diffuse	3.334	(3_3) 6p
RB182	549.53	181 977	Very broad diffuse	4.28	(1_1) 7p
RB184	543.44	184 017	Very broad diffuse	5.27	(1_1) 8p
RB186	541.146	184 793	AS (q - ve)	4.35	(3_3) 7p
RB187	539.93	185 210	Broad diffuse	6.31	(1_1) 9p
(RB189)	538.061	185 853	Weak	7.20	(1_1)10p
RB190	537.583	186 018	Quite strong AS (q-ve)	4.34	(4_1) 7p
RB191	536.587	186 363	Moderate AS (q-ve)	8.26	(1_1)11p

Code	λ(Å)	ν(cm^{-1})	Appearance	n*	Possible Assignment
RB192	535.898	186 603	Quite Strong AS (q-ve)	5.25	(3_3) 8p
RB194	534.903	186 950	Weak	10.37	(1_1) 13p
RB195	534.519	187 084	Quite broad	3.23	(7_1) 6p
RB196	534.321	187 153	Quite sharp	5.78	(2_2) 6f
RB197	533.488	187 446	Quite sharp	4.99	(4_1) 5f
RB198	533.180	187 554	Broad diffuse	3.29	(7_1) 6p
RB201	531.757	188 056	Diffuse	5.38	(4_1) 8p
RB203	531.601	188 144	Quite sharp	3.23	(8_2) 6p
(RB204)	527.487	189 220	Broad unclear	3.39	(9_1) 6p
(RB EDGE)	481.49	207 691	Edge, unclear (AS q-ve)		$4p^5 5d$ nl
(RB206)	473.41	211 236	Quite diffuse		$4p^5 5d$ nl

These are absorption features unless otherwise indicated. Those lines with their code numbers in brackets are not as certain Rb features as the other lines.

All these assignments are, of course, very tentative. The 3 features RB182, RB184 and RB187 do seem to form the lower members of a series but otherwise the assignments are merely indicative of how transitions of this type can account for all the features seen in this region.

It is not clear whether or not transitions to np or nf levels produce these features and, of course, a mixture could be present. The analysis of these lines is discussed further in 5.4.4.

The two $4p^5 5d$ nl features are doubtful but they do seem to be distinct enough from the background to be worth recording.

5.4 Analysis

5.4.1 The $4p^5(4d + 5s)$ Limits

From broad energetic considerations the only excitation scheme expected to be operating in the region in which the strongest part of the spectrum occurs (565-810Å) is $4p^6 5s\ ^2S_{\frac{1}{2}} \rightarrow 4p^5 5s$ ns, nd and $4p^5 4d$ ns, nd ($J = {}^1/2,\ {}^3/2$).

The limits of these series are the $4p^5 5s$, $4p^5 4d$ levels of Rb II, listed in 5.3 Table I. These levels were measured by Laporte, Miller and Sawyer (91). 4 levels, with J=0, 1, 2 are possible for the $4p^5 5s$ configuration and 12 levels with J=0,1, 2, 3, 4 are expected for $4p^5 4d$. Laporte, Miller and Sawyer found 12 of these 16 levels, those with J=0, 1, 2.

Laporte, Miller and Sawyer had characterised 4 of these levels as $4p^5 5s$, expecting the splittings of the upper (J=0, 1) and lower (J=2, 1) levels to be nearly equal in an intermediate coupling scheme that they expected to apply. Connerade (93), however, re-examined this characterisation using the formula of Condon and Shortley (94) for the $l^{n-1}s$ configuration.

$$\frac{({}^3/2,\ {}^1/2)_1 - ({}^3/2,\ {}^1/2)_2}{({}^1/2,\ {}^1/2)_1 - ({}^1/2,\ {}^1/2)_0} = -\frac{(2l + 1)}{l}\frac{({}^3/2,\ {}^1/2)_1 - ({}^3/2,{}^1/2)_2}{({}^1/2,\ {}^1/2)_0 - ({}^3/2,{}^1/2)_2}\frac{+l+1}{l}$$

Here n is the number of l electrons required to form a closed shell.

This formula enables the value of l to be calculated from the positions of the 4 $l^{n-1}s$ levels in any coupling scheme. (J_c, j) notation is used in the formula in this case.

Connerade established the 2 lower $4p^5 5s$ (J=2, 1) levels as (3_2) and (4_1) by subtracting the Rb III $4p^5$ splitting (95) from the possible combinations for the upper levels (J=0, 1), one of which must be (6_0) or (8_0), the 2 J=0

levels. He found that the (3_2), (4_1) levels lay in the most nearly correct positions (in which the centres of gravity of the upper and lower levels are separated by an energy approximately equal to the $4p^5$ splitting). This choice of (3_2), (4_1) is confirmed by the hyperfine structure analysis of Reinheimer (96).

Taking these assignments for the lower levels as established Connerade then applied the above formula for $l^{n-1}s$ to the various possible combinations of these 2 levels with J=0, 1 upper levels. He found that none of these combinations was satisfactory. Only the (3_2), (4_1), (6_o), (7_1) and (3_2), (4_1), (8_o), (10_1) combinations gave positive values for l, the first group being nearer l=1 (l=1.8) than the second group (l=2.6) that had been chosen by Laporte, Miller and Sawyer.(91).

It is clear therefore that no 4 levels can be characterised purely as $4p^5 5s$ and that possibly all $4p^5 4d$ levels with J=0, 1, 2 contain some admixture of $4p^5 5s$. (The 4 unknown J=3, 4 levels cannot mix with $4p^5 5s$)

In view of this mixing it is not meaningful to analyse this spectrum in terms of LS notation based on parent ions characterised as $4p^5 4d$, $4p^5 5s$. Therefore a generalised $(J_c K)$ notation has been adopted, treating the $4p^5$ (4d + 5s) configuration as an extended core specified only by its J value.

It does seem, though, from the experimental results, that the (3_2), (4_1), (6_o), (7_1) and (8_o), (10_1) levels have more $4p^5 5s$ character than the highest and lowest $4p^5$ (4d + 5s) levels, (1_1), (2_2) and (11_2), (12_1). This is indicated by Connerade's assignments of the $4p^5$ (4d + 5s) 6s lines that show the transitions to levels obtained by adding a 6s electron to the (3_2), (4_1), (6_o), (7_1), (8_o) and (10_1) limits to be the strongest and also by the fact that the 4 groups of high series members seen in the present experiment go to

3 of these levels (4_1), (7_1) and (10_1). Thus a general assumption might be made that series to these six levels should be more of a single electron transition nature and should thus be expected to be stronger and better developed. The fact that series to the (11_2) and (12_1) limits do not appear above the (10_1) limit also supports this assumption.

5.4.2 The $4p^5$ (4d + 5s) ns configuration

When n=5, the $4p^5 5s$ ns configuration becomes $4p^5 5s^2$ $(^2P_{1/2,3/2})$ with a $5s^2$ closed shell. This doublet is easily identified as the two strong long wavelength lines RB 1 and RB 6 . This original assignment of Beutler's has been shown by Connerade (15) to be supported by Tomboulian's (95) assignments of the $4p^5$ configuration of Rb III which he assigned from work on the Br I isoelectronic sequence. In Rb III the splitting of $4p^5$ $(^2P_{3/2,1/2})$ doublet is 7380cm^{-1}. In the present experiment the $4p^5 5s^2$ $(^2P_{3/2,1/2})$ splitting is 6812cm^{-1}, the energy difference being reduced slightly by a reduction of the spread of the $4p^5$ core by the $5s^2$ closed shell.

Connerade assigned the broad group of $4p^5$ (5s + 4d) 6s lines in the following way. The $4p^5$ (5s + 4d) ns configuration can produce 17 J=$^1/2,^3/2$ levels, 2 levels for each J=1 Rb II level and 1 for each J=0 or 2 Rb II level. The other possible low energy configuration is $4p^5$ (5s + 4d) 4d; this can produce at least 29 levels (see 5.4.3). The lowest energy levels of any strength, other than the $4p^5 5s^2$ $(^2P_{3/2,1/2})$ doublet, are the broad group of absorption lines 139 000 and 159 000 cm^{-1}. There are in fact about 17 of these levels and when the effective quantum numbers of this group, referred to the Rb II J=0, 1, 2 levels of Laporte, Miller and Sawyer, are calculated the

value obtained, around $n^* = 2.3$, is very reasonable for the second member (6s) of an ns series. Thus Connerade is able to establish this group quite well as $4p^5$ (4d + 5s) 6s.

Using the value obtained above for the s electron quantum defect ($\sim$ 3.7) Connerade was able to make tentative $4p^5$ (4d + 5s) ns assignments for many of the other Rb I^b features using Laporte, Miller and Sawyer's Rb II limits, which fortunately include all the J=0, 1, 2 levels relevant to ns electrons. He considered that, in the Rb I^b spectrum, the existence of a 5s electron not present in Rb II, screened the d electrons from the core and thus improved their characterisation. Thus the mixing of overlapping ns and nd levels should not be as much of a problem as in Rb II.

In the present analysis this method is applied to the additional Rb I^b features listed in 5.3.1 to 5.3.4. In many ways this extension of Connerade's analysis has supported the arguments on which he based his analysis. Most of the stronger features have been attributed to the $4p^5$ (4d + 5s) ns configuration and, in particular, the stronger series to the (10_1) limit, the best developed series observed has a quantum defect very much in accord with the typical value for a s electron used by Connerade and in the present analysis.

Thus the strong features in 5.3 have been assigned using crude assessments of the positions of ns levels calculated from the quantum defect and the ion limits, and from assuming a steady decrease of intensity along a series with the levels better characterised as $4p^5 5s$ being assumed to be stronger. Also, in the region of strong interactions (600-560Å), a similarity of autoionizing profile has been expected. However in a spectrum so rich in configuration interactions many exceptions to the above assumptions are found such as irregularities in quantum defect, intensity and profile anomalies, the sudden appearance of unexpected transitions and missing series members.

Connerade (105) worked out the order of levels for the $p^5 ss'$ configuration from Merrill's (97) work on the $l^k ss'$ configuration. This order is as follows for the $J={}^1/2$, ${}^3/2$ levels relevant to the present analysis:-

$4p^5$	$4p^5 5s$	$4p^5 5s\ ns$
Rb III	Rb II	Rb I[b]
$^2P_{3/2}$	$({}^3/2, {}^1/2)_2$	[2] $3/2$
		[1] $3/2$
	$({}^3/2, {}^1/2)_1$	[1] $\frac{1}{2}$
$^2P_{1/2}$	$({}^1/2, {}^1/2)_0$	[0] $\frac{1}{2}$
		[1] $\frac{1}{2}$
	$({}^1/2, {}^1/2)_1$	[1] $3/2$

Then, considering that all 12 J=0, 1, 2 levels of $4p^5$ (4d + 5s) possessed some $4p^5 5s$ character, Connerade expected that the $p^5 ss'$ order of levels should be obeyed locally as all $4p^5$ (4d + 5s) ns levels should possess some $p^5 ss'$ character. In this way the $[K]_J$ assignments for ns electrons in 5.3 have been made. When the local order of Rb II levels is not the same as that expected for $p^5 s$, but inverted, it has been assumed that inverted levels converge on inverted limits. One further assumption of this method of predicting the order of levels is that the s′ electron does not introduce new strong configuration mixing. The order of $4p^5$ (4d + 5s) ns levels predicted in this way has been used in the present analysis.

5.4.3 The $4p^5$ (4d + 5s)nd configuration

For n=4, this configuration is difficult to analyse. Normally the Pauli principle would restrict the number of $4p^5 4d^2$ levels to 18 with $J={}^1/2, {}^3/2$; however, as most of the parent $4p^5 4d$ ion levels seem to have some $4p^5 5s$ character for which the Pauli restriction on the number of 4d levels does not apply, it is difficult to predict the number of 4d levels built on each limit,

though, for the unknown J=3, 4 $4p^5 4d$ ion levels of course the $4p^5 4d^2$ configuration is well characterised. For these reasons the $4p^5$ (4d + 5s) 4d levels have been assigned keeping only within the total Pauli restriction for the $4p^5 4d^2$, $4p^5 5s4d$ configurations i.e. 29 levels. 19 such features have been tentatively assigned in 5.3.4, two of them being assigned as $4p^5 4d^2$ built on the unknown J=3, 4 limits. These are all sharp, but not particularly strong, absorption lines.

It seems possible however, that for 4d electrons the mixed configuration could be of the type $4p^5$ $(4d + 5s)^2$ and thus describing these levels as well-characterised $4p^5$ (4d + 5s) 4d levels built on the $4p^5$ (4d + 5s) ion levels through a $(J_c K)$ scheme would not be very meaningful in this case. Assignments in 5.3.4 of $4p^5$ (4d + 5s) 4d features have been made in this way, but, in view of the possibility of $4p^5$ $(4d + 5s)^2$ interactions, these assignments must be more tentative than the other assignments of the table. A similar configuration interaction seems to be significant in potassium (6.4.3).

In relation to the discussion of the $4p^5$ $(4d + 5s)^2$ configuration, the weak diffuse absorption features between 750 and 810Å noted at the end of 5.3.4 should be mentioned. These features, too weak for measurement in the present experiment were thought by Connerade to be due to molecular compounds of Rb. Another possibility is that they belong to the $4p^5$ $(4d + 5s)^2$ configuration, although they do seem to be rather different in appearance from the rest of the spectrum; they are more diffuse than other low lying features.

In addition there is the possibility of an interaction with the $4p^5 5p^2$ configuration, although estimations of the positions of transitions to this configuration (based on a knowledge of the $4p^5 5p$ ion levels and a typical p electron quantum defect in the valence spectrum) indicate that they should lie between 166 000 and 180 000 cm^{-1}, a long way above the

$4p^5$ (4d + 5s) 4d levels. The $4p^5 5p^2$ configuration is discussed in 5.4.4.

The remaining $4p^5$ (4d + 5s) nd assignments of 5.3 have been made in the same way as the $4p^5$ (4d + 5s) ns assignments of the previous section were made, with much the same considerations of intensities, profiles and likely configurations being taken into account and with similar anomalies being expected. The nd levels have been largely assumed to be weaker than the ns levels in view of the fact that the strong broad levels between 139000 and 159 000 cm^{-1}, had been assigned to the 6s, rather than the 4d configuration.

The nd configurations can produce many more levels than the ns configurations, a total of 47 different series being possible for each nd added to the 16 J=0, 1, 2, 3, 4 levels of $4p^5$ (4d + 5s) in Rb II. The number of levels assigned to each nd did not approach 47 though and it was not possible to assign K and J values to these nd levels. Except for the two $4p^5 4d^2$ lines mentioned earlier it was not necessary to assign any further features to the unknown J=3, 4 levels. In fact, in this case, as the $4p^5 4d$ of the ion is well characterised, these are genuine two-electron transitions and would therefore be expected to be weaker. As the $4p^5$ (4d+5s) levels are so greatly mixed it is not possible to estimate the regions in which these J=3, 4 levels should lie from a knowledge of the other ion levels.

The typical quantum defect used for crude estimations of the positions of nd levels was about 1.2, similar to that of Connerade's analysis. This is a reasonable value for a d electron and it is confirmed by the n* of the one nd series assigned, the (10_1) nd series in 5.3.3 (ii). This series also confirms the assumption, described earlier, 5.4.2, that the nd series are weaker than ns series, the (10_1) nd series being weaker than the (10_1) ns series in this case.

5.4.4 Two Electron Excitation $4p^6 5s\ ^2S_{\frac{1}{2}} \rightarrow 4p^5 5p$ np, nf

Beyond the (12_1) limit further discrete features are observed in the continuous absorption that follows the $4p^5$ (4d + 5s) limits. These features, with 2 rather doubtful exceptions lie between 560 and 525Å. They are listed in 5.3.5.

Energetically the next single electron transitions expected in Rb are those from the 4s shell. Characteristic X-ray data (89) indicate that these features would be built on limits at about 29.3eV (420Å); therefore structure between 560 and 525Å could not be due to this kind of excitation.

The alternative is that these are two-electron transitions. Energetically the $4p^5 5p$ ion levels (Table I, 5.3) would be expected to be the next possibilities as limits after the RbI^b spectrum and the energies of these limits certainly make them likely parent ions for features in this region. The possible excitation schemes for a final J= $^1/2$, $^3/2$ are $4p^6 5s\ ^2S_{\frac{1}{2}} \rightarrow 4p^5 5p$ np, nf.

The positions of np levels can be roughly predicted from a knowledge of the $4p^5\ 5p^4$ RbII limits and the typical quantum defect for a p electron in the valence spectrum. The predictions place the $4p^5 5p^2$ levels between 166 000 and 180 000 cm^{-1}, amongst the complex features of the RbI^b spectrum. It is not surprising, therefore, that they are not detected as they should be much weaker than the "single electron" RbI^b spectrum, though they could of course add to the complexity of the latter spectrum through interactions with levels from it. Some transitions to $4p^5 5p\ 6p$ levels may also be lost in the RbI^b spectrum. Thus the appearance of these features in a region which would indicate $n > 6$, without obvious lower lying features does not invalidate the possibility of transitions to np states. Furthermore some of these features between 560Å and 525Å are quite broad, indicating np

electrons rather than the almost hydrogenic nf electrons. In particular the 3 broad diffuse features RB182, 184 and 187 seem to be quite well identified as 7p, 8p, 9p features to the $4p^5 5p\ (1_1)$ limit with a quantum defect similar to that of p electrons in the valence electron. The 5p line would lie in the midst of the intense RbI^b spectrum. The 6p line would lie just beyond the onset of continuous absorption from the $4p^5\ (4d + 5s)\ (10_1)$ limit, and while there does appear to be a broad absorption peak there, it would be difficult to distinguish this feature from the continuous absorption.

The nf electrons, almost hydrogenic in the valence spectrum, should begin with $n^* \sim 4$, and, if the $4p^5 5p$ nf configuration were dominant, this could also account for the fact that the lowest two-electron features occur in a region with $n^* \sim 3.5$. Some of the features do seem to be fairly sharp and these could be attributable to transitions to nf levels.

It is, therefore, difficult to establish whether the nf or the np configurations are dominant. In 5.3.5 the possible assignments are largely np though there are a few nf assignments for sharp lines. These tentative assignments have little meaning in detail, therefore, but merely establish that transitions of this type can account for all the features seen in this region.

5.4.5 The Region 525-350Å

Only 2 rather doubtful discrete features (5.3.5) are detected at wavelengths below 525Å and these are very roughly assigned to $4p^5 5d$ nl. These are considered to lie at energies too low for excitation from the 4s shell.

Otherwise the continuous absorption, following the RbI^b limits, continues

until the limit of observation at about 350Å is reached, although it does weaken steadily to shorter wavelengths. There is no sign of excitation from the 4s shell. If it does occur around 420Å it should be detected, though, admittedly, it would have to consist of fairly strong well-defined features to be easily distinguished against the background intensity, which is much diminished by continuous absorption at high pressures. Such a 4s shell limit $4s4p^6 5s$ could in fact just lie above the RbII ionization potential at 254 443 cm^{-1} and the spectrum would in that case be converging on an autoionising level of the RbII ion, making the series less clear still.

5.5. Conclusions

At least 80 new features of the RbI^b spectrum have been added to the 73 measured by Connerade (15). Connerade's measurements have largely been confirmed although 20 or so features measured by him at wavelengths below 598Å have on the whole been ignored as they have been made at different parts of line profiles to those measurements made in the present experiment.

Connerade's method of analysis has been extended and, to some extent, confirmed. In particular the observation of 4 groups of series members has been important in this respect. The detailed assignments remain tentative though the overall scheme seems to explain the abundance and intensities of ~~levels~~ lines quite well. Reliable theoretical calculations of all the possible configuration interactions will be required before assignments can be made with any certainty.

At least 15 new two-electron resonances have been recorded and an initial survey of the excitation scheme has been performed.

The RbI^b measurements at energies below the $4p^5$ (4d + 5s) limits are satisfactory experimentally largely due to the low level of continuous absorption in that region. However knowledge of the spectrum above these limits could probably be usefully extended by the use of faster light sources and faster photographic emulsions which would make it possible to fill in troublesome background features by the use of longer exposures.

CHAPTER VI POTASSIUM

6.1 Introduction and Experimental Details

Beutler (11) had been able to observe only the first 2 features of the KI^b spectrum, the leading doublet, $3p^6 4s\ ^2S_{\frac{1}{2}} \rightarrow 3p^5 4s^2(^2P_{1/2,\ 3/2})$ at 662 and 653Å. As might be expected from an examination of the limits of the KI^b spectrum, the $3p^5 4s$ and $3p^5 3d$ KII levels, the remainder of the KI^b spectrum lay at wavelengths below the short wavelength limit of the He_2 continuum (600Å). Hudson and Carter (38), in their measurements of the continuous photoionization cross section of KI with the Hopfield continuum, from 1000Å to 580Å, record 6 further discrete features, but these are considerably weaker than the leading doublet. They assign these features to $3p^5 4s3d$.

Extension of the KI spectrum beyond 600Å should therefore reveal the KI^b spectrum, $3p^6 4s\ ^2S_{\frac{1}{2}} \rightarrow 3p^5\ (3d+4s)$ ns, nd, a spectrum that could be as rich in resonances as the RbI^b spectrum of Chapter V.

Experimentally potassium proved more difficult to work with than rubidium. Although it should have been a less reactive element it required the use of higher furnace temperatures to reach the potassium pressures needed for strong absorption and the 12in. quartz furnace was necessary for the attainment of these higher temperatures. In the time used for an exposure, typically an hour, the hot potassium could etch the quartz quite heavily in spite of the stainless steel lining placed in the heated part of the furnace and, although a furnace was never punctured in this way, a danger always existed in view of the violent reaction of hot potassium with air.

The experimental procedure of 2.4 was employed, using a 1gm capsule of potassium. Temperatures from 360 to 440°C were used in the furnace. These

corresponded to K vapour pressures from 1.5 to 8mm Hg, although, again, the amount of internal furnace baffling employed seemed to be equally important in achieving a high degree of absorption. High K absorption was quite easily achieved.

As with Rb, the low level of continuous absorption present at wavelengths far below the first ionization potential of K at 2856Å was ideal for the BRV continuum source. When observed through the hot K vapour, the continuum appeared to be cleaner and a little more intense; again as with Rb, this could be brought about by a gettering action of the alkali metal. The continuous absorption at energies above the $3p^5$ (3d+4s) limits, however, made the recognition of further KI absorption features difficult.

Photographs were taken of the KI absorption spectrum over a great range of pressures and thus the spectrum was seen at many different intensities. Spectra at high, medium and low pressures were measured. The standards were considered to be very reliable in the region of interest here (450-580Å) (2.3.3).

Lastly, potassium was cleaned from the furnace in the same way as rubidium (5.1). Some of the potassium did not always oxidise though, and minor reactions of the potassium with the water did take place. The quartz tended to flake a little as it cooled down after being attacked by the hot potassium.

6.2 Appearance of the KI Spectrum (Plate IX)

Plate IX indicates the appearance of the KI spectrum at 2 different pressures, the long wavelength photograph (b) being taken at a higher pressure and the shorter wavelength photograph (a) being taken at a medium pressure.

K I Absorption Spectrum

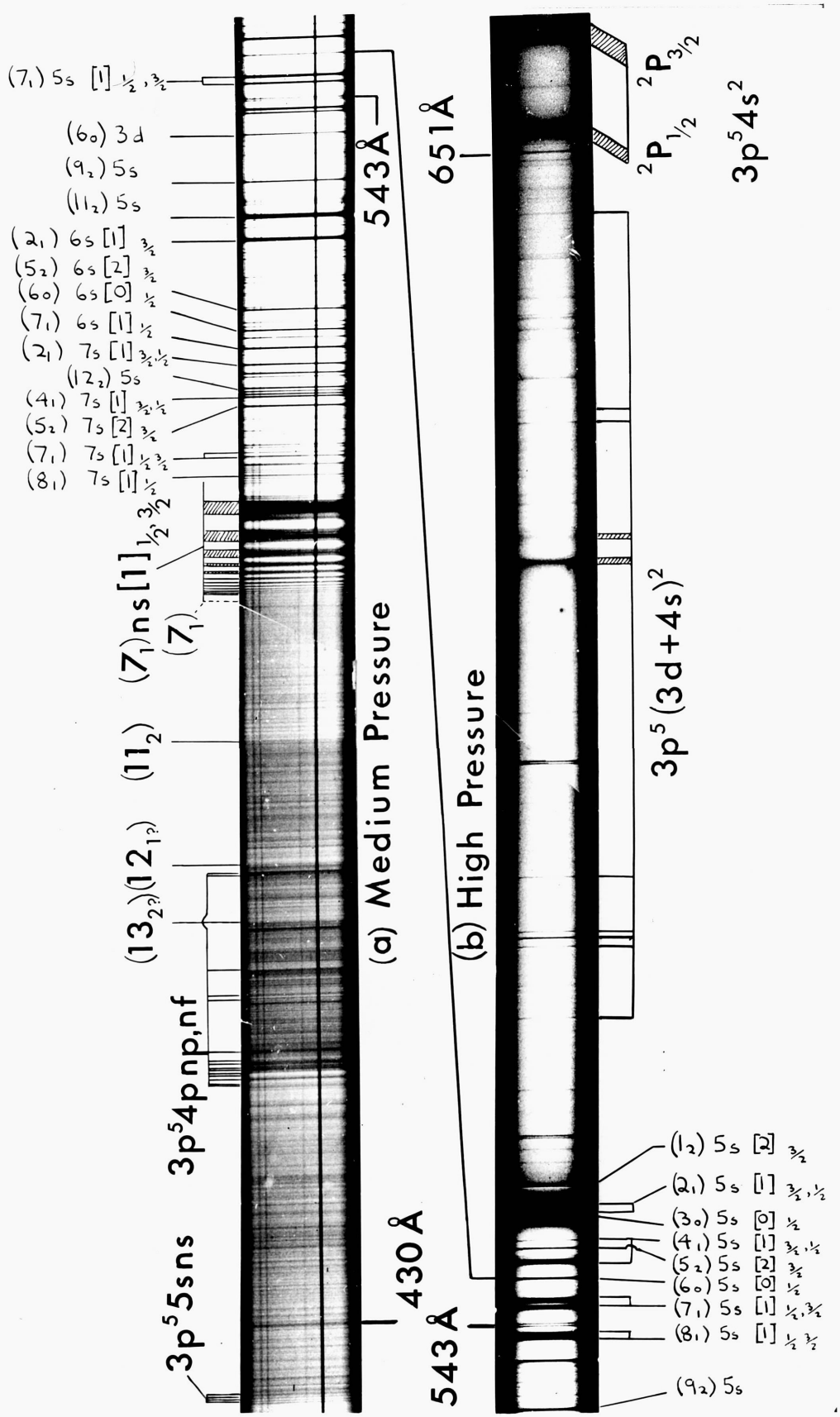

The KI^b spectrum at wavelengths above 500Å consists of a large number of very well defined absorption lines, sharper than the lines of the RbI^b spectrum, though still exhibiting some autoionization broadening. At higher pressures these features above 500Å retained their symmetric absorption profiles, the only exception being a sharp feature which appeared as an absorption line at low pressures but which assumed an asymmetric profile as it interacted with the wing of the broad line, K17, at high pressure. The sharp absorption features appear in many cases to be of a doublet structure. Apart from the leading doublet the strongest lines of the spectrum lie at wavelengths between 560 and 530Å.

Towards 500Å the lines become sharper and more densely grouped although no obvious series can be picked out. Then the spectrum is suddenly terminated by a very strong and well-developed series to a limit at about 495Å. This series possesses very broad lower members.

At higher energies, above this strong series, there is quite a high level of continuous absorption. In this continuous absorption a few steps can be detected, one being quite strong, and then between 465Å and 450Å some further features with varying autoionizing profiles are seen. Finally a group of absorption features around 425Å is seen and then one, possibly two, further absorption lines around 406Å can be detected.

The level of continuous absorption, which can be high above the strong series limit at high pressure, diminishes steadily at shorter wavelengths. The limit of observation for this spectrum was about 330Å at moderate pressures.

6.3 Results for Potassium

TABLE I KII level notation used in analysis

Notation Atomic Energy Levels Vol.III - de Bruin	Present Notation	Configuration	Energy (cm^{-1}) From KI ground state	J
X_2	1_2	$3p^5(3d+4s)$	197 517	2
X_3	2_1	"	198 247	1
X_4	3o	"	198 446	0
X_5	4_1	"	199 506	1
X_6	5_2	"	199 942	2
X_7	6o	"	200 160	0
X_8	7_1	"	201 472	1
	8_1	"	202 329 ?	1 ?
	9_2	"	204 643 ?	2 ?
X_9	10_3	"	205 845	3
X_{10}	11_2	"	206 537	2
	12_2	"	211 567 ?	2 ?
	13_1	"	214 087 ?	1 ?
P_1		$3p^5(^2P_{3/2})4p$	218 218	1
P_2		"	221 399	3
P_3		"	221 696	2
P_4		"	222 541	1
P_5		"	223 164	2
P_6		$3p^5(^2P_{1/2})4p$	224 254	1
P_7		"	224 672	2

Notation Atomic Energy Levels Vol.III - de Bruin	Present Notation	Configuration	Energy (cm^{-1}) From KI ground state	J
P_8		$3p^5(^2P_{3/2})4p$	224 782	0
P_9		$3p^5(^2P_{1/2})4p$	225 145	1
P_{10}		"	229 786	0
Y_4		$3p^5(^2P_{1/2})5s$	249 737	0
Y_5		"	250 029	1
Y_6		$3p^5(^2P_{3/2})4d$	250 415	0
Y_{10}		"	254 206	2

Excepting the levels (8_1), (9_2), (12_2) and (13_1), these levels are taken from a paper of Bowen (98) in which he supplements the measurements of de Bruin (99) with his own observations in the vacuum ultraviolet.

The levels (8_1), (9_2), (12_2) and (13_1) are suggested in the present work in order to enable a more complete analysis to be made. The evidence for these levels is discussed in 6.4.1

6.3.1 Series to the (7_1) Limit.

Code	λ (Å)	ν (cm^{-1})	n*	Assignment
KS 1	505.16 ±0.2	197 959	5.59	(7_1) 8s $[1]_{1/2, 3/2}$
KS 2	502.74 ±0.1	198 911	6.55	9s
KS 3	501.13 ±.05	199 549	7.554	10s
KS 4	500.049	199 980	8.576	11s
KS 5	499.332	200 268	9.547	12s
KS 6	498.770	200 493	10.587	13s

Code	λ(Å)	ν(cm^{-1})	n*	Assignment
KS 7	498.360	200 658	11.611	(7_1) 14s $[1]_{1/2,\ 3/2}$
KS 8	498.057	200 780	12.593	15s
KS 9	497.819	200 876	13.554	16s
KS10	497.624	200 955	14.569	17s
KS11	497.472	201 017	15.53	18s
KS12	497.330	201 074	16.61	19s
KS13	497.205	201 124	17.75	20s
KS14	497.138	201 152	18.52	21s

The members of this series are very strong broad diffuse absorption lines, different in character from the well-defined absorption lines at longer wavelengths.

The breadths of the first 3 members 8s, 9s, 10s of the series are so great that a large error is attached to their measurement, in fact the windows between these broad absorption features are sharper and more amenable to measurement than the absorption lines. The windows on either side of the 12s absorption feature are slightly weaker than they would be expected to be from their positions in the series. This could be attributable to the (6o) limit (Table I) that lies close to the 12s series member.

Superimposed on the first 3 members are many sharp absorption lines. These are listed and tentatively assigned in 6.3.2. Also in this table are tentative assignments for the 5s, 6s, 7s $[1]_{1/2,\ 3/2}$ series members and some (7_1) nd assignments. In addition to the (7_1) 8s assignment to the broad first series member above two sharp features within this feature are tentatively assigned (7_1) 8s $[1]_{1/2,\ 3/2}$ in 6.3.2.

The choice of an ns assignment rather than nd for this series was made because $3p^5$ (3d+4s) ns appeared to be the dominant configuration rather than $3p^5$ (3d+4s) nd in the analysis of 6.4. The quantum defect for the series is quite reasonable for an ns electron, a little smaller than the typical value for an ns electron in this analysis.

6.3.2 Other $3p^5$ (3d+4s) ns, nd Features with Tentative Assignments

With Rb (5.4.1) it was decided that the $4p^5 4d$ RbII levels possessed some $4p^5 5s$ character. In 6.4.1 it is concluded that a similar situation exists in KII i.e. that the $3p^5 3d$ and $3p^5 4s$ levels with J=0, 1, 2 are mixed. Thus transitions of the type $3p^6 4s\ ^2S_{\frac{1}{2}} \rightarrow 3p^5 3d$ ns, nd and $3p^5 4s$ ns, nd are listed together in this section as $3p^6 4s\ ^2S_{\frac{1}{2}} \rightarrow 3p^5$ (3d+4s) ns, nd, in effect as one-electron transitions.

There are 2 lists, the first comprising lines that are judged to be distinct from source features and the second, a short list in this case, comprising possible K features.

(i) Line list of $3p^5$ (3d+4s) ns, nd features with tentative assignments

For convenience the leading doublet is listed among the tentative assignments in this list although its assignment is well established. (6.4.2)

Code	λ(Å)	ν (cm^{-1})	n*	Tentative Assignment	Appearance
K 1	662.22	151 008		$3p^5 4s^2(^2P_{3/2})$	Very broad, strong
K 1A	653.23	153 085		$3p^5 4s^2(^2P_{1/2})$	"
K 2	645.602	154 894		$3p^5(3d+4s)^2$	Weak, diffuse
K 4	627.481	159 367		"	Very weak, sharp
K 5	626.262	159 678		"	Moderate strength, sharp

Code	λ(Å)	ν(cm^{-1})	n*	Tentative Assignment	Appearance
K 6	615.748	162 404		$3p^5(3d+4s)^2$	Very broad, weak, diffuse
K 7	613.473	163 006		"	Very broad, moderate, diffuse
K 9	579.298	172 623		"	Moderate, sharp
K10	578.705	172 800		"	Strong sharp
K11	577.892	173 043		"	Moderate sharp
K14	571.307	175 037		"	Moderate sharp
K15	555.908	179 886	2.497	(1_2) 5s $^2{}_{3/2}$	Strong AS in the wing of K17
K15A	555.802	179 920		$3p^5(3d+4s)^2$	Sharp
K17	553.860	180 551	2.490	(2_1) 5s $[1]_{3/2}$	Very broad, Strong
K18	553.125	180 791	2.507	(2_1) 5s $[1]_{1/2}$	Very broad, Strong
K19	552.945	180 850	2.497	(3_o) 5s$[0]_{1/2}$	Broad Strong
K20	550.913	181 517	2.470	(4_1) 5s $[1]_{3/2}$	Sharp Moderate
K21	550.229	181 742	2.456	(5_2) 5s $[2]_{3/2}$	Strong Sharp
K22	548.993	182 152	2.515	(4_1) 5s $[1]_{1/2}$	Broad Strong
K23	547.492	182 651	2.503	(6_o) 5s $[0]_{1/2}$	Very Strong
K24	545.490	183 322	2.447	(7_1) 5s $[1]_{1/2}$	Broad, Very Strong
K25	544.864	183 532	2.473	(7_1) 5s $[1]_{3/2}$	Broad, Very Strong
K26	542.470	184 342	2.470	(8_1) 5s $[1]_{1/2}$	Very Strong
K27	542.094	184 470	2.479	(8_1) 5s $[1]_{3/2}$	Very Strong
K28	540.094	185 153	2.724	(6_o) 3d	Strong
K29	537.047	186 203	2.691	(7_1) 3d	Weak
K30	535.745	186 656	2.470	(9_2) 5s	Strong
K31	534.742	187 006	2.609	(8_1) 3d	Moderate Sharp
K34	533.596	187 408	2.624	(8_1) 3d	Sharp
K35	532.464	187 806	2.420	(11_2) 5s	Very broad, Strong

Code	λ(Å)	ν(cm^{-1})	n*	Tentative Assignment	Appearance
K36	531.779	188 048	2.572	(9_2) 3d	Moderate Sharp
K37	531.497	188 148	3.422	(1_2) 6s $[2]_{3/2}$	Sharp
K38	530.321	188 565	3.367	(2_1) 6s $[1]_{3/2}$	Broad, Strong
K39	529.467	188 869	3.562	(1_2) 4d	Moderate
K40	529.151	188 982	3.442	(2_1) 6s $[1]_{1/2}$	Sharp. Quite Strong
K41	528.535	189 202	3.633	(1_2) 4d	Sharp. Quite Strong
K43	526.799	189 826	3.610	(2_1) 4d	Sharp. Quite Strong
K44	526.594	189 900	3.626	(2_1) 4d	Moderate
K45	526.294	190 008	3.606	(3_o) 4d	Strong
K46	525.309	190 364	3.463	(4_1) 6s $[1]_{3/2}$	Sharp Moderate
K47	525.114	190 434	3.472	(4_1) 6s $[1]_{1/2}$	Sharp Moderate
K49	523.984	190 846	3.560	(4_1) 4d	Strong
K49A	523.826	190 903	3.571	(4_1) 4d	Moderate
K50	523.718	190 942	3.492	(5_2) 6s $[2]_{3/2}$	Strong
K51	522.578	191 359	3.670	(4_1) 4d	Quite Strong
K52	522.168	191 509	3.607	(5_2) 4d	Quite Strong
K53	521.810	191 641	3.589	(6_o) 6s $[0]_{1/2}$	Very Strong
K55	521.126	191 892	3.692	(5_2) 4d	Strong
K55A	521.060	191 916	3.648	(6_o) 4d	Strong
K56	520.444	192 144	4.519	(1_2) 7s $[2]_{3/2}$	Moderate
K57	520.154	192 251	3.450	(7_1) 6s $[1]_{1/2}$	Broad Strong
K58	519.869	192 356	4.611	(1_2) 5d	Weak
K59	519.550	192 474	3.492	(7_1) 6s $[1]_{3/2}$	Moderate
K60	518.608	192 824	4.498	(2_1) 7s $[1]_{3/2,1/2}$	Strong
K60A	517.960	193 065	4.516	(3_o) 7s $[0]_{1/2}$	Weak

Code	λ(Å)	ν(cm^{-1})	n*	Tentative Assignment	Appearance
K61	517.808	193 122	3.452	(8_1) 6s $[1]_{1/2}$	Strong
K62	517.481	193 244	3.475	(8_1) 6s $[1]_{3/2}$	Strong
K63	517.296	193 313	4.624	(3_o) 5d	Moderate
K64	516.436	193 635	2.474	(12_2) 5s	Strong
K65	516.133	193 749	3.576	(8_1) 4d	Strong
K66	516.856	193 853	5.473	(1_2) 8s $[2]_{3/2}$	Strong
K67	515.602	193 948	4.443	(4_1) 7s $[1]_{3/2\ 1/2}$	Strong
K68	515.283	194 068	5.641	(1_2) 6d	Moderate
K69	514.733	194 275	4.401	(5_2) 7s $[2]_{3/2}$	Strong
K70	514.294	194 441	4.655	(4_1) 5d	Moderate
K71	514.106	194 512	5.420	(2_1) 8s $[1]_{3/2}$	Moderate
K72	513.951	194 571	5.464	(2_1) 8s $[1]_{1/2}$	Moderate
K73	513.714	194 661	4.467	(6_o) 7s $[0]_{1/2}$	Quite Strong
K74	513.537	194 728	5.433	(3_o) 8s $[0]_{1/2}$	Quite Strong
K75	513.119	194 887	4.659	(5_2) 5d	Moderate
K76	512.900	194 969	4.698	(5_2) 5d	Moderate
K77	512.738	195 031	6.644	(1_2) 7d	Weak
K78	512.430	195 149	3.400	(9_2) 6s	Strong
K79	512.210	195 232	4.719	(6_o) 5d	Moderate
K80	511.910	195 347	2.420	(13_1) 5s	Moderate
K82A	511.209	195 615	6.456	(2_1) 9s $[1]_{3/2}$	Strong
K82B	511.121	195 648	6.498	(2_1) 9s $[1]_{1/2}$	Strong
K83	510.944	195 716	2.444	(13_1) 5s	Strong
K84	510.640	195 833	6.481	(3_o) 9s $[0]_{1/2}$	Weak
K85	510.442	195 908	4.441	(7_1) 7s $[1]_{1/2}$	Strong

Code	λ(Å)	ν(cm^{-1})	n*	Tentative Assignment	Appearance
K86	510.240	195 986	8.466	(4_1) 11s [1] $_{3/2,\frac{1}{2}}$	Weak
K87	510.057	196 057	4.502	(7_1) 7s [1] $_{3/2}$	Strong
K88	509.889	196 121	5.694	(4_1) 6d	Quite Weak
K88A	509.800	196 155	5.723	(4_1) 6d	Weak
K89	509.572	196 243	5.447	(5_2) 8s [2] $_{3/2}$	Quite Weak
K90AA	509.374	196 319	7.544	(2_1) 10s [1] $_{3/2,1/2}$	Strong
K90AB	509.263	196 362	3.640	(9_2) 4d	Strong
K90B	509.076	196 434	7.383	(3_o) 10s [0] $_{1/2}$	Diffuse
K90C	508.841	196 525	5.494	(6_o) 8s [0] $_{1/2}$	Moderate
K91	508.650	196 599	7.708	(3_o) 8d	Moderate
K92	508.496	196 658	5.598	(6_o) 6d	Moderate
K93	508.341	196 718	4.422	(8_1) 7s [1] $_{1/2}$	Strong
K94	508.062	196 826	4.466	(8_1) 7s [1] $_{3/2}$	Quite Strong
K95	507.843	196 911	8.455	(3_o) 11s [0] $_{1/2}$	Quite Strong
K96	507.634	196 992	8.688	(3_o) 9d	Quite Strong
K97	507.320	197 114	4.587	(8_1) 5d	Weak
K98	507.055	197 217	4.634	(8_1) 5d	Weak
K99	506.878	197 286	9.726	(3_o) 10d	Moderate
K100	506.739	197 340	6.494	(5_2) 9s [2] $_{3/2}$	Moderate
K102	506.384	197 479	3.484	(11_2) 6s [2] $_{3/2}$	Diffuse
K103	506.170	197 562	6.499	(6_o) 9s [0] $_{1/2}$	Strong
K104	505.905	197 665	7.519	(4_1) 10s [1]	Diffuse
K105	505.695	197 748	3.682	(10_3) 4d	Strong
K106	505.556	197 802	5.468	(7_1) 8s [1] $_{1/2}$	Strong
K107	505.452	197 843	5.499	(7_1) 8s [1] $_{3/2}$	Weak

Code	λ(Å)	ν(cm^{-1})	n*	Tentative Assignment	Appearance
K108	505.337	197 888	3.562	(11_2) 4d	Weak
K109	505.196	197 943	3.573	(11_2) 4d	Diffuse
K110	504.925	198 049	5.662	(7_1) 6d	Diffuse
K114	502.532	198 992	6.652	(7_1) 7d	Moderate
K115	502.396	199 046	6.726	(7_1) 7d	Moderate
K115A	502.197	199 125	4.459	(9_2) 7s $[2]_{3/2}$	Diffuse
K129	483.98	206 619		(11_2) Limit	Strong Edge
EDGE	472.66	211 569		(12_2) Limit	Moderately Strong Edge
EDGE	467.10	214 087		(13_1) Limit	Moderately Strong Edge

All these features are measured as absorption lines unless otherwise stated. AS denotes asymmetric.

The edges at 472.66, 467.10Å were measured from a microdensitometer trace.

(ii) Line list of possible $3p^5$ (3d+4s) ns, nd features with tentative assignments.

Code	λ(Å)	ν(cm^{-1})	n*	Tentative Assignment	Appearance
K 8	584.333	171 135		$3p^5$ $(3d+4s)^2$	Moderate strength
K 29A	536.489	186 397	2.698	(7_1) 3d	Very Weak
K 30A	535.052	186 898	2.744	(7_1) 3d	Very Weak
K 31A	534.419	187 119	2.686	(8_1) 3d	Very Weak
K 42	527.666	189 514	3.703	(1_2) 4d	Diffuse Weak
K 48	524.654	190 602	2.624	(11_2) 3d	Diffuse Weak
K 74A	513.405	194 778	5.624	(2_1) 6d	Weak
K110A	504.303	198 293	7.667	(6_0) 8d	Diffuse

Code	λ(Å)	ν(cm^{-1})	n*	Tentative Assignment	Appearance
K112	502.974	198 817	6.429	(7_1) 9s $[1]_{1/2,3/2}$	Moderate
K113	502.686	198 931	9.449	(6_0) 12s $[0]_{1/2}$	Quite Strong
K117	501.091	199 565	7.586	(7_1) 8d	Moderate
K117A	500.855	199 659	4.692	(9_2) 5d	Very Strong

The line K8 is quite strong and seems to be distinct from source features. However it appeared as intensely at low pressures as at high pressures and is therefore included in the possible list.

Of all the features listed in 6.3.1 and 6.3.2 only 4 have been observed previously. The leading doublet K1, K1A was measured first by Beutler (11) and has also been investigated by Hudson and Carter (38). The values of the present experiment differ from Beutler's values of 662.38, 653.31Å but this is not unreasonable, considering the experimental error involved in measuring such broad lines. The two other features that have been observed previously are the lines K6 and K7; these can be correlated with Hudson and Carter's features at 616.0 and 613.6Å. Hudson and Carter report 4 other features in the range under examination here; these are all considerably weaker than the leading doublet. 2 of these, at 645.0 and 625.0Å, could possibly be associated with the lines K2 and K5, although this is unlikely. These 4 features could have been detected by Hudson and Carter at high number densities than those used in the present experiment; if this is the case the Hudson and Carter lines are certainly very minor features of the KI spectrum.

6.3.3 Simultaneous Excitation of Two Electrons

The $3p^5 4p$, $3p^5 5s$ and $3p^5 4d$ KII levels are listed in Table I and the notation of the "Possible Assignments" column refers to these parent ion levels.

(i) Line list of KI two-electron transitions with possible assignments

Code	λ(Å)	ν (cm^{-1})	Appearance	n*	Possible Assignment
K132	462.679	216 131	Quite strong broad AS (q+ve)	4.441	$P_3 6p$
K132A	461.820	216 534	Moderate window	4.274	$P_4 6p$
K133	460.388	217 207	Diffuse A	4.292	$P_5 6p$
K134	460.080	217 352	Sharp A	4.345	$P_5 6p$
K135	455.171	219 696	Strong A	3.298	$P_{10} 5p$
K135A	454.165	220 183	Moderate A	5.192	$P_6 7p$
K135B	453.973	220 276	Moderate A	5.252	$P_6 7p$
K135W	453.882	220 320	Window between K135B/C	5.282	$P_6 7p$
K135C	453.680	220 418	Moderate A	5.079	$P_7 7p$
K135D	453.468	220 521	Moderate	5.142	$P_7 7p$
K136	453.112	220 695	Sharp Window	5.182	$P_8 7p$
K137	452.923	220 787	Sharp Window	5.241	$P_8 7p$
K138	452.654	220 938	A between K137 and K136A	5.107	$P_9 7p$
K138A	452.475	221 007	Sharp Window	5.150	$P_9 7p$
K139A	452.303	221 091	Sharp Window	5.203	$P_9 7p$
		. . .	. . . . .		
K141	424.277	235 695	Diffuse A	2.796	$Y_4 5s$
K142	423.922	235 892	Diffuse A	2.815	$Y_4 5s$
K143	423.620	236 061	Sharp A	2.803	$Y_5 5s$
K144	423.382	236 193	Sharp A	2.817	$Y_5 5s$
K148	406.754	245 849	Moderate A	3.628	$Y_{10} 6s$

(ii) Line list of possible KI two-electron transitions with possible assignments.

Code	λ(Å)	ν(cm^{-1})	Appearance	n*	Possible Assignment
K130	471.784	211 961	Diffuse A (AS q+ve)	3.221	$P_4 5p$
K131	471.500	212 089	Weak Diffuse A	3.240	$P_5 5p$
B2A	464.289	215 396	W	4.276	$P_2 6p$
B2B	463.433	215 780	Edge before W	4.307	$P_3 6p$
K145	423.171	236 311	Sharp A	2.789	$Y_6 5s$
K147	407.161	245 603	Diffuse A	4.775	$Y_6 7s$

There is a fairly sharp decrease in the continuous absorption starting with the window K136 (453.1Å).

AS = asymmetric, A = absorption peak, W = window. Many of the two-electron features listed above possess complex profiles and, on the whole, measurements have been taken at the sharpest parts of profiles where the most accurate measurements can be made, though in many cases these points where measurements have been made may not necessarily be the most significant points of a feature's profile.

All assignments in this section are very tentative in detail; in general they are indicative of the configurations that can account for the features observed in this region. In particular the lines assigned as $3p^6 4s\ ^2S_{\frac{1}{2}} \rightarrow 3p^5 4p\ np\ (J={}^1/2,\ {}^3/2)$ in the tables above can, equally plausibly, be assigned as transitions to $3p^5 4p\ nf\ (J={}^1/2,\ {}^3/2)$ states or a mixture of the two configurations. The assignment of two-electron features is discussed further in 6.4.4.

6.4 Analysis

This analysis for potassium follows closely the analysis described for rubidium in the previous chapter.

6.4.1 The $3p^5$ (3d+4s) Limits

Energetically the excitation scheme operating in the region where the strongest features of the KI^b spectrum occur (670-495Å) is expected to be $3p^6 4s\ ^2S_{\frac{1}{2}} \rightarrow 3p^5 4s$ ns, nd and $3p^5 {}^3d$ ns, nd ($J={}^1/2,\ {}^3/2$).

The limits of these series are the $3p^5 4s$, $3p^5 3d$ levels of KII (6.3 table I) Unfortunately only 8 of the 12 possible levels of these configurations with J=0, 1, 2 are known (98,99) and any analysis of the KI^b spectrum must, necessarily, be more speculative than the equivalent analyses of RbI^b or CsI^b.

Firstly it is useful to examine the $3p^5 4s$ characterisation of the known KII levels. The KII assignments of Bowen (98) were largely based on a comparison with Meissner's analysis of the same configuration in ArI (100) and do not take account of the possibility of $3p^5 4s$, $3p^5 3d$ mixing.

As with Rb two methods are used to examine the 4 possible combinations of KII levels with the order expected for the $p^5 s$ configuration i.e. J=2, 1, 0, 1. Firstly, the splittings of the centres of gravity of the upper (0, 1) and lower (2, 1) levels are compared with the $3p^5$ ($^2P_{3/2,\ 1/2}$) splitting of KIII (2162cm^{-1}) (101) and, secondly, these 4 possible combinations of levels are inserted into the Condon and Shortley formula for the splittings of the $l^{n-1}s$ configuration (95). This formula, given in 5.4.1 enables the l value to be calculated for any coupling scheme.

The possible combinations of KII levels and the results of these methods of investigation are listed in Table II.

TABLE II

Level Combination	Splitting of Centres of Gravity of Upper and Lower Levels (cm^{-1}).	I
1_2 2_1 6_o 7_1	3353	6.70
1_2 2_1 3_o 4_1	1452	0.17
1_2 4_1 6_o 7_1	2881	0.12
1_2 2_1 3_o 7_1	2924	0.26

It is clear from this Table that none of these combinations, including Bowen's choice (1_2), (2_1), (6_o), (7_1), can be satisfactorily described as pure $3p^5 4s$. It seems likely therefore that all the $3p^5 3d$ levels possess some $3p^5 4s$ mixture and that a ($J_c K$) scheme, built on $3p^5$ $(3d+4s)_J$ mixed configuration KII levels will be the most appropriate coupling scheme to use, as it was with Rb.

In order that any attempt at analysis of the KI^b spectrum should be fairly complete it is useful to gain some knowledge of the positions of the unknown KII $3p^5$ (3d+4s) levels, in particular those with J=0, 1, 2. To achieve this two kinds of evidence of the positions of these levels have been sought. Firstly the continuous absorption at energies above the (7_1) limit has been searched for absorption edges which would indicate the existence of a series limit and, secondly, attempts have been made to correlate strong low lying lines, that are difficult to associate with known limits, with higher series members and thus with unknown limits.

The strongest absorption edge beyond the (7_1) limit is at 206 619cm^{-1} (5.3.2). This can be correlated with the (11_2) limit at 206 537cm^{-1}. The discrepancy (0.2Å) between these 2 values for the energy of this level is

much greater than the error normally attached to measurement in this region (0.02Å), but it is not an unreasonable discrepancy in view of the difficulty encountered in measuring an ill-defined feature of this sort. It does seem, therefore, that this method, of associating KII levels with absorption edges, has some validity.

The particular evidence for the four ion levels proposed by these methods is listed below.

(8_1) 202 329 cm^{-1}

The existence of a limit at about this energy was suspected from the difficulty in assigning the strong features K26, K27. The positions of higher series members were then estimated and the lines K61, K62 (6s) and K93, K94 (7s) were all found to be suitable choices as higher members as far as intensity and separation were concerned. This level was therefore proposed as a J=1 level with 2 possible levels, (8_1) ns $[1]_{1/2, 3/2}$, for each ns electron. The error in estimating the position of a limit from the positions of low series members in this way is expected to be large; no evidence of an absorption edge corresponding to this limit was found. 6 features are assigned as transitions to nd levels built on this limit.

(9_2) 204 643 cm^{-1}

This level was proposed as a result of difficulty in assigning the fairly strong lines K30 and K78 as transitions to ns levels. This particular KII level is very much tentative e.g. the strong line K38 (assigned as (2_1) 6s $[1]_{3/2}$) in 5.3.2) could also be the lowest member, 5s, of a series built on a J=2 ion level. The error involved in estimating the energy of this limit is large, no evidence being found of an absorption edge at this energy. Three (9_2) nd assignments are made.

(12_2) 211 567 cm^{-1}

This level is proposed to account for the moderate absorption edge at 211 567 cm^{-1}. A fairly strong line, K64, is assigned as a transition to a 5s level built on this ion level. The edge is not very well-defined and an error of up to 0.25Å is possible in its measurement.

(13_1) 214 087 cm^{-1}

Finally this last KII level is proposed to account for another moderate absorption edge at 214 087 cm^{-1}. 2 lines, K80 and K81 are assigned as transitions to the (13_1) 5s $[1]_{1/2,\ 3/2}$ levels. The error in measurement of this edge must also be about ±0.25Å.

For both the (12_2) and (13_1) limits, the possibility that these edges could be due to asymmetric features of the two-electron transition spectrum (6.4.4) must be acknowledged, and, as the higher members of series to these limits would lie among the strong series members to the (7_1) limit or in the region of continuous absorption without discrete features beyond this limit, it is difficult to obtain further evidence to support these choices. No features are assigned as transitions to (12_2) nd or (13_1) nd levels.

In view of the strong mixing of the $3p^5 3d$, $3p^5 4s$ configurations it is difficult to estimate the expected positions of unknown levels of this mixed configuration from the positions of known levels, although, in fact, the energies of these 4 additional levels are found to be quite reasonable from a comparison with Meissner's ArI levels (100) and possible J values are suggested for these levels from a comparison with the ArI spectrum. The J=1 for the (8_1) level is better established in view of the regular doublet structure found for transitions to ns levels built on this limit.

The unknown J=3, 4 levels are considered to be less likely to be

detected as, only being able to give rise to well characterised $3p^5 3d$ nd levels, which involve genuine two-electron transitions, features associated with these limits should be correspondingly weaker.

From the evidence listed above it can be seen that none of the 4 limits suggested can be regarded as well-established and that measurements of the energies of these limits are liable to large error. However they should be indicative of the effects of these missing levels and should enable a more complete attempt at analysis to be made than would otherwise have been possible.

6.4.2 The $3p^5$ (3d+4s) ns Configuration (cf Rb 5.4.2)

For n=4, the $3p^5 4s^2$ ($^2P_{3/2, 1/2}$) leading doublet is well-established. First identified by Beutler (11), the splitting of this doublet (2077cm^{-1}) is slightly less than the $3p^5$ ($^2P_{3/2, 1/2}$) splitting of KIII (101) (2162cm^{-1}). This decrease in energy difference is accounted for by a reduction of the spread of the $3p^5$ core by the $4s^2$ closed shell.

There are 17 possible $3p^5$ (3d+4s) ns levels with J= $^1/2$, $^3/2$, 2 being built on each J=1 ion level on one on each J=0, 2 ion level. The strongest group of lines, apart from the leading doublet, lie between 180 000 and 189 000cm^{-1} corresponding roughly to effective quantum numbers, n * of about 2.50 when referred to the known $3p^5$ (3d+4s) limits. This value would suggest a 5s electron rather than the more hydrogenic 3d electrons (6.4.3) and there are about 17 of these strong levels observed. Furthermore, some of these levels seem to possess a doublet structure. These doublets can be correlated well with the J=1 ion levels that should produce doublets for the addition of ns electrons in (J_cK) coupling. These levels have, therefore, been fairly well-established as $3p^5$ (3d+4s) 5s, some of them being built on the ion levels suggested in the previous section.

Using the $3p^5$ (3d+4s) KII limits, and the value obtained in the previous paragraph for the quantum defect of a s electron (about 2.53), to predict the positions of $3p^5$ (3d+4s) ns features, most of the stronger lines of 6.3.2 have been assigned to the $3p^5$ (3d+4s) ns (J= $^1/2$, $^3/2$) configuration. As with Rb, the existence of a 4s electron (5s for Rb) is considered to lead to the screening of d electrons from the core and thus the mixing of ns, (n-1)d levels should not be as much of a problem as in the ion levels.

The $3p^5$ (3d+4s) ns levels have been assigned from these crude estimates of their respective positions from the ion levels and a quantum defect of about 2.53. There are the usual anomalies expected from configuration interactions (5.4.2) and assignments are, of course, tentative.

The one strong series, to the (7_1) limit, has a quantum defect in reasonable agreement with the typical value for ns electrons in this analysis. In 6.4.1 it was concluded that all J=0, 1, 2 $3p^5 3d$, $3p^5 4s$ KII levels possessed some $3p^5 4s$ character. From the strengths of lines noted in this analysis and the strength of the (7_1) ns series it seems likely that this characterisation is greater for the lower ion levels. No series or discrete features, are attributed to the KI^b spectrum beyond the (7_1) limit.

The order of the $3p^5$ (3d+4s) ns levels is determined from Merrill's work (97) on the $1^k ss'$ configuration in the same way as Connerade had determined the order of the equivalent configuration in Rb (5.4.2). The assumptions are that all $3p^5$ (3d+4s) ion levels with J=0, 1, 2 possess some $3p^5 4s$ admixture and, therefore, that all $3p^5$ (3d+4s) ns levels possess $p^5 ss'$ character. It is also assumed that the s′ electron does not introduce new strong configuration mixing. Thus a local $p^5 ss'$ ordering is assumed, built on the local $p^5 s$ (2,1,0,1) order. When this local order is inverted, inverted levels are assumed to converge on inverted limits.

This method has been used in 6.3.2 to assign $3p^5\ (3d+4s)_{J_c}ns[K]$ features that are built on the known ion levels and also the (8_1) level that is regarded as quite well-established as J=1. The other 3 levels proposed in 6.4.1 are not considered to be certain enough in their J values to justify complete assignments, specifying the J_c and K values, to be made built on these parent ion levels.

6.4.3 The $3p^5\ (3d+4s)$ nd Configuration

When n=3, the $3p^5\ (3d+4s)$ 3d configuration can give rise to a total of 29 levels, 18 for the $3p^5 3d^2$ configuration (from the Pauli restriction) and 11 for the $3p^5 4s3d$ configuration. In view of the difficulty in characterising the $3p^5\ (3d+4s)$ levels, the number of levels assigned to this configuration has been determined by this total restriction rather than by the number of levels that can be built on each limit. 19 lines of this sort have been tentatively assigned.

With Rb it was noted (5.4.3) that mixing of the type $4p^5\ (4d+5s)^2$ could be significant i.e. configuration interactions could involve both 4d electrons. This effect seems to be much more prominent in KI. It is difficult to assign any of the levels below 175 000cm^{-1} to parent ion levels because the energy range over which these levels are spread is much greater than that of the limits. Furthermore effective quantum numbers of these levels are unreasonable for 5s or 3d elections added to a parent ion e.g. the strong line K7 has an effective quantum number of 1.783 when referred to the lowest known limit (1_2). Of course it is possible that unknown J=3, 4 levels lying at energies lower than the known levels could act as parents for these low lying features. However it is extremely unlikely that these ion levels should lie so far below

the others and, in any case, the numbers of lines and their intensities could hardly be accounted for by the $(3p^5 3d)_{3,4}$ 3d configuration which would involve well-characterised two-electron transitions.

Therefore these features below 175 000cm^{-1} have been assigned to the $3p^5$ $(3d+4s)^2$ configuration without reference to the ion levels. Some higher weak lines have been tentatively assigned as 3d electrons referred to ion limits but these assignments are not very meaningful. It should be noted that $3p^5 4p^2$ (6.4.4) may also have an influence on this configuration though such levels would be expected to lie at somewhat higher energies, 196 000 to 208 000cm^{-1}.

The difficulty in assigning these lower $3p^5$ $(3d+4s)^2$ features more specifically is unfortunate as it means that a typical value for the quantum defect of a 3d electron in this spectrum cannot be determined from the positions of these lines. The quantum defect used in making rough assessments of the positions of $3p^5$ (3d+4s) nd levels has therefore been chosen from considerations such as the abundance of weaker lines not identified as $3p^5$ (3d+4s) ns and the values of the effective quantum numbers for 3d electrons in the valence spectra of ArI, KI and CaI.

A value of about 0.35 for the quantum defect was therefore used as a typical value for a nd electron in estimating the positions of $3p^5$ (3d+4s) nd. The assignments of this type of transition in 6.3.2 have been made in this way, assuming also that parent ions that give rise to strong ns lines should also produce comparatively strong nd lines. 47 different series are possible for each nd added to the 16 J=0, 1, 2, 3, 4 ion levels $3p^5$ (3d+4s), $3p^5 3d$. The number of lines assigned was considerably less than 47 for each n. Unfortunately no series are observed that can help establish the typical quantum defect for nd electrons.

In view of the difficulty in establishing a typical quantum defect for nd electrons, assignments for the $3p^5$ (3d+4s) nd configuration are much more tentative than the assignments of the previous section and should only be taken as indicative of how this configuration can easily account for the number of weaker absorption features of 6.3.2. Furthermore it is by no means established that configuration interactions involving the outer d electron apply only to the case where n=3.

6.4.4 Two-Electron Excitation

Listed in 6.3.3 are KI absorption features between 475 and 400Å. It might be thought that these features could belong to the $3p^6 4s\ ^2S_{\frac{1}{2}} \rightarrow$ $3p^5$ (3d+4s) ns, nd (J= $^1/2$, $^3/2$) excitation scheme discussed in the 3 previous sections e.g. they could be high members of series to unknown high-lying $3p^5$ (3d+4s) KII levels. However these features are rather too strong to be accounted for in this way and KII levels on which features around 460Å would be built would be expected to be as much as 15 000cm^{-1} above the known KII levels. Energies of this magnitude (220 000cm^{-1}) are unlikely for the KII $3p^5$ (3d+4s) configuration.

The next single electron excitation possibility is excitation from the 3s shell. The energy required for this kind of transition may be estimated roughly from the characteristic X-ray spectrum of potassium. The energy required for the removal of a 3s electron in potassium (X-ray M_1 edge) is 33.9eV (89) corresponding to 365Å. Thus transitions of this sort are unlikely to be responsible for the features in the region 475-400Å.

Therefore, as with Rb, features of this sort seem to be due to two-electron excitation. Energetically the $3p^6\ ^2S_{\frac{1}{2}} \rightarrow 3p^5 4p$ np, nf (J=$^1/2$, $^3/2$)

transitions are expected to possess the lowest energies. The parent ion levels for this configuration are the KII $3p^5 4p$ levels listed in Table I.

Crude estimates of the positions of $3p^5 4p$ np, nf levels can be made from a knowledge of the KII limits and the typical quantum defects of np and nf electrons in the normal spectrum. The nf electrons are hydrogenic, the lowest lying configuration being $3p^5 4p4f$. As with the similar transitions in Rb, it is very difficult to predict whether the transitions observed are due to transitions to np or nf configurations. The lowest lying features suggest effective quantum numbers of about 4 when referred to the $3p^5 4p$ levels. This at first suggests nf levels; however, when the positions of the transitions to $3p^5 4p^5$ and $3p^5 4p$ 5p levels are calculated they are found to lie in the region of the KII $3p^5$ (3d+4s) limits and, as two-electron features are normally weaker than single electron features, it is quite possible that these lower levels are entirely lost in interactions with the KI^b spectrum.

The features between 475Å and 450Å have been given possible assignments as transitions to $3p^5$ 4p np levels, mainly because this configuration yields more low-lying levels than the $3p^5$ 4p nf configuration. However this choice is very arbitrary and transitions to $3p^5$ 4p nf levels are also likely. It is noted in 6.3.3 that these complex features are difficult to measure in a significant way and this should also be taken into account when assessing these assignments.

Further features are seen beyond the highest $3p^5 4p$ limits and these have been given possible assignments as transitions to the $3p^5 5s$ ns and $3p^5$ 4d ns configurations. Transitions of this sort are considered to be more likely than transitions to $3p^5 5s$ nd and $3p^5 4d$ nd from a comparison with the KI^b

spectrum. Again these assignments have little detailed meaning but merely indicate transitions which could account for these features.

6.4.5 The 3s Shell. Continuous Absorption

There is no sign of excitation from the 3s shell at wavelengths around 365Å (6.4.4). The intensity of light in this region is very low at higher pressures and features would have to be quite strong and well-defined to be detectable. Furthermore, as with sub shell s excitation in RbI (5.4.5), the $3s\ 3p^6\ 4s$ KII limit could just lie above the KII ionization potential at 291 647cm^{-1} (measured from the KI ground state). In this case any sub shell series would be converging on an autoionizing limit.

The continuous absorption cross section of KI is of interest. It was measured by Hudson and Carter (38) between 1000Å and 580Å. Their results differed from the theoretical predictions of Sheldon (102) who used the quantum defect method to calculate the continuous cross section in this region. This discrepancy became greater at shorter wavelengths, Hudson and Carter finding the magnitude of the absorption to be greater than the theoretical predictions. An attempt was made to find some indication of the extent of the continuous absorption in the present experiment by comparing a microdensitometer trace of the KI spectrum with a trace of the undiminished background. The level of continuous absorption, apart from the discrete features, was so low as not to be detectable in the region above 550Å. In fact, as mentioned in 6.1, the gettering effect of the alkali metals tended to clean up the continuum a little.

The level of continuous absorption beyond the (7_1) limit was great at high pressure. It decreases steadily towards shorter wavelengths with irregularities in the form of the (11_2) (12_2) and (13_1) absorption edges

(see 6.4.1) and a fairly sharp decrease in continuous absorption accompanying the window features around 453Å.

6.5. Conclusions

In this investigation at least 146 new transitions of the KI spectrum have been measured. At wavelengths above 495Å the accuracy of measurement should be very good though, below this wavelength, measurements could probably be improved, at higher pressures, by the use of a faster light source and a faster photographic emulsion that would make the source features less obtrusive.

A tentative analysis of the KI^{b} $3p^6 4s\ ^2S_{\frac{1}{2}} \rightarrow 3p^5\ (3d+4s)$ ns, nd ($J = {}^1/2$, ${}^3/2$) spectrum has been proposed. Assignments for nd electrons are very much speculative. From this analysis possible positions for the unknown KII $3p^5$ (3d+4s) levels have been suggested and an investigation of the $3p^5 4s$ characterisation of the known $3p^5 3d$, $3p^5 4s$ levels has indicated strong (3d+4s) mixing. A strong series to one of these known limits has been observed. More certain assignments for this spectrum must await reliable theoretical calculations of all the possible configuration mixing effects.

Finally a survey of the new two-electron resonances in potassium has been made and the dominant configurations for this kind of transition have been suggested.

CHAPTER VII SODIUM

7.1 Introduction and Experimental Details

No discrete features of the NaI spectrum have previously been observed at energies above the first ionization potential at 41 450cm^{-1}. Hudson and Carter (37) have measured the continuous photoionization cross section of NaI between 600 and 1000Å using the Hopfield background continuum, but have not observed any discrete features.

Investigation of the NaI spectrum at wavelengths below 600Å should therefore reveal the $2p^6 3s\ ^2S_{\frac{1}{2}} \rightarrow 2p^5 3s$ ns, nd (J= $^1/2$, $^3/2$) NaI^b spectrum, a spectrum that should be much simpler than the equivalent RbI^b, KI^b spectra as, in the absence of a 2d shell, there is no longer the possibility of (n-1) p^5 ns, (n-1) p^5 (n-1)d mixing in the parent ion levels.

The experimental problems encountered with potassium (6.1) became more serious with sodium in the furnace. The quartz furnace was required to attain the higher temperatures necessary for strong Na absorption and hot sodium vapour could attack the quartz vacuum housing considerably in the time of an exposure, in spite of the stainless steel lining in the heated part of the furnace. In particular, as the furnace cooled down, the quartz that had been attacked by sodium flaked away considerably. Because of the extent of this attack by sodium a longer quartz furnace, 26in. long, was employed when it was necessary to attain a higher degree of absorption, rather than a higher temperature in the 12in. furnace.

The experimental procedure of 2.4 was used although the sodium samples were not enclosed in capsules. The metal was cut into 2-3gm. samples in an argon tent and was then stored in an atmosphere of argon before being inserted into the furnace in a stainless steel boat. A thin surface oxide layer

formed on the sodium while it was being stored but, although this oxide layer probably reduced the sodium vapour pressure, it was considered that effects of this sort could be overcome by the use of higher temperatures. Temperature ranges of 430 to 610°C (for the 12in. quartz furnace) and 500 to 560°C (for the 26in. quartz furnace) were employed; these corresponded to sodium vapour pressures from 0.7 to 10.5mm Hg (12in. furnace) and 2.5 to 5.5mm Hg (26in. furnace). It was difficult to obtain a sufficiently high level of sodium absorption, however, because, while attempts to increase the level of sodium absorption by increasing the temperature and the amount of internal furnace baffling were effective at first, a saturation point seemed to be reached where the sodium condensed more rapidly at the end pieces but did not absorb any more intensely. As explained in the previous paragraph, higher temperatures risked serious attacks on the quartz and for this reason a longer furnace was employed instead.

Even with the use of a longer absorbing cell sodium absorption could never be obtained at the level at which it was required. Although continuous absorption, beyond the $2p^5 3s\ (^1P_1)$ limit, could be fairly high, the discrete features at lower energies were not as strong as the equivalent features in Rb and K. The level of continuous absorption at energies below the $2p^5 3s\ (^1P_1)$ limit was low, Na producing a gettering effect similar to that of K or Rb.

The lower members of the NaI^b spectrum could be observed with the 3m normal incidence spectrograph, but the higher members, in particular the higher series members converging on the $2p^5 3s\ (^1P_1)$ limit, fell in the region of fast diminishing grating reflection and the 2m grazing incidence spectrograph was needed for wavelengths below 325Å. This was unfortunate because the

illuminiation at the photographic plate for the grazing incidence instrument, with the 26in. furnace inserted, was poor. To compensate for this loss of illumination the slit width had to be broadened to 15μ, with some loss of resolution.

Most of the sodium features at wavelengths above 325Å were measured 3 times, twice with plates from the normal incidence spectrograph and once with a plate from the grazing incidence spectrograph. The region 350-300Å in which most measurements were made was not a satisfactory region as far as accuracy of measurement was concerned, (2.3.3), because measurements depended largely on source standards measured by extrapolation from standards at longer wavelengths. The measurements made on the inert gas spectra of Madden and Codling (Chapter III) support the use of these standards but, while there is no particular reason to suspect the accuracy of measurements of the NaI^b spectrum, they are undoubtedly not as reliable as the Hg, Rb or K measurements. Furthermore, as mentioned previously, the use of a 15μ slit for the grazing incidence instrument brought about some loss of resolution. The regularity of the quantum defect of the series to the $2p^5 3s\ (^1P_1)$ limit, which should be a sensitive pointer to errors of measurement, was quite satisfactory.

7.2 Appearance of the Na I Spectrum (Plate X)

Energetically, the lowest lying feature of the NaI^b spectrum, at about 400Å, is a strong doublet. Proceeding to shorter wavelengths, no further features are encountered until 346Å is reached. Here a group of quite sharp absorption lines is seen; some are moderately strong. Then towards shorter wavelengths many more rather weak absorption lines are observed (a pair of lines at 336Å being moderately strong). Finally the spectrum finishes with

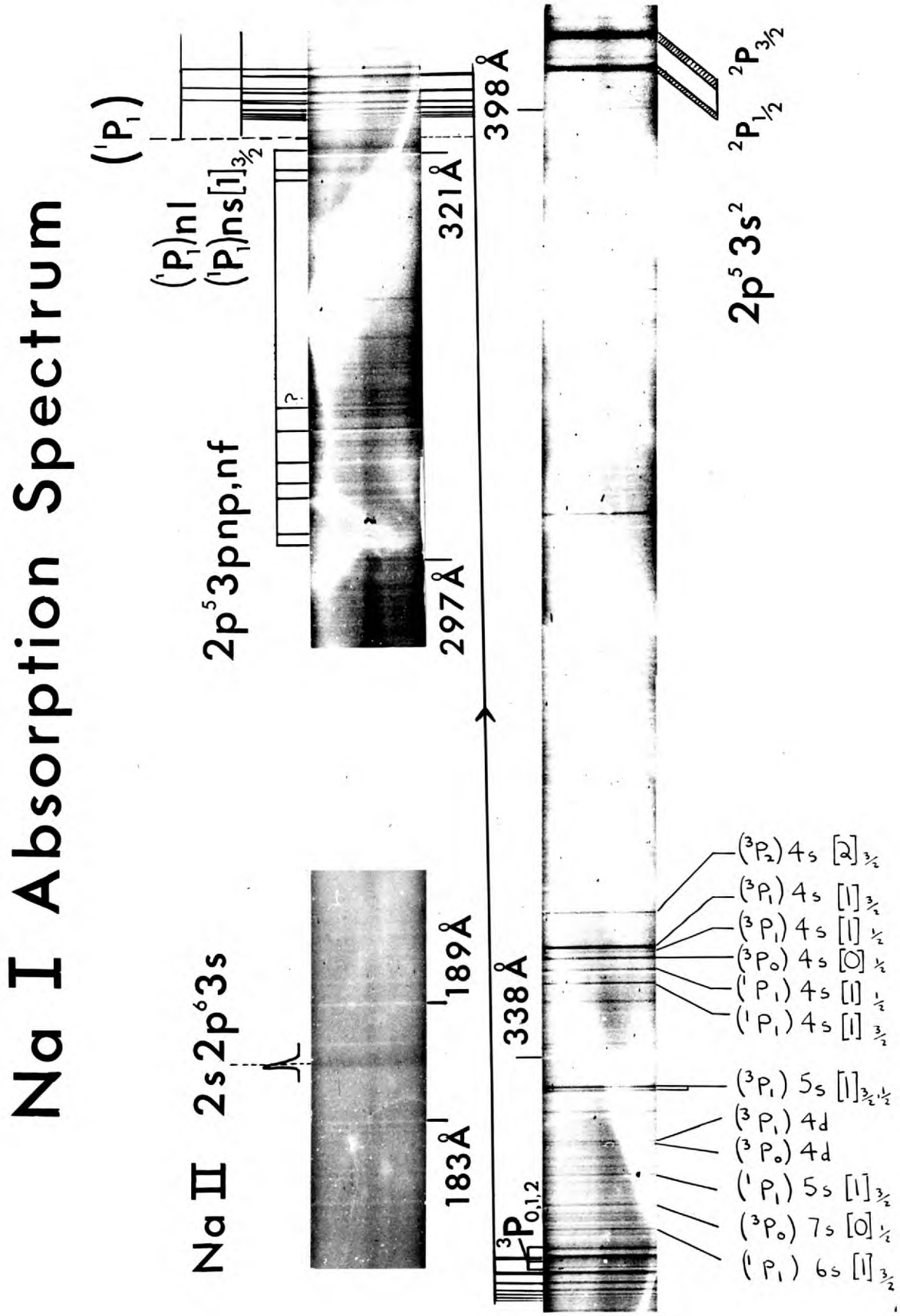
Na I Absorption Spectrum
Na II 2s2p⁶3s
183Å
189Å
338Å
297Å
321Å
398Å
2p⁵3pnp,nf
(¹P₁)nl
(¹P₁)ns[1]3/2
(¹P₁)
2p⁵3s²
²P3/2
²P1/2
³P0,1,2
(³P₂)4s [2]3/2
(³P₁)4s [1]3/2
(³P₁)4s [1]1/2
(³P₀)4s [0]1/2
(¹P₁)4s [1]1/2
(¹P₁)4s [1]3/2
(³P₁)5s [1]3/2,1/2
(³P₁)4d
(³P₀)4d
(¹P₁)5s [1]3/2
(³P₀)7s [0]1/2
(¹P₁)6s [1]3/2

the higher members of 2 series, one quite strong, converging on the same limit. All these features, at wavelengths above 323Å, are fairly well-defined absorption peaks, broadened by autoionization. At the pressures attained in the present experiment these lines are weaker than the equivalent lines of the RbI[b] and KI[b] spectra.

At wavelengths below 323Å a few further features are seen. One, the asymmetric feature at 305Å is strong. The level of continuous absorption is very low at wavelengths above 323Å but can be quite strong below this wavelength; it then decreases steadily towards shorter wavelengths.

Finally one broad diffuse absorption feature is seen at 186Å. The grazing incidence instrument records BRV emission lines at wavelengths as low as 90-100Å; however, with the long furnace inserted, the short wavelength limit of usable continuum is about 150Å and this was the limit of observation for the NaI spectrum in the present experiment.

7.3. Results for Sodium

TABLE I NaII level notation used in this analysis.

Notation Atomic Energy Levels Vol. I	Configuration	J	Energy (cm^{-1}) measured from NaI ground state
$^3P_2$	$2p^5\ (^2P_{3/2})\ 3s\ (^3P_2)$	2	306 378
$^3P_1$	$2p^5\ (^2P_{3/2})\ 3s\ (^3P_1)$	1	307 143
^3P_o	$2p^5\ (^2P_{1/2})\ 3s\ (^3P_o)$	0	307 735
$^1P_1$	$2p^5\ (^2P_{1/2})\ 3s\ (^1P_1)$	1	310 215
$3p_{10}$	$2p^5\ (^2P_{1\frac{1}{2}})\ 3p$	1	334 674
$3p_9$	"	3	338 703

Notation Atomic Energy Levels Vol. I	Configuration	J	Energy (cm^{-1}) measured from NaI ground state
$3p_8$	$2p^5\ (^2P_{1\frac{1}{2}})\ 3p$	2	339 089
$3p_7$	"	1	339 619
$3p_6$	"	2	340 644
$3p_5$	$2p^5\ (^2P_{1/2})\ 3p$	1	341 339
$3p_4$	"	2	341 558
$3p_3$	$2p^5\ (^2P_{1\frac{1}{2}})\ 3p$	0	341 842
$3p_2$	$2p^5\ (^2P_{1/2})\ 3p$	1	341 961
$3p_1$	"	0	350 315

These levels are taken from Söderquist (103).

7.3.1 The Leading Doublet $2p^5 3s^2\ (^2P_{3/2,\ 1/2})$

λ (Å)	ν (cm^{-1})	Assignment	Appearance
402.968	248 159	$2p^5 3s^2\ (^2P_{3/2})$	Very Strong
400.796	249 503	$2p^5 3s^2\ (^2P_{1/2})$	Very Strong

This doublet, not previously observed, is the strongest feature of the NaI^b spectrum. It is readily identified as $2p^5 3s^2\ (^2P_{3/2,\ 1/2})$ (7.4.1). As with the leading doublets of Cs (9), Rb (Chapter V) and K (Chapter VI) the $^2P_{3/2}$ line is broader than the $^2P_{1/2}$ line.

7.3.2 Series to the $(^1P_1)$ limit

(i) Strong series. $2p^5 3s\ (^1P_1)\ ns[1]_{3/2}$

Code	λ(Å)	ν (cm^{-1})	n*	Assignment
NA33	325.855	306 885	5.747	$2p^5 3s\ (^1P_1)\ 7s\ [1]_{3/2}$
NA35	324.901	307 786	6.719	8s
NA37	324.275	308 381	7.731	9s
NA38	323.883	308 753	8.658	10s
NA39	323.589	309 034	9.631	11s
NA40	323.40	309 214	10.46	12s
NA40A	323.25	309 361	11.32	13s

This series is made up of broad absorption peaks. The limit on the number of members seen is set by the resolving power of the grazing incidence spectrograph with a 15 μ slit. The error of measurement on the last 2 members is quite large and, therefore, the irregular n* for these two members is not surprising.

It seems likely that the $2p^5 3s$ ns configuration is stronger than the $2p^5 3s$ nd configuration (7.4.1) and therefore this series is assigned as an ns series. It is specifically assigned as the $[1]_{3/2}$ series as the series following (ii) is possibly the $[1]_{1/2}$ series. If this latter assignment is incorrect the above series is probably the result of a merging of the 2 series $[1]_{3/2}, {}_{1/2}$.

Possible assignments are made in 7.3.3 for the 4s, 5s, 6s members of this series.

(ii) Weaker series to the $(^1P_1)$ limit. $2p^5 3s\ (^1P_1)$ nl.

Code	λ (Å)	ν (cm^{-1})	n*
NA32	326.320	306 448	5.396
NA34	325.193	307 510	6.367
NA36	324.512	308 155	7.295

This series becomes too weak for further observation after the line NA36, although NA32 is moderately strong compared with other features of the spectrum.

The effective quantum numbers for these 3 lines are considered to be unlikely values for the effective quantum numbers of a $2p^5 3s\ (^1P_1)$ nd series, nd electrons being almost hydrogenic in the NaI valence spectrum. The other possibility is that this series is the $ns\left[1\right]_{1/2}$ series to the $(^1P_1)$ limit. The large separation of the 2 series to the $(^1P_1)$ limit however makes this interpretation unlikely. The splittings are certainly too large for (J_cK) coupling and are unreasonable for LS coupling too. In addition the splitting observed for the $2p^5 3s^2\ (^2P_{3/2,\ 1/2})$ doublet (7.3.1) and the splittings of the $2p^5 3s4s$ levels (as tentatively assigned in 7.3.3) would also lead to the expectation of much smaller separations between the two sets of higher members of the $(^1P_1)$ $ns\left[1\right]_{1/2,\ 3/2}$ series than those measured here.

As this series is not easily amenable to identification as $(^1P_1)$ ns or nd it is simply labelled $(^1P_1)$ nl. It is possibly a series of mixed configuration resulting from interactions between the outer ns and (n-1)d electrons.

7.3.3 Other $2p^5 3s$ ns, nd Lines with Tentative Assignments

As has been the practice previously, two lists are given, the first comprising lines clearly distinguishable from the source features and the second comprising possible NaI lines. In particular the NaI features between 333 and 327Å are mostly quite weak and difficult to distinguish from source features.

In view of the difficulty encountered in making detailed assignments for

these features in 7.4.1 the effective quantum number, n^* , of each feature is given for each of the four $2p^5 3s$ ($^3P_{0,\ 1,\ 2}$, $^1P_1$) limits.

(i)

Code	λ(Å)	ν(cm^{-1})	n* (to 4 limits) $(^3P_2)$	$(^3P_1)$	(^3P_o)	$(^1P_1)$	Tentative Assignment	Appearance
NA 3	346.675	288 455	2.474	2.423	2.386	2.246	$(^3P_2)4s\ [2]_{3/2}$	Sharp
NA 4	346.421	288 666	2.489	2.437	2.399	2.257		Weak
NA 5	344.555	290 229	2.607	2.547	2.504	2.343	$(^3P_1)4s\ [1]_{3/2}$	Very strong
NA 5A	344.265	290 474	2.627	2.566	2.521	2.358	$(^3P_1)4s\ [1]_{1/2}$	Weak
NA 6	343.875	290 803	2.654	2.591	2.546	2.377	$(^3P_o)4s\ [0]_{1/2}$	Strong
NA 7	343.161	291 408	2.707	2.649	2.600	2.422	$(^1P_1)4s\ [1]_{1/2}$	Quite Strong
NA 8	342.350	292 099	2.772	2.705	2.658	2.468	$(^1P_1)4s\ [1]_{3/2}$	Strong
NA13	335.959	297 656	3.547	3.401	3.300	2.956	$(^3P_1)5s\ [1]_{3/2}$	Strong
NA14	335.727	297 861	3.589	3.438	3.332	2.980	$(^3P_1)5s\ [1]_{1/2}$	Quite Strong
NA15	333.067	300 240	4.228	3.987	3.826	3.316	$(^3P_1)4d$	Moderate
NA16	332.665	300 603	4.359	4.096	3.932	3.379	$(^3P_o)4d$	Moderate
NA16A	332.453	300 794	4.433	4.157	3.976	3.413	$(^3P_2)6s\ [2]_{3/2}$	Weak
NA20	330.660	302 426	5.337	4.875	4.590	3.777	$(^1P_1)5s\ [1]_{3/2}$	Quite Strong
NA21	330.213	302 835	5.646	5.101	4.781	3.882	$(^3P_2)7s\ [2]_{3/2}$	Moderate, diffuse
NA25	328.894	304 049	6.864	5.955	5.456	4.218	$(^3P_o)7s\ [0]_{1/2}$	Quite Strong

Code	λ (Å)	ν (cm^{-1})	n* (to 4 limits) ($^3P_2$)	($^3P_1$)	(^3P_o)	($^1P_1$)	Tentative Assignment	Appearance
NA26	328.404	304 503	7.65	6.447	5.827	4.382	($^3P_1$)8s [1]$_{3/2,1/2}$	Moderate
NA27	328.135	304 752	8.22	6.775	6.065	4.481	(^3P_o)7s [0]$_{1/2}$	Moderate
NA28	327.966	304 910	8.65	7.01	6.233	4.547	($^3P_2$)10s [2]$_{3/2}$	Moderate
NA29	327.684	305 172	9.54	7.46	6.543	4.664	($^1P_1$)6s [1]$_{1/2}$	Moderate
NA30	327.456	305 385	10.51	7.90	6.833	4.766	($^1P_1$)6s [1]$_{3/2}$	Quite strong
NA31	327.137	305 681	12.55	8.66	7.31	4.919	($^1P_1$)5d	Diffuse

These are all fairly well-defined absorption peaks.

(ii) Possible $2p^5$ ns, nd features with tentative assignments

Code	λ (Å)	ν (cm^{-1})	n* (to 4 limits) ($^3P_2$)	($^3P_1$)	(^3P_o)	($^1P_1$)	Tentative Assignment	Appearance
NA11	338.618	295 318	3.150	3.046	2.973	2.714	($^1P_1$)3d	Moderate
NA12	338.378	295 528	3.180	3.074	2.998	2.733	($^1P_1$)3d	Moderate
NA18	331.158	301 971	4.990	4.606	4.363	3.648	($^1P_1$)5s [1]$_{1/2}$	Moderate
NA19	330.950	302 161	5.101	4.693	4.437	3.691	(^3P_o)6s [0]$_{1/2}$	Weak
NA22	329.744	303 260	5.938	5.320	4.955	3.973	($^1P_1$)4d	Very Weak, diffuse
NA23	329.582	303 415	6.086	5.425	5.040	4.017	($^3P_1$)7s [1]$_{3/2}$	Very Weak, diffuse
NA24	329.278	303 695	6.395	5.641	5.212	4.102	($^3P_1$)7s [1]$_{1/2}$	Weak

Again these are all absorption peaks.

7.3.4 Two-Electron Excitation

Code	λ (Å)	ν (cm^{-1})	n*	Possible Assignment	Appearance
NA41A	321.568	310 977	2.152	$3p_{10}$ 3p	Diffuse A (AS q -ve)
(NA41B)	320.320	312 188	2.034	$3p_9$ 3p	Diffuse A
(NA41C)	319.706	312 787	2.058	$3p_9$ 3p	Diffuse W
NA43	304.886	327 991	3.201	$3p_9$ 4p	Strong AS (q -ve)
(NA44)	302.972	330 064	3.052	$3p_5$ 4p	Diffuse W
NA45	301.674	331 484	5.87	$3p_{10}$ 7p	Diffuse W
NA46	300.899	332 338	4.15	$3p_9$ 5p	Diffuse W
(NA47)	298.831	334 638	5.20	$3p_9$ 6p	Weak W
(NA48)	298.329	335 200	4.15	$3p_4$ 5p	Weak W

Those features with their code numbers bracketed are doubtful Na features. AS denotes asymmetric, W denotes window and A denotes absorption. Many of the features of this section are confused with the background source features. Between 308 and 306Å some familiar source features are suppressed but it is difficult to distinguish any new features.

These two-electron features are given possible assignments as excitation to $2p^5 3p$ np configurations. However, as with the similar excitations in Rb (5.4.4) and K (6.4.4), excitation to the $2p^5 3p$ nf configuration is also likely, though the lower energy features, NA41A, NA41B, NA41C and NA43 are more likely to be attributable to $2p^5 3p$ np. These configurations are discussed in 7.4.3.

7.3.5 Excitation from the 2s shell

One further feature is observed, at shorter wavelengths; this is a broad

absorption feature at 186.5Å. This feature is asymmetric in as much as the absorption cross section falls more sharply on the short wavelength side than on the long wavelength side. A measurement at this point at which the cross section changes most rapidly yields a wavelength of 185.8Å (538 126cm^{-1}). The error attached to this measurement is large, (±0.3Å), firstly because the feature is diffuse and, secondly, because the standards are inadequate in this region, relying heavily on the line measured to be 158.45Å (2.3.2).

This feature is assigned as due to transitions of the type $2s^2 2p^6 3s\ ^2S_{\frac{1}{2}} \rightarrow 2s2p^6 3s$ np, nf (J= $^1/2$, $^3/2$). The region in which the cross section changes rapidly could in fact be the highest $2s2p^6 3s\ ^1S_o$, $^3S_1$ NaII level. This feature is discussed further in 7.4.4.

7.4 Analysis

The discrete NaI spectrum in the region under examination is expected, on broad energetic grounds, to be mainly due to transitions of the type $2p^6 3s\ ^2S_{\frac{1}{2}} \rightarrow 2p^5 3s$ ns, nd (J= $^1/2$, $^3/2$). The limits of this spectrum are the $2p^5 3s$ ($^3P_{o,\ 1,\ 2}$, $^1P_1$) NaII levels (Table I). In the absence of a $2p^5 2d$ configuration there is no longer the possibility of configuration mixing in the parent ion levels and the $2p^5 3s$ levels are well characterised, unlike the equivalent levels of KII and RbII. The NaI^b spectrum is immediately simpler than the KI^b and RbI^b spectra as can be seen in Plate X.

It should also be noted that the distribution of the levels of $2p^5 3p$ configurations of NaII is much closer to LS coupling than to (jl) coupling. Thus, while a (J_cK) notation is used in the same way that it was used to describe the KI^b, RbI^b spectra, the possibility that a LS scheme is more appropriate for the $2p^5 3s$ ns, nd levels, is constantly considered. The

$\Delta S = 0$ selection rule could apply to some extent and the separations of levels might be greater than would be expected if a $(J_c K)$ coupling scheme was operating.

7.4.1 The $2p^5 3s\ ns$ configuration

When n=3 this configuration becomes $2p^5 3s^2\ (^2P_{3/2,\ 1/2})$. The leading doublet (7.3.1) is easily assigned to this configuration. The splitting of the doublet ($1344 cm^{-1}$) is close to the splitting of the $2p^5\ (^2P_{3/2,\ 1/2})$ levels of NaIII ($1364 cm^{-1}$) (104). For NaI the spread of the $2p^5$ core is reduced by the presence of a $3s^2$ shell, thus reducing the $2p^5\ (^2P_{3/2,\ 1/2})$ splitting. This reduction is smaller than the equivalent reductions of the $(n-1)p^5\ ns^2\ (^2P_{3/2,\ 1/2})$ splittings in Rb and K (5.3.4, 6.3.2), presumably because the 2p shell of Na is more tightly bound than the 3p shell of K or the 4p shell of Rb. The position of the $2p^5 3s^2\ (^2P_{1/2,\ 3/2})$ levels of NaI has been computed by Froese (105), from Hartree-Fock calculations, to be at about 245 $000 cm^{-1}$, quite close to the value of the present experiment.

There are no further NaI features between 400Å and 350Å as is expected in the absence of a 2d shell. The next group of lines lies between 288 000 and 293 000 cm^{-1} (7.3.3). There are 7 of these lines, one strong, four quite strong and 2 weak. The next $2p^5 3s\ ns$ configuration expected is $2p^5 3s4s$. There can be six of these levels, the order is given below; it is the order obtained by Connerade (106) from Merrill's work on the $1^{n-1} ss'$ configuration (97) c.f Rb 5.4.2.

TABLE II

$(J_c K)$ Notation	J	LS Notation
$2p^5 3s\ (^3P_2)4s\ [2]_{3/2}$	$1\frac{1}{2}$	$2p^5 3s\ (^3P_2)4s\ (^4P_{3/2})$
" $(^3P_1)4s\ [1]_{3/2}$	$1\frac{1}{2}$	" $(^3P_1)4s\ (^2P_{3/2})$
" $(^3P_1)4s\ [1]_{1/2}$	$\frac{1}{2}$	" " " $(^4P_{1/2})$
" $(^3P_0)4s\ [0]_{1/2}$	$\frac{1}{2}$	" $(^3P_0)4s\ (^2P_{1/2})$
" $(^1P_1)4s\ [1]_{1/2}$	$\frac{1}{2}$	" $(^1P_1)4s\ (^2P_{1/2})$
" $(^1P_1)4s\ [1]_{3/2}$	$1\frac{1}{2}$	" " " $(^2P_{3/2})$

It seems therefore that this configuration, which can produce 6 levels (4 in strict LS coupling), is not able to account for all 7 transitions in this energy range.

The lowest $2p^5 3s$ nd configuration should be $2p^5 3s3d$. This configuration can give rise to 11 levels, $^4F_{3/2}$, $^4D_{3/2,1/2}$, $^4P_{3/2,1/2}$, $(^3P)\ ^2P_{3/2\ 1/2}$, $(^3P)\ ^2D_{3/2}$, $(^1P)\ ^2P_{3/2,1/2}$, $(^1P)\ ^2D_{3/2}$, in LS coupling. However the quantum defects of the 7 features between 288 000 and 293 000cm^{-1}, when referred to the ion limits, can be seen (7.3.3) to be about 0.5, an improbably high value for a 3d electron which is almost hydrogenic in the valence spectrum. If strict LS coupling applies in this case transitions to 6 levels are expected, so, to obtain 7 features from this configuration, it must be assumed that LS coupling breaks down in one case; the 4 transitions that would not be seen in LS coupling would be those to 4 of the quartet terms. However if, as might be expected, the terms of higher multiplicity lie deeper, the remaining 7 transitions should be referred to the higher ion limits making the quantum defects greater than 0.5, an even more unreasonable value for a 3d electron.

In view of the unreasonable quantum defects for 3d electrons obtained

For the 6 stronger lines in this region these lines have been described (7.3.3) as transitions to the $2p^5 3s4s$ configuration. The effective quantum numbers are reasonable for 4s electrons and in some ways these assignments correspond well to the LS notation of Table II, the quartet terms being weaker than the doublet terms and the $J=\frac{1}{2}$ levels being weaker than the $J=3/2$ levels.

In making these assignments the 7th line NA4 has been left unassigned. It is a weak line but, by the criteria applied in distinguishing lines from source features, it would normally be accepted as a feature of the element under study. Possible explanations for its presence are a mixing between the $2p^5 3s4s$ and $2p^5 3s3d$ configurations or a mixing between these configurations and the $2p^5 3p^2$ configuration. A mixing with this latter configuration is less likely as levels of this type would be expected to lie at energies above 310 000cm^{-1} (7.4.3).

Further evidence that there are configuration interactions involving the orbiting electrons is obtained when the positions of the lower members of the 2 series to the ($^1P_1$) NaII limit (7.3.2) are estimated. No lines are observed that have anything like the intensity expected for lower members of the ($^1P_1$) ns $[1]_{3/2}$ series; lines in the region where the 6s member is expected are particularly weak. The series only becomes evident at energies above the ($^3P_{0,1,2}$) ion levels which lie around the 7s member of the ($^1P_1$) ns $[1]_{3/2}$ series. The difficulty encountered in making a plausible ($^1P_1$) ns or ($^1P_1$) nd assignment for the weaker series of 7.3.2 also suggests a mixed configuration.

The significance of configuration mixing involving the outer electron is great because it has been an important assumption of the analyses of Cs (15), Rb (Chapter V) and potassium (Chapter VI) that the outer electron does not

introduce additional strong new configuration interactions; the outer electron is considered to be screened from the core by the 6s (Cs)/5s (Rb)/4s (K) electron of the extended core and thus better characterised. The possibility of mixing involving the outer electron is discussed in Chapter VIII.

In view of the tentative identification of the strong longer wavelength features as transitions to $2p^5 3s4s$ levels, most of the other features in 7.3.3 have been tentatively assigned as transitions to $2p^5 3s\ ns$ but there are many anomalies as would be expected in the presence of configuration interactions. For each feature in 7.3.3 the effective quantum number, n^*, is given for each of the four $2p^5 3s$ ($^3P_{0,1,2}$, $^1P_1$) limits and the most likely identification is then given in the "tentative assignment" column.

7.4.2 The $2p^5 3s\ nd$ Configuration

It was shown in the previous section that transitions are possible to 11 levels of the $2p^5 3s\ nd$ configuration, 6 of these transitions being to doublet terms and 5 to quartet terms. In the valence spectrum of NaI nd electrons are almost hydrogenic and in the valence spectrum of MgI nd electrons possess quantum defects of about 0.25, but as was explained in the previous section, it is very difficult to make $2p^5 3s3d$ assignments with quantum defects near to these "reasonable" values.

As a result of this difficulty of assigning features so as to give reasonable quantum defects for nd electrons, few assignments have been made for the $2p^5 3s\ nd$ configuration in 7.3. The number of lines assigned for each n does not approach the 6 lines expected in strict (LS) coupling. However it seems likely that this configuration does manifest itself in configuration mixing with the $2p^5 3s\,ns$ configuration.

As it is not possible to assign any features satisfactorily as transitions to the $2p^5 3s3d$ configuration, it is difficult to establish a typical value for the quantum defect of a nd electron and the $2p^5 3s$ nd assignments of 7.3.3 are necessarily very tentative.

7.4.3 Two-Electron Excitation

Energetically, the next single electron excitation expected in NaI is excitation from the 2s shell. A rough estimate of the energy involved in transitions of this type can be made from characteristic X-ray data. The energy of the L_1 absorption edge in Na is 63.3eV (196Å) (89), therefore the features listed in 7.3.4 could hardly be attributed to transitions of this sort.

The NaII ion levels following the $2p^5 3s$ levels in energy are those due to the $2p^5 3p$ configuration (Table I). Transitions based on these parent ions are of the type $2p^6 3s\ ^2S_{\frac{1}{2}} \rightarrow 2p^5 3p$ np, nf. Rough estimates of the positions of these levels have been made from a knowledge of the energies of the ion levels and the typical quantum defects of np and nf (hydrogenic) in the valence spectrum of NaI. It is interesting that the lowest level estimated in this way, $2p^5 3p\ (^3P_{10})\ 3p$, lies at about 310 200cm^{-1}, about the same energy as the highest $2p^5 3s$ limit. It seems therefore that the $2p^5 3p^2$ levels would not be expected to overlie the higher $2p^5 3s$ ns, nd levels to the same extent as the equivalent configurations of KI and RbI overlapped.

Many of the lines of 7.3.4 can be assigned, equally plausibly, as $2p^5 3p$ np or $2p^5 3p$ nf. The 3 lowest lines, however, possess effective quantum numbers that, when referred to the lowest $2p^5 3p$ limit, $3p_{10}$, are too low for 4f electrons ($n^* \sim 4$). These 3 features are much more likely to be due to

transitions to the $2p^5 3p$ np configuration. Furthermore the strong asymmetric feature NA43 gives a n^* of 4.022 when referred to $3P_{10}$ limit and $n^* < 3.2$ when referred to the other limits. Therefore this feature, the strongest of the two-electron spectrum, seems also to be due to a transition to a $2p^5 3p$ np level rather than a $2p^5 3p$ nf level.

Unlike the case of the similar transitions in Rb and K, therefore, it does seem that the np configurations are better established than nf in many cases, though the assignments are still very much speculative, merely indicating how transitions of this sort can account for features in this region.

7.4.4 Excitation from the 2s Shell

It was mentioned in the previous section that excitation from the 2s shell would be expected at about 196Å. It seems very likely, therefore, that the feature mentioned in 7.3.5, at 186Å, is due to transitions of this type. The energy at which the feature occurs (538 126cm^{-1}) is above the ionization potential of NaII measured from the ground state, 422 978cm^{-1}. It is therefore built on an autoionizing level of NaII and this may account for its diffuseness to some extent. The span of a Rydberg series is small in this region and, as explained in 3.1.3, the increasing dominance of Auger transitions in determining the breadth of lines due to excitation from low lying shells means that a series soon loses contrast and higher members are not resolved experimentally.

Thus this feature may represent the merging of all the members of a series converging on a NaII $2s2p^6 3s$ ($^1S_0$, $^3S_1$) limit; the sharp change of cross section on the short wavelength side of the feature may represent a series limit.

7.4.5 The Continuous Absorption Cross Section

The continuous photoionization cross section of NaI has been measured by Hudson and Carter (37) between 1000 and 600Å using a Hopfield continuum as a background. As with their similar measurements of the continuous photoionization cross section of potassium (6.4.5), their values for the cross section became progressively greater than the values calculated by Cooper (107) and Sheldon (102) as the energy increased.

An attempt to obtain an indication of how the continuous absorption cross section varied in the present experiment was made by comparing microdensitometer traces of the background, with and without NaI absorption, at high pressure. At wavelengths above 350Å the continuous absorption was too small to be detectable. At wavelengths below the $2p^5 3s\ (^1P_1)$ limit, however, quite a substantial continuous absorption set in. The level of absorption lessened progressively towards shorter wavelengths, however, and it was quite low at the limit of observation in the present experiment, about 150Å.

7.5 Conclusions

In the present experiment at least 38 new features of the NaI spectrum have been observed and measured, the first features of NaI to be observed at energies above the first ionization potential of sodium.

Experimentally it should be possible to improve and extend the present results in 2 ways. Firstly the superposition of external wavelength standards on this spectrum should enable more reliable values for the wavelength measurements to be obtained and, secondly, the use of faster light sources and faster photographic emulsions would mean that the slit could be narrowed,

improving resolution, and that higher levels of Na absorption could be achieved because higher temperatures could be reached with less risk in shorter exposures.

Only the leading doublet has been assigned with any certainty but a tentative analysis has been performed that at least establishes that configuration interactions involving the outer electron cannot be neglected, an important finding in as much as it may affect the assumptions made in the equivalent analyses of other alkali spectra. Calculations of these configuration interactions will be necessary before a more certain analysis can be made.

Finally a feature has been observed that can be attributed to transitions from a lower lying shell, the first time such a feature has been observed in the atomic absorption spectra of group I elements.

CHAPTER VIII EXCITATION FROM THE SUB-VALENCE p SHELL IN THE ALKALI METALS

8.1 Introduction

It is now useful to summarise and compare the results obtained, in Chapters V to VII of this thesis, and in the work of Connerade (15), for transitions of the type $(n-1)\ p^6 ns \rightarrow (n-1)\ p^5\ \left[(n-1)d + ns\right]$ ms, md in neutral atoms of the alkali metals.

It is evident that it is not possible to find a line by line correspondence between these p shell spectra, as was possible in Connerade's results for the inner d shell excitation of the Zn-like sequence (14) or in Madden and Codling's results for subshell d excitation in the inert gases (41). The reason for this is, of course, that the mixing of the $(n-1)p^5\ (n-1)d$ and $(n-1)p^5$ ns levels of KII, RbII and CsII, on which the I^b spectra are built, takes a different form for each element depending on the relative positions of these overlapping configurations. The NaI^b spectra is different again in the absence of a $(n-1)\ p^5\ (n-1)d$ configuration in NaII.

8.2 Parent Ion Levels. Coupling Scheme

Investigations of the $(n-1)\ p^5$ ns characterisation of the mixed $(n-1)\ p^5\ \left[(n-1)d + ns\right]$ ion levels show mixing to be considerable in all the alkalis, with the exception of Na which does not posses a (n-1)d shell. For Cs this mixing occurs more strongly with the J= 0, 1, 2 upper levels, for Rb it occurs for all J= 0, 1, 2 levels and for K there is some indication that the mixing occurs more strongly for the lower levels (with J= 0, 1, 2).

The most convenient notation for describing these spectra has been the

(J_cK) scheme of Racah (64). This scheme can incorporate mixed limits, characterised only by their J values. The pronounced doublet appearance of many features of these spectra also indicates that the (J_cK) model is a reasonable first approximation. Only in Na is there any indication that an IS scheme might be more appropriate.

8.3 The $(n-1)\ p^5\ [(n-1)d + ns]\ ms$ Configuration

When n=m this configuration produces the very strong $(n-1)\ p^5\ ns^2$ $(^2P_{3/2,\ 1/2})$ leading doublet that provides the lowest lying features for each of the alkali spectra.

Transitions to the next levels of this configuration, where m=n + 1, have also been quite well established for each element as the next strong group of lines following the leading doublet. For Rb this configuration is particularly well established and for the other alkalis plausible assignments have been made, the positions of strong lines corresponding well to the $(n-1)\ p^5\ ns$ characterisation of the ion levels. For K of course some of the ion levels were not known and thus assignments are accordingly less certain for this element. It is notable that all obvious series observed in these spectra are to J=1 limits which have pronounced $(n-1)\ p^5\ ns$ character.

Most of the other strong features of the I^b spectra have been assigned to this configuration assuming it to be dominant. An analysis of this sort has assumed that the orbiting ms, md electrons are well characterised, screened from the core by the ns electron which is not present in the case of the ion. However there are indications that this assumption can break down (8.5).

A summary of typical quantum defects of ms electrons in the alkali I^b

spectra (based on the (n + 1) s lines), and of the quantum defects of ns electrons in the valence spectra of neutral atoms of group VIII, I and II elements is given below.

TABLE I

Group	VIII	I	II	I (I^b)(present spectra)
Transition	$p^6 \rightarrow p^5ns$	$p^6s \rightarrow p^6ns$	$p^6s^2 \rightarrow p^6sns$	$p^6s \rightarrow p^5sns$
	Ne 1.33	Na 1.35	Mg 1.62	Na 1.50
Quantum	Ar 2.16	K 2.19	Ca 2.45	K 2.53
Defects	Kr 3.12	Rb 3.14	Sr 3.36*	Rb 3.75
	Xe 4.05	Cs 4.07	Ba 4.30*	Cs 4.75

*irregular quantum defects

8.4 The (n-1) p^5 [(n-1)d + ns] md Configuration

For each element transitions to this configuration have been used to assign the sharper features not accounted for by the (n-1) p^5 [(n-1)d + ns] ms configuration. The number of lines assigned in this way has been considerably less than the number of lines possible for this configuration, although assignments for the m = (n-1) configuration (restricted by the Pauli principle) have been fairly numerous.

Transitions to this configuration were able to account for the weaker low-lying features of Cs, though, admittedly, Connerade was restricted from observing the region around the leading doublet $5p^56s^2$ ($^2P_{3/2,\ 1/2}$) by the upper wavelength limit of the He_2 continuum. For Rb this configuration accounted for the low-lying sharp lines with 2 exceptions but for K it was evident that an additional interaction was taking place (8.5). Thus for K

and Na, assignments involving this configuration are not very satisfactory.

A summary of typical quantum defects for nd electrons in the present spectra and in the valence spectra of group VIII, I, II elements is given in Table II. The values for the I^b spectra of K and Na are hardly meaningful though, for the reasons noted above.

TABLE II

Group	VIII	I	II	I (I^b)(present spectra)
Transition	$p^6 \rightarrow p^5nd$	$p^6s \rightarrow p^6nd$	$p^6s^2 \rightarrow p^6snd$	$p^6s \rightarrow p^5snd$
	Ne 0.02	Na 0.01	Mg 0.24	Na 0.1
Quantum	Ar 0.27	K 0.20	Ca 0.95	K 0.35
Defects	Kr 1.25	Rb 1.30	Sr 1.85*	Rb 1.20
	Xe 2.39	Cs 2.47	Ba 2.90*	Cs 2.28

* irregular quantum defect

8.5 Configuration Interactions of the Orbiting Electron

The coupling notation and method of analysis used for all these spectra have taken account of the considerable mixing of the parent ion levels on which all these levels are built but has presumed largely that the orbiting electrons are well characterised, with occasional anomalies expected when levels lie close together.

The spectrum of Na, however, which has pure (n-1) p^5 ns limits enables an estimation of additional configuration mixing effects to be made. Although the Na spectrum possesses less features than the other alkali I^b spectra, it also bears similarities in as much as it consists broadly of a group of well defined lower energy features followed by a complex region of weaker lines

which finally give way to a strong series converging on the highest limit of the spectrum. This series emerges above the 3 other limits of the NaI[b] spectrum. Estimations of the positions of lower members of the series and difficulty encountered in assigning all the lower energy features (7.4.1) indicate that additional configuration interactions do take place.

In addition, difficulties in assigning many of the weaker lower features of the K spectrum (6.4.3) indicate a configuration interaction involving the $3p^5\ (3d+4s)^2$ configuration. There is no particular indication of a similar problem in Cs and Rb, and it may be that these additional interactions are not general features of these spectra and that they apply more with Na and K and with md configurations rather than ms. The $(n-1)\ p^5 \left[(n-1)d + ns\right]$ $(n+1)s$ assignments, for example, may still have particular validity.

In conclusion, however, it is evident that complete analyses of these spectra will not be possible until reliable theoretical calculations can be made firstly of the mixing of the ion limits, secondly of the possible configuration interactions involving orbiting electrons and thirdly of the possible configuration mixing effects of the $(n-1)\ p^5\ np^2$ configuration with the $(n-1)\ p^5\ \left[(n-1)d + ns\right]$ ms, md configurations.

REFERENCES

1) J.J. HOPFIELD
Astr.J. 72, 133 (1930)

2) Y.TANAKA
J.Opt.Soc.Amer. 48, 304 (1958)

3) R.E.HUFFMAN. Y.TANAKA AND J.C.LARABEE
Appl.Opt. 4, 1581 (1965)

4) H.BEUTLER (General)
Zeit. für Phys. 86, 495 (1933)

5) H.BEUTLER (Ar, Kr, Xe)
Zeit. für Phys. 93, 177 (1935)

6) H. BEUTLER (Hg)
Zeit. für Phys. 86, 710 (1933)

7) H. BEUTLER (Cd)
Zeit. für Phys. 87, 19 (1933)

8) H.BEUTLER AND K.GUGGENHEIMER (Zn)
Zeit. für Phys. 87, 176 (1933)

9) H.BEUTLER AND K.GUGGENHEIMER (Cs)
Zeit. für Phys. 88, 25 (1934)

10) H.BEUTLER (Rb)
Zeit. für Phys. 91, 131 (1934)

11) H.BEUTLER AND K. GUGGENHEIMER (K)
Zeit. für Phys. 87, 188 (1933)

12) H.BEUTLER AND W.DEMETER (Tl)
Zeit. für Phys. 91, 218 (1934)

13) W.KOSSEL
Zeit. für Phys. 1, 119 (1920)

14) W.R.S. GARTON AND J.P. CONNERADE (Zn, Cd and Hg)
Astr.J. 155, 667 (1969)

15) J.P.CONNERADE (Rb, Cs, Tl)
Thesis (London) 1968. To be published Astr. J.

16) J.F. LOWRY, D.L. EDERER AND D.H.TOMBOULIAN
Phys.Rev. 137, A1054 (1964)

17) D.J. BAKER, D.E. BEDO AND D.H.TOMBOULIAN
Phys. Rev. 124, 1471 (1961)

18) PO LEE AND G.L. WEISSLER
Phys. Rev. 99, 540 (1955)

19) D.L. EDERER AND D.H.TOMBOULIAN
Phys. Rev. 133, A1525 (1964)

20) J.A.R. SAMSON
J.Opt. Soc. Am. 55, 935 (1965)

21) R.W. DITCHBURN
Proc. Phys. Soc. LXXV, 461 (1960)

22) R.E. HUFFMAN, Y.TANAKA AND J.C. LARABEE
J. Chem. Phys. 39, 902 (1963)

23) N.WAINFAN, W.C. WALKER AND GL. WEISSLER
Phys.Rev. 99, 542 (1955)

24) P.H. METZER AND G.R. COOK
J.Opt. Soc. Am. 55, 516 (1965)

25) O.P. RUSTGI
J.Opt.Soc. Am. 54, 464 (1964)

26) J.A.R. SAMSON
J. Opt. Soc. Am. 54, 420 (1964)

27) R.W. ALEXANDER, D.L. EDERER AND D.H. TOMBOULIAN
Bull. Am. Phys. Soc. 9, 626 (1964)

28) R.E. HUFFMAN, Y. TANAKA AND J.C. LARABEE
Appl. Opt. 2, 947 (1963)

29) O.P. RUSTGI, E.I. FISHER, C.H. FULLER
J. Opt. Soc. Am. 54, 745 (1964)

30) A. PERY-THORNE AND W.R.S . GARTON
Proc. Phys. Soc. B76, 833 (1960)

31) J.A.R. SAMSON (Ar Resonances)
Phys. Rev. 132, 2122 (1963)

32) G.L.WEISSLER
J . Quant. Spectr.Rad.Trans. 2, 383 (1962)

33) D.L. EDERER
Phys. Rev. Letters 13, 760 (1964)

34) J.A.R.SAMSON (Kr and Xe Resonances)
Phys. Letts. (Neths) 8, 107 (1964)

35) W.R.S. GARTON
J.Sci. Instrum. 36, 11 (1959)

36) J.E.G. WHEATON
Appl. Opt. 3, 1247 (1964)

37) R.D. HUDSON AND V.L. CARTER
J.Opt.Soc.Am. 57, 651 (1967)

38) R.D. HUDSON AND V.L. CARTER
J.Opt.Soc.Am.57, 1471 (1967)

39) R.P. MADDEN AND K. CODLING (General)
Phys. Rev. Letters 10, 516 (1963)

40) R.P. MADDEN AND K . CODLING (Kr,Xe)
J. Opt. Soc. Am. 54, 268 (1964)

41) K. CODLING AND R.P. MADDEN (Kr,Xe)
Phys. Rev. Letters 12, 106 (1964)

42) R.P. MADDEN AND K. CODLING (He)
Astr. J. 141, 364 (1965)

43) K. CODLING AND R.P. MADDEN (Kr, Xe)
Appl. Opt. 4, 1431 (1965)

44) K. CODLING, R.P. MADDEN AND D.L. EDERER (Ne)
Phys. Rev. 155, 26 (1967)

45) R.P. MADDEN, D.L. EDERER AND K. CODLING (Ar)
Phys. Rev. 177, 136 (1969)

46) D.H.TOMBOULIAN AND P.L. HARTMAN
Phys. Rev. 102, 1423 (1956)

47) D.H. TOMBOULIAN AND D.E. BEDO
J. Appl. Phys. 29, 804 (1958)

48) D.E. BEDO, D.H. TOMBOULIAN AND J.A. RIGGERT
J. Appl. Phys. 31, 2289 (1960)

49) M. NAKAMURA ET AL.
Phys. Rev. Letts. 21, 1303 (1968)

50) W.S. WATSON AND F.J. MORGAN
J. Phys. B. (Proc. Phys.Soc.) 2, 277 (1969)

51) R. WHIDDINGTON AND H. PRIESTLEY
Proc. Roy. Soc. A, 145, 462 (1934)

52) J. AROL SIMPSON, S.R. MIELCZAREK AND J. COOPER
J. Opt. Soc. Am. 54, 269 (1964)

53) J. AROL SIMPSON, G.E. CHAMBERLAIN AND S.R. MIELCZAREK
Phys. Rev. 139, A1039 (1965)

54) C.E. KUYATT AND J. AROL SIMPSON
Proc. of the 2nd Int. Conf. on the Phys. of Electronic and Atomic collisions (1963). North Holland

55) M.E. RUDD
Phys. Rev. Letts. 13, 503 (1964)

56) M.E. RUDD
Phys. Rev. Letts. 15, 580 (1965)

57) M.E. RUDD, T.JORGENSEN AND D.J. VOLZ
Phys. Rev. 151, 28 (1966)

58) M. E. RUDD AND D.V. LANG
4th Int. Conf. on the Phys. of Electronic and Atomic Collisions. Science Bookcrafters Inc. N.Y. (1965) p.153.

59) J. ROMAND
J. Quant. Spectr. Rad. Trans. 2, 691 (1962)

60) H. DAMANY, J.-Y. RONCIN AND N. DAMANY-ASTOIN
Appl. Opt. 5, 297 (1966)

61) U. FANO
Phys. Rev. 124, 1866 (1961)

62) U. FANO AND J.W. COOPER
Phys. Rev. 137, A1364 (1965)

63) C.B. ELLIS AND R.A. SAWYER
Phys. Rev. 49, 145 (1936)

64) G. RACAH
Phys. Rev. 61, 537 (1942)

65) J. COOPER, U. FANO AND F. PRATS
Phys. Rev. Letts. 10, 518 (1963)

66) A.P. LUKIRSKI, T.M. ZIMKINA AND I.A. BRITOV
Izv. Akad. Nauk.SSSR, Ser. Fiz. 28, 772 (1964)

67) A.H. GABRIEL, J.R. SWAIN AND W.A. WALLER
J. Sci. Instr. 42, 94 (1965)

68) N. ASTOIN, B. VODAR AND J. ROMAND
J. de Phys. et Rad. 16, 491 (1955)

69) W.A. RENSE AND T. VIOLETT
J. Opt. Soc. Am. 49, 139 (1959)

70) W.M. BURTON
Optical Transmission Data for Thin Al Films (1966) UKAEA Culham Report CLM-R64

71) W.R. HUNTER AND R. TOUSEY
J. de Phys. 25, 148 (1964)

72) W.R. HUNTER, D.W. ANGEL AND R. TOUSEY
Appl. Opt. 4, 891 (1965)

73) K. CODLING AND R.P. MADDEN
Phys. Rev. 167, 587 (1968)

74) H.W.B.SKINNER, T.G. BULLEN AND J.E. JOHNSTON
Phil. Mag. 45, 1070 (1954)

75) D.E. CARTER AND M.P. GIVENS
Phys. Rev. 101, 1469 (1956)

76) B.VODAR AND N.ASTOIN
Nature, 166, 1029 (1950)

77) B.VODAR AND N.ASTOIN
J. Phys. Rad. 14, 494 (1953)

78) G. BALLOFET, J. ROMAND AND B.VODAR
Comptes Rendus, 252, 4139 (1961)

79) B. EDLÉN
Rep. Prog. Phys. 26, 181 (1963)

80) G. HERZBERG
Trans. Int. Astronom. Union 11A, 97 (1962)

81) R.L. KELLY
Atomic Emission Lines below 2000Å. H-Ar. Naval Research
Lab. Washington D.C. (1968)

82) R.L. KELLY
Vacuum Ultraviolet Emission Lines below 2000Å.
University of California. UCRL 5612 (1959)

83) J.W. COOPER
Phys. Rev.Letters 13, 762 (1964)

84) R.P. MADDEN AND K. CODLING
Autoionization Spectra of the Noble Gases. P.129 of "Autoinnization"
Ed. A. Temkin. Mono Book Corp. Baltimore (1966)

85) F. PASCHEN
Akad. Wiss., Berlin (Phys.-Math. Kl) Sitz. Pts. 31-33 p.536 (1928)

86) J.C. MCLENNAN, A.B. McLAY, AND M.F. CRAWFORD
Proc. Roy. Soc. (A) 134, 41 (1931)

87) J.P. CONNERADE
1968 Thesis (London) P.50.

88) E.U. CONDON AND G.H. SHORTLEY
The Theory of Atomic Spectra. Cambridge. P.312.

89) J.A. BEARDEN
X-ray Wavelengths and X-ray Atomic Energy Levels. National Standard Reference Data Series - NBS 14, Rev.Mod. Phys. 31, No.1 (1967)

90) S.T.MANSON AND J.W.COOPER
Phys.Rev. 165, 126 (1968)

91) O.LAPORTE, G.R. MILLER AND R.A.SAWYER
Phys.Rev. 38, 843 (1931)
Correction in
Phys.Rev. 39, 458 (1932)

92) J.P.CONNERADE
Thesis (London) 1968, P.109

93) J.P. CONNERADE
Thesis (London) 1968, P.112. Note that the $l^{n-1}s$ formula is incorrectly quoted by Connerade. The $(3/2, 1/2)_1$ term should read $(3/2, 1/2)_2$ and -2l + 1 should be - (2l + 1).

94) E.U.CONDON AND G.H. SHORTLEY
The Theory of Atomic Spectra. Cambridge Univ. Press P.305

95) D.H.TOMBOULIAN
Phys.Rev. 54, 350 (1938)

96) H.REINHEIMER
Ann. der Phys. 71, 162 (1923)

97) R.A. MERRILL
Phys.Rev. 46, 487 (1934)

98) I.S.BOWEN
Phys.Rev. 31, 499 (1928)

99) T.L. de BRUIN
Zeit. für Phys. 38, 94 (1926)
Proc. Royal Acad. Amsterdam 29, No.5, 713 (1926)
Arch. Néerl. Sci. exactes et naturelles (IIIA) 11, 75 (1928)

100) K.W. MEISSNER

Zeit. für Phys. 39, 172 (1926)

40, 839 (1927)

101) B.EDLÉN

Zeit. für Phys. 104, 410 (1937)

102) J.W.SHELDON

J.Appl.Phys. 37, 2928 (1966)

103) J.SÖDERQVIST

Nova Acta Reg. Soc. Sci. Uppsala IV, 9 No. 7, 22 (1934)

104) D.H. TOMBOULIAN

Phys.Rev. 54, 347 (1938)

105) Calculation of C.FROESE quoted from article by L. GOLDBERG "Astrophysical Implications of Autoionization" in "Autoionization" Ed. A.TEMKIN, Mono Book Corp., Baltimore (1966) P.21.

106) J.P.CONNERADE

Thesis (London) 1968, P.116

107) J.W. COOPER

Phys.Rev. 128, 681 (1962)